Chapter 2
Chemical Applications of Mössbauer Spectroscopy

Philipp Gütlich and Yann Garcia

Abstract The Tutorial Lecture begins with a brief recapitulation of the hyperfine interactions and the relevant parameters observable in a Mössbauer spectrum. The main chapter with selected examples of chemical applications of Mössbauer spectroscopy follows and is subdivided into sections on: basic information on structure and bonding; switchable molecules (thermal spin transition in mono- and oligonuclear coordination compounds, light-induced spin transition, nuclear-decay-induced spin transition, spin transition in metallomesogens); mixed-valency in biferrocenes and other iron coordination compounds, and in an europium intermetallic compound; electron transfer in Prussian blue-analog complexes; molecule-based magnetism; industrial chemical problems like corrosion; application of a portable miniaturized Mössbauer spectrometer for applications outside the laboratory and in space. The Lecture ends with concluding remarks and an outlook to future developments.

Abbreviations

δ	Isomer shift
ΔE_Q	Quadrupole splitting
ΔE_M	Magnetic splitting
EFG	Electric field gradient
B_c	Fermi contact field
B_D	Spin dipolar field
eQ	Quadrupole moment

P. Gütlich (✉)
Institute of Inorganic and Analytical Chemistry, University of Mainz, 55099, Mainz, Germany

Y. Garcia
Institute of Condensed Matter and Nanosciences, MOST-Inorganic Chemistry, Université Catholique de Louvain, 1348, Louvain-la-Neuve, Belgium

Y. Yoshida and G. Langouche (eds.), *Mössbauer Spectroscopy*,
DOI: 10.1007/978-3-642-32220-4_2, © Springer-Verlag Berlin Heidelberg 2013

β_N	Nuclear Bohr magneton
g_N	Nuclear Landé factor
g	Landé splitting factor
H_{eff}	Effective hyperfine field
H_{ext}	External field
HS	High-spin
LS	Low-spin
SCO	Spin crossover
ST	Spin transition
LIESST	Light induced excited spin state trapping
NIESST	Nuclear decay-induced excited spin state trapping
ZFS	Zero-field splitting
AF	Antiferromagnetic
$T_{1/2}$	Transition temperature
LC	Liquid-crystal
1D	One-dimensional
EXAFS	Extended X-ray absorption fine structure
DSC	Differential scanning calorimetry
TGA	Thermo-gravimetric analysis
MAS	Mössbauer absorption spectroscopy
MES	Mössbauer emission spectroscopy
MIMOS	Miniaturized Mössbauer spectrometer
APXS	Alpha particle X-ray spectrometer
MER	Mars exploration rover
RAT	Rock abrasion tool
NFS	Nuclear forward scattering
NIS	Nuclear inelastic scattering
PDOS	Partial density of states
ptz	1-propyl-tetrazole
mtz	1-methyl-tetrazole
phen	1,10-phenanthroline
phdia	4,7-phenanthroline-5,6-diamine
bpym	Bipyrimidine
pmatrz	4-amino-3,5-bis{[(2-pyridyl-methyl)amino]methyl}-4*H*-1,2,4-triazole
iptrz	4-isopropyl-1,2,4-triazole
hyetrz	4-(2′-hydroxy-ethyl)-1,2,4-triazole
C_{10}-tba	3,5-bis(decyloxy)-*N*-(4*H*-1,2,4-triazol-4-yl)benzamide
C_{12}-tba	3,5-bis(dodecyloxy)-*N*-(4*H*-1,2,4-triazol-4-yl)benzamide
C_n-tba	3,5-bis(alkoxy)-*N*-(4*H*-1,2,4-triazol-4-yl)benzamide
TB-LMTO-ASA	Tight-binding linear Muffin-Tin Orbital atomic-sphere approximation

2.1 Introduction

Shortly after the discovery of *recoilless nuclear resonance fluorescence of gamma radiation* by Rudolf Mössbauer [1–4], physicists and chemists explored the possibility to use this effect as a basis for a new physical technique in materials science. One of the first publications, by Kistner and Sunyar [5] reported the magnetic hyperfine splitting of α-Fe_2O_3 (Fig. 2.1a). This was the first spectrum of a material that reflected all three types of hyperfine interactions between nuclear moments and electrons penetrating the nucleus that can be observed in a Mössbauer spectrum: the electric monopole interaction resulting in the *isomer shift*, the electric quadrupole interaction causing the *quadrupole splitting* and the magnetic dipole interaction giving rise to *magnetic splitting of degenerate nuclear levels*. These interactions are all taken into account in Fig. 2.1b (middle) in the case of Fe_2O_3, and are compared on the left side of Fig. 2.1b with metallic iron which shows a magnetic splitting only and on the right side with stainless steel that displays an isomer shift only. This report demonstrated the usefulness of the Mössbauer effect as a new spectroscopic technique—Mössbauer spectroscopy—for the non destructive characterization of materials and initiated overwhelming research activities in physics, chemistry, geo- and earth sciences, and even industrial applications.

The purpose of this tutorial lecture is to demonstrate how Mössbauer spectroscopy can help solving chemical problems. There are several thousands of excellent examples that have appeared in the literature since the discovery of the Mössbauer effect [6–17]. Because of limited space we shall present a selection of chemical applications of Mössbauer spectroscopy mainly from our own work dealing with investigations of transition metal compounds featuring:

- Bonding and structural properties
- Valence state
- Solid state reactions
- Electron transfer reactions
- Mixed valency
- Spin crossover
- Magnetic properties

The major part of the chapter will be devoted to the phenomenon of thermally induced spin crossover in iron complex compounds. This research topic has recently gained increasing interest by chemists and physicists for the promising potential of technical applications as devices. It will be demonstrated that Mössbauer spectroscopy, together with magnetic measurements, is particularly suited to follow the electronic structure dynamics of such materials under various conditions.

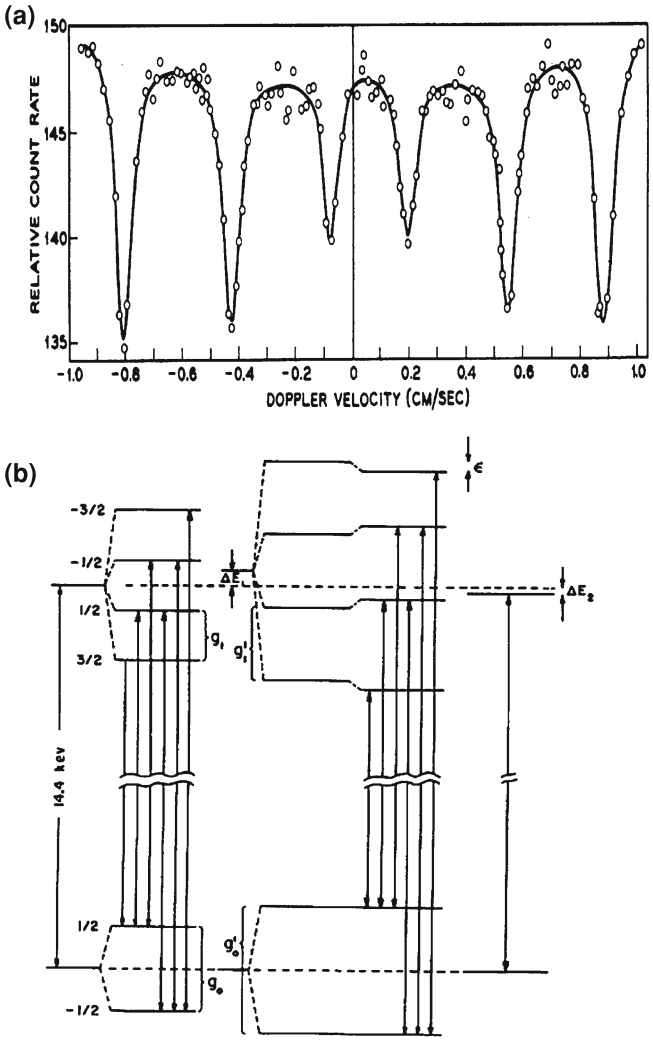

Fig. 2.1 **a** Room temperature Mössbauer spectrum of Fe_2O_3. **b** Schematic representation of the nuclear sub states of the ground and the 14.4 keV excited states of ^{57}Fe bound in metallic iron (*left*), Fe_2O_3 (*middle*) and stainless steel (*right*) [5]

2.2 Hyperfine Interactions and Mössbauer Parameters

Three kinds of hyperfine interactions may be observed in a Mössbauer spectrum:

Electric monopole interaction between protons of the nucleus and electrons (mainly s-electrons) penetrating the nuclear field. The observable Mössbauer parameter is the "isomer shift δ". Isomer shift values give information on the oxidation state, spin state, and bonding properties such as covalency and electronegativity.

Table 2.1 Conditions for hyperfine interactions and resulting Mössbauer parameters

Type of interaction	Nuclear condition	Electronic condition	Consequence
Electric monopole interaction	$R_e^2 \neq R_g^2$	$\|\Psi(0)\|_A^2 \neq \|\Psi(0)\|_S^2$	Different shift of nuclear levels $\Rightarrow$ *Isomer shift* $\boldsymbol{\delta}$
Electric quadrupole interaction	Electric quadrupole moment $eQ \neq 0$ ($I > 1/2$)	$EFG \neq 0$	Nuclear states split into $I + ½$ substates $\|I, \pm m_I>$ (twofold degenerate) $\Rightarrow$ *Quadrupole splitting* $\boldsymbol{\Delta E_Q}$
Magnetic dipole interaction	Magnetic dipole moment $\mu \neq 0$ ($I > 0$)	$H \neq 0$	Nuclear states $\|I>$ split into $2I + 1$ substates $\|I, m_I>$ with $m_I = +I, +I\text{-}1, \ldots, -I$ $\Rightarrow$ *Magnetic dipole splitting* $\boldsymbol{\Delta E_M}$

Electric quadrupole interaction between the nuclear quadrupole moment and an inhomogeneous electric field at the nucleus. The observable Mössbauer parameter is the "quadrupole splitting ΔE_Q". The information derived from the quadrupole splitting refers to oxidation state, spin state and site symmetry.

Magnetic dipole interaction between the nuclear magnetic dipole moment and a magnetic field at the nucleus. The observable Mössbauer parameter is the "magnetic splitting ΔE_M". This quantity gives information on the magnetic properties of the material under study.

The following table summarizes the conditions, regarding the electronic and the nuclear properties, that lead to the three kinds of hyperfine interactions observable in a Mössbauer spectrum (Table 2.1).

2.2.1 Electric Monopole Interaction: Isomer Shift

Electric monopole interaction is the Coulomb interaction between protons of the nucleus and electrons (mainly s-electrons) penetrating the nuclear field. In a typical Mössbauer experiment, the source (S) material (e.g. ^{57}Co embedded in Rh metal) is generally different from the absorber (A) material under study. The nuclear radius in the excited state is different (in the case of ^{57}Fe, it is smaller) than that in the ground state: $R_e \neq R_g$. If the source and absorber materials are different, the electronic densities set up by all s-electrons (1s, 2s, 3s, etc.) of the electronic shells are different at the nuclei of the source and the absorber: $|\Psi(0)|_A^2 \neq |\Psi(0)|_S^2$. The result is that the electric monopole interactions are different in the source and the absorber and therefore affect the nuclear ground and excited state levels to a different extent. This leads to the measured isomer shift δ (see Fig. 2.2).

The isomer shift depends directly on the s-electron densities (as sum of contributions from all s-electron shells), but may be influenced indirectly via shielding

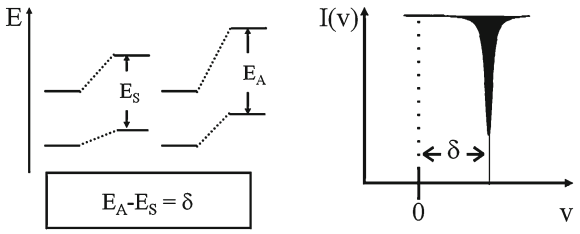

Fig. 2.2 Electric monopole interaction between electrons and protons perturbs the energy levels of the nuclear ground and excited states (with different radii). The energy changes are different in the source (*S*) and absorber (*A*) as a result of different electron densities at the source and absorber nuclei, the result is manifested as isomer shift in the Mössbauer spectrum

effects of p-, d- and f-electrons, which are not capable (if neglecting relativistic effects) of penetrating the nuclear field. Results from Hartree–Fock calculations of the contributions of s-orbitals to the total electron density at the iron nucleus as a function of oxidation state and configuration have shown that (a) nominally the largest contributions originate from the filled 1s and 2s shells (1s $\sim 10^4$ au^{-3}, 2s $\sim 10^3$ au^{-3}, 3s $\sim 10^2$ au^{-3}), and (b) significant changes in the electron densities arise from the noticeably different contributions from the 3s shell populations due to different shielding effects of $3d^n$. The reason becomes apparent on inspecting the strongly overlapping distribution functions of 3s and 3d electrons.

Chemical bonds between metal ion and ligands in coordination compounds can be viewed as the result of the balance between σ-donation (s-electrons from ligands are donated into s-orbitals of the metal) and d_π–p_π back donation (d-electrons move from d-orbitals of the metal to empty π-orbitals of the ligands). Both bonding mechanisms influence the isomer shift in the same direction, but to different extent, depending on the nature of the ligands and thus on the weight of the atomic orbitals of the metal and ligands participating in the molecular orbitals (covalency effects). This is the reason why isomer shift scales for different compounds of the same oxidation state often cover a broad range of values. The most valuable information derived from isomer shift data refers to the valence state of a Mössbauer-active atom embedded in a solid material as shown in Fig. 2.3.

2.2.2 Electric Quadrupole Interaction: Quadrupole Splitting

Electric quadrupole interaction occurs if at least one of the nuclear states involved possesses a quadrupole moment eQ (which is the case for nuclear states with spin $I > 1/2$) and if the electric field at the nucleus is inhomogeneous. In the case of ^{57}Fe the first excited state (14.4 keV state) has spin $I = 3/2$ and therefore also an electric quadrupole moment.

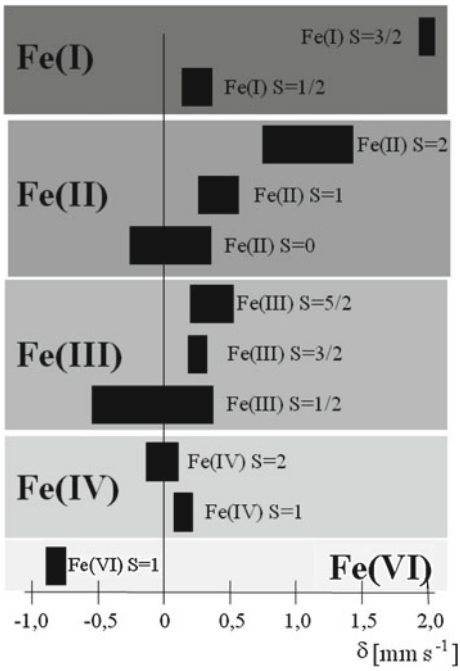

Fig. 2.3 The figure shows ranges of isomer shift values as expected for different oxidation and spin states. The most positive isomer shift occurs with formally Fe^{I} compounds with spin S = 3/2. In this case, the seven d-electrons exert a very strong shielding of the s-electrons towards the nuclear charge, this reduces markedly the s-electron density ρ_A giving a strongly negative quantity $|\Psi(0)|_A^2 \neq |\Psi(0)|_S^2$. As the nuclear factor $(R_e^2 - R_g^2)$ is negative for ^{57}Fe, the measured isomer shift becomes strongly positive. At the other end of the isomer shift scale are strongly negative values expected for formally Fe^{VI} compounds with spin S = 1. The reason is that iron Fe^{VI} compounds have only two d-electrons, the shielding effect for s-electrons is very weak in this case and the s-electron density ρ_A at the nucleus becomes relatively high which—multiplied by the negative nuclear factor $(R_e^2 - R_g^2)$—pushes the isomer shift value strongly in a negative direction. It is seen from the figure that some isomer shift regions do not overlap, e.g. Fe^{II} HS compounds with S = 2 can be easily assigned from a Mössbauer spectrum. In other cases with more or less strong overlapping δ values unambiguous assignment to certain oxidation and spin states may not be possible. In such cases the quadrupole splitting parameter ΔE_Q will be included in the analysis and leads to a conclusive characterization in most cases

If the electric field gradient (EFG) is non-zero, for instance due to a non-cubic valence electron distribution and/or non-cubic lattice site symmetry, electric quadrupole interaction as visualized by the precession of the quadrupole moment vector about the field gradient axis sets in and splits the degenerate $I = 3/2$ level into two substates with magnetic spin quantum numbers $m_I = \pm 3/2$ and $\pm 1/2$ (Fig. 2.4). The energy difference between the two substates ΔE_Q is observed in the spectrum as the separation between the two resonance lines. These two resonance lines in the spectrum refer to the two transitions between the two substates of the

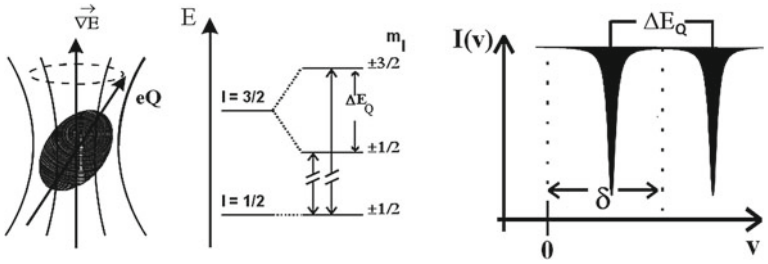

Fig. 2.4 In the case of a non-zero electric field gradient (EFG), electric quadrupole interaction as visualized by the precession of the quadrupole moment vector about the field gradient axis sets in and splits the degenerate I = 3/2 level into two substates with magnetic spin quantum numbers $m_I = \pm 3/2$ and $\pm 1/2$. This gives rise to two transition lines with equal probability (intensity). The energy difference between the two sub states ΔE_Q is observed in the spectrum as the separation between the two resonance lines

split excited state and the unsplit ground state. The ground state with $I = 1/2$ has no quadrupole moment and remains therefore unsplit, but still twofold degenerate. This degeneracy can be lifted by magnetic dipole interaction (Zeeman effect, see below). The same holds for the two substates of the excited $I = 3/2$ level, which are still twofold degenerate after electric quadrupole interaction. This becomes apparent by looking at the expression for the quadrupolar interaction energies E_Q derived from perturbation theory:

$$E_Q(I, m_I) = \left(\frac{eQV_{zz}}{4I(2I-1)}\right)\left[3m_I^2 - I(I+1)\right] \quad (\text{for axial symmetry}).$$

For ^{57}Fe Mössbauer spectroscopy, electric quadrupole interaction in the absence of magnetic dipole interaction leads to a doublet, the separation of the two resonance lines giving the quadrupole interaction energy ΔE_Q which is proportional to the quadrupole moment eQ and the electric field gradient. The electric field E at the nucleus is the negative gradient of the potential, $-\nabla V$, and the electric field gradient EFG is given by the nine components $V_{ij} = \left(\partial^2 V/\partial i \partial j\right)$ $(i, j = x, y, z)$ of the 3×3s rank EFG tensor. Only five of these components are independent because of the symmetric form of the tensor, i.e. $V_{ij} = V_{ji}$ and because of Laplace's equation which requires that the tensor be traceless: $\nabla V_{ii} = 0$. In the principal axes system the off-diagonal elements vanish, and for axial symmetry (fourfold or threefold axis of symmetry passing through the Mössbauer nucleus yielding $V_{xx} = V_{yy}$) the EFG is then solely given by the tensor component V_{zz}. For non-axial symmetry the asymmetry parameter $\eta = (V_{xx} - V_{yy})/V_{zz}$ is required in addition. When choosing the principal axes ordering such that $V_{zz} \geq V_{xx} \geq V_{yy}$, the asymmetry parameter range becomes $0 \leq \eta \leq 1$.

In principle, there are two sources which can contribute to the total EFG: (1) charges (or dipoles) on distant ions surrounding the Mössbauer atom in non-cubic symmetry, usually termed *lattice contribution* to the EFG; (2) anisotropic (non-cubic) electron distribution in the valence shell of the Mössbauer atom, usually

called *valence electron contribution* to the EFG. The latter comes about mainly in two ways: (1) Anisotropic population of the metal d-orbitals visualized in the frame of simple crystal field theory with axial distortion to molecular symmetry lower than O_h (an example is given below); (2) anisotropic covalency effects in molecular orbitals between the metal center and ligands with different σ-bonding and π-back bonding capability. It is understood that both sources of valence electron contributions are jointly operative and cannot be separated.

The electric quadrupole splitting gives information on the oxidation state, the spin state and the local symmetry of the Mössbauer atom. Note that the isomer shift parameter δ is given by the distance of the barycenter of the quadrupole doublet from zero Doppler velocity (Fig. 2.4).

2.2.3 Magnetic Dipole Interaction: Magnetic Splitting (Nuclear Zeeman Effect)

The requirements for magnetic dipole interaction (nuclear Zeeman effect) to be observed are that (1) the nuclear states involved must possess a magnetic dipole moment and (2) a magnetic field must be present at the nucleus. A nuclear state with spin $I > 1/2$ possesses a magnetic dipole moment μ. This is the case for both the ground state with $I = 1/2$ and the first excited state with $I = 3/2$ of ^{57}Fe. Magnetic dipole interaction (visualized as the precession of the magnetic dipole moment vector about the axis of the magnetic field; Fig. 2.5) leads to splitting of the states $|I, m_I>$ into $2I + 1$ substates characterized by the magnetic spin quantum numbers m_I. Thus the excited state with $I = 3/2$ is split into four, and the ground state with $I = 1/2$ into two substates. These substates are no longer degenerate. The energies of the sublevels are given from first-order perturbation theory by

$$E_M(m_I) = -\mu B m_I / I = -g_N \beta_N B m_I,$$

where g_N is the nuclear Landé factor and β_N the nuclear Bohr magneton. Note that the sign of the magnetic spin quantum numbers m_I of the sublevels have a different

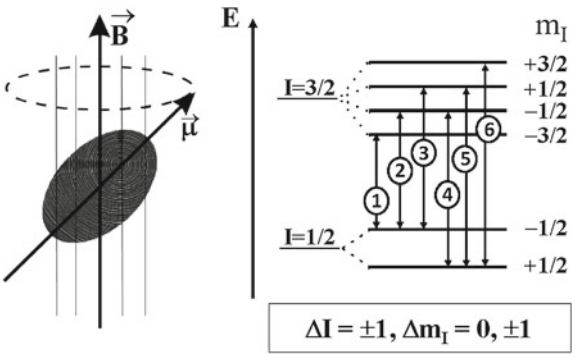

Fig. 2.5 Magnetic dipole interaction (visualized as the precession of the magnetic dipole moment vector about the axis of the magnetic field) leads to splitting of the states $|I, m_I>$ into $2I + 1$ substates characterized by the magnetic spin quantum numbers m_I

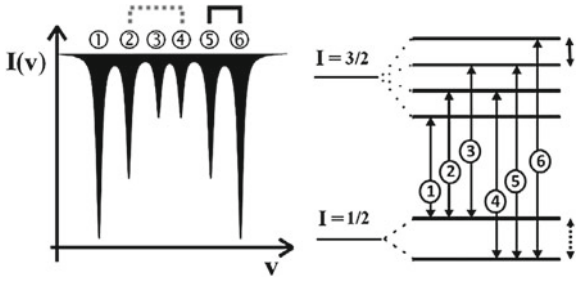

Fig. 2.6 Typical ^{57}Fe Mössbauer spectrum resulting from magnetic dipole interaction. The energies of the ground and excited state splitting can be determined as depicted in the figure and described in the text

sequence in the excited state and the ground state, this being due to the different signs of the magnetic moments of the two states. The allowed gamma transitions between the sublevels of the excited state and those of the ground state are given by the selection rules for magnetic dipole transitions: $\Delta I = \pm 1$, $\Delta m_I = 0, \pm 1$. The six allowed transitions in the case of ^{57}Fe are shown in Figs. 2.5 and 2.6.

The separation between the lines 2 and 4 (also between 3 and 5) refers to the magnetic dipole splitting of the ground state. The separation between lines 5 and 6 (also between 1 and 2, 2 and 3, 4 and 5) refers to the magnetic dipole splitting of the excited $I = 3/2$ state (Fig. 2.6). The magnetic hyperfine splitting enables one to determine the effective magnetic field (size and direction) acting at the nucleus. Such a field can be externally applied. But many substances can also create a magnetic field of their own through various mechanisms, e.g.:

- The *Fermi contact field* B_C arises from a net spin-up or spin-down s-electron density at the nucleus as a consequence of spin polarization of inner filled s-shells by spin-polarized partially filled outer shells;
- a contribution B_L may arise from the *orbital motion* of valence electrons with the orbital momentum quantum number L;
- a contribution B_D, called *spin-dipolar field*, may arise from the total electron spin of the atom under consideration.

All contributions may be present and add to the total effective magnetic field $B_{\mathrm{eff}} = B_{\mathrm{C}} + B_{\mathrm{L}} + B_{\mathrm{D}}$. By applying an external magnetic field of known size and direction one can determine the size and the direction of the intrinsic effective magnetic field B_{eff} of the material under investigation.

Magnetic dipole interaction and electric quadrupole interaction may be present in a material simultaneously (together with the electric monopole interaction which is always present). The perturbations are treated depending on their relative strengths. In the case of relatively weak quadrupole interaction the nuclear sublevels $|I, m_I>$ arising from magnetic dipole splitting are additionally shifted by the quadrupole interaction energies $E_Q(I, m_I)$; as a result, the sublevels of the excited $I = 3/2$ state are no longer equally spaced. The shifts by E_Q are upwards or downwards depending on the direction of the EFG. This enables one to determine the sign of the quadrupole splitting parameter ΔE_Q (Fig. 2.7).

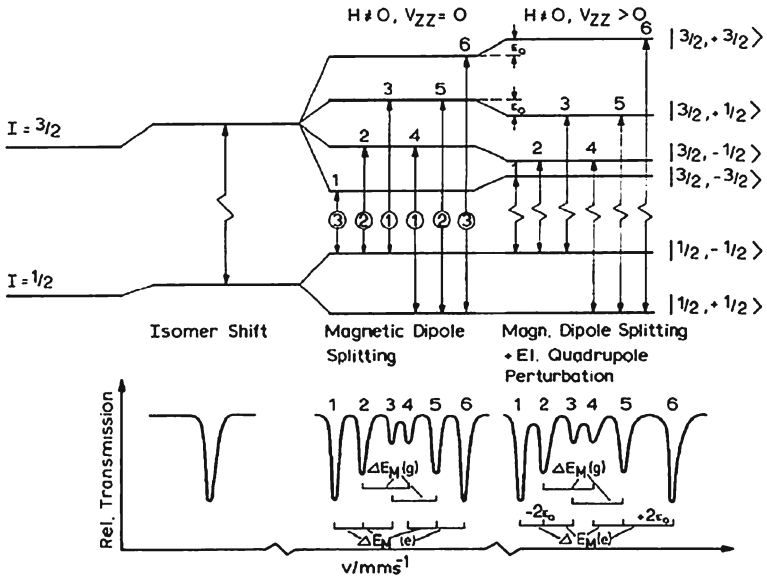

Fig. 2.7 Nuclear energy level scheme (^{57}Fe) for electric monopole interaction (causing the isomer *shift*, *left*), pure magnetic dipole interaction (causing magnetic *splitting*, *middle*), and combined magnetic dipole interaction and electric quadrupole interaction (*right*)

2.3 Selected Applications

2.3.1 Basic Information on Structure and Bonding

2.3.1.1 Quadrupole Splitting in Three Typical Fe^{II} Compounds

Figure 2.8 shows the Mössbauer spectra of three selected Fe^{II} compounds.

Ferrous sulphate, formulated as $[Fe(H_2O)_6]SO_4{\cdot}H_2O$, is a high-spin (HS) compound with spin $S = 2$ and shows a large quadrupole splitting of ca. 3 mm s^{-1}. $K_4[Fe(CN)_6]$ is a low-spin (LS) compound with $S = 0$ and cubic (O_h) molecular symmetry and shows no quadrupole splitting. $Na_2[Fe(CN)_5NO]$ is also LS with $S = 0$, but strong tetragonal distortion from O_h symmetry due to the replacement of one of the six CN^- ligands by NO, gives rise to a significant quadrupole splitting. The occurrence of quadrupole splitting in $[Fe(H_2O)_6]$-$SO_4{\cdot}H_2O$ and $Na_2[Fe(CN)_5NO]{\cdot}2H_2O$ and the absence of it in $K_4[Fe(CN)_6]$ are explained in Figs. 2.9 and 2.10.

For HS Fe^{II} with $3d^6$ electron configuration, the six 3d electrons are distributed under O_h symmetry as shown in Fig. 2.9 (left). The two degenerate e_g orbitals carry one electron each, and the three degenerate t_{2g} orbitals are occupied by $1^{1/3}$ electrons on average. As the t_{2g} and e_g orbitals are cubic subgroups, there is no valence electron contribution to the EFG independent of the number of electrons

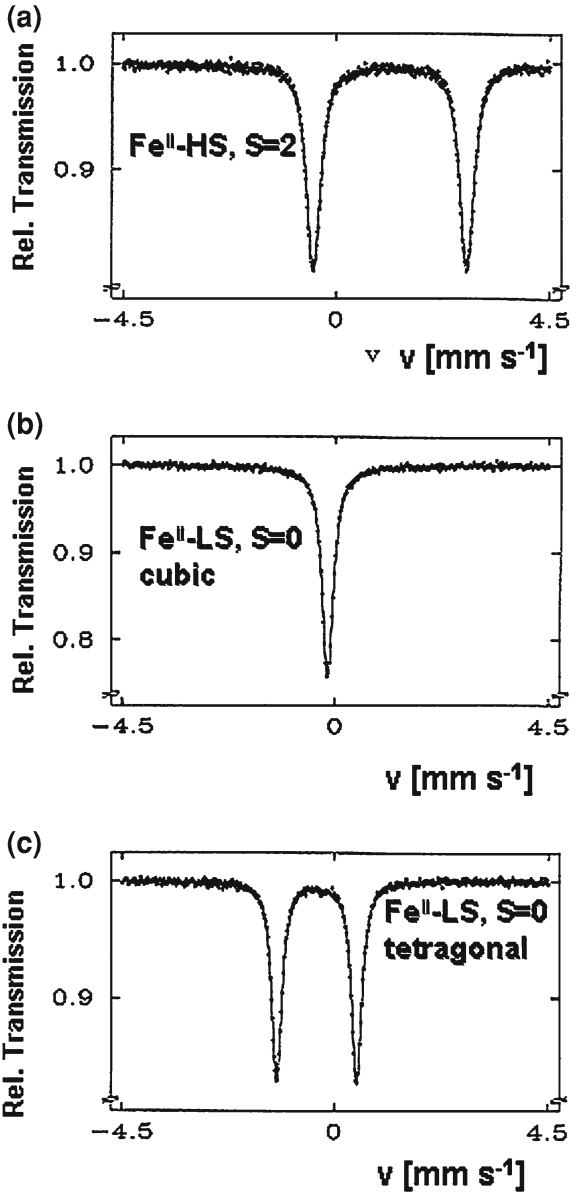

Fig. 2.8 Mössbauer spectra of three selected Fe^{II} compounds. The occurrence of quadrupole splitting in $[Fe(H_2O)_6]SO_4 \cdot H_2O$ (*A*) and $Na_2[Fe(CN)_5NO] \cdot 2H_2O$ (*C*) and the absence of it in $K_4[Fe(CN)_6]$ (*B*) are explained in the text in connection with Figs. 2.9 and 2.10

occupying them. There is also no lattice contribution to the EFG arising from the coordination sphere of six identical H_2O ligands arranged with O_h symmetry. Thus, there is no quadrupole splitting expected under O_h symmetry. $[Fe(H_2O)_6]^{2+}$, however, is a "Jahn–Teller-active" complex ion. It is unstable under O_h symmetry. It undergoes axial distortion with symmetry lowering to (e.g.) D_{4h} as schematized in Fig. 2.9 (right), either compressing or elongating the octahedron in z-direction.

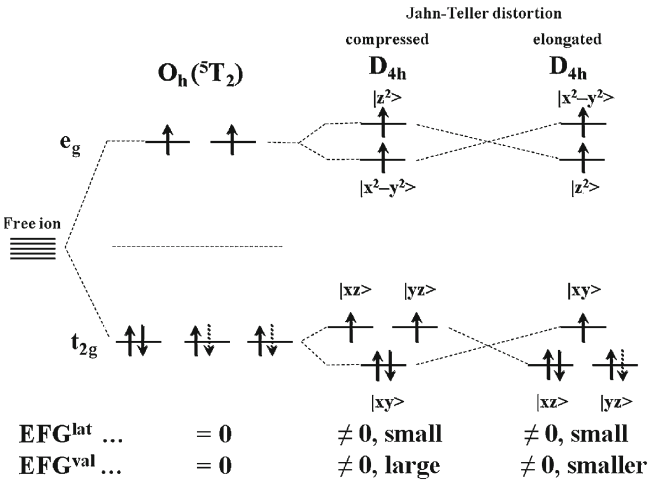

Fig. 2.9 Quadrupole splitting in the HS $[Fe(H_2O)_6]^{2+}$ complex ion arises from a non-cubic valence electron distribution due to Jahn–Teller distortion with lowering of symmetry from O_h (EFG = 0) to D_{4h} with valence electron population in a compressed octahedron as shown in the figure and described in the text

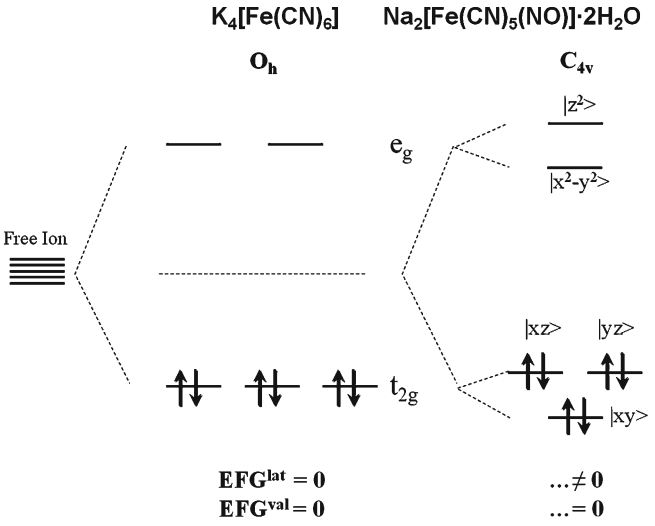

Fig. 2.10 $K_4[Fe(CN)_6]$ is a $3d^6$ LS complex with O_h symmetry, where all six electrons are accommodated in the three t_{2g} orbitals. Both contributions $(EFG)^{val}$ and $(EFG)^{lat}$ vanish; there is no quadrupolar interaction. $Na_2[Fe(CN)_5NO]\cdot 2H_2O$ has C_{4v} symmetry with d-orbital splitting as shown on the right. Its LS behavior requires that all six electrons are accommodated in the lowest three orbitals arising from the tetragonal splitting of the former cubic t_{2g} (O_h) subgroup. $(EFG)^{val}$ is still zero, but $(EFG)^{lat} \neq 0$ arises from the ligand replacement in he iron coordination sphere

Compression is preferred because in this case the ground state is an orbital singlet with the doubly occupied xy orbital being lowest in energy. Suppose all d-orbitals are singly occupied, as for instance in the case of $\left[Fe(H_2O)_6\right]^{3+}$(HS), $(EFG)^{val}$ would be zero. But the sixth electron placed in the lowest xy orbital in the case of $\left[Fe(H_2O)_6\right]^{2+}$ accumulates more charge in the xy plane than along the z-axis and, thus, causes a large $(EFG)^{val} \neq 0$ and the observed quadrupole splitting.

2.3.1.2 Structure of $Fe_3(CO)_{12}$

On the basis of single crystal X-ray diffraction measurement three possible molecular structures had been suggested for the metalorganic compound $Fe_3(CO)_{12}$ [18]. In all cases the iron atoms form a triangle, but with different surroundings by the CO groups. In the upper two structures of Fig. 2.11 the three iron atoms have identical surroundings, the Mössbauer spectrum is expected to show only one type of resonance signal. The lower structure has two identical iron positions and a different one for the third iron atom. In this case the Mössbauer spectrum is expected to show two different types of resonance signals with an area ratio of 2:1. A Mössbauer effect study performed by Greatrex and Greenwood in 1969 [19] indeed showed two types of resonance signals, a quadrupole doublet A and a singlet B with an area ratio of 2:1 confirming the presence of two types of iron positions in $Fe_3(CO)_{12}$ (Fig. 2.11).

2.3.1.3 Effect of π-Backdonation in $\left[Fe(CN)_5X^{n-}\right]^{(3+n)-}$

The following example demonstrates that Mössbauer spectroscopy can help to characterize chemical bond properties. Taking from the literature [7] the isomer shift data for the pentacyano complexes of Fe^{II} with a different sixth ligand X and normalizing the isomer shifts to that of the pentacyanonitrosylferrate complex as

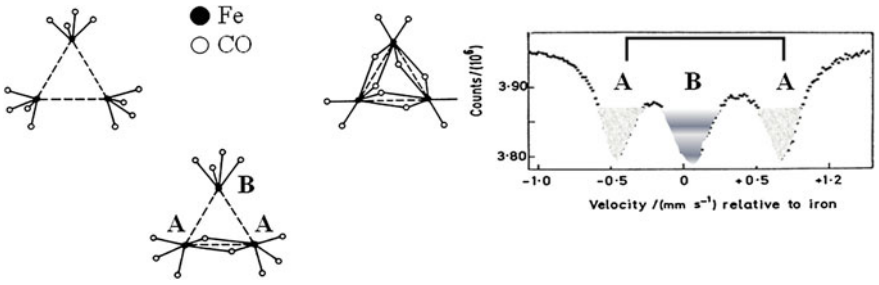

Fig. 2.11 The Mössbauer spectrum of $Fe_3(CO)_{12}$ shows a quadrupole doublet *A* and a singlet *B* with area ratio 2:1, which confirms that the structure with two inequivalent lattice sites of iron, *A* and *B*, is the correct structure [19]

Table 2.2 Effect of π-back donation in $[Fe(CN)_5X^{n-}]^{(3+n)-}$

Ligand X	δ/mm s^{-1}	$d_\pi \rightarrow p_\pi$	d-shield	ρ(0)
NO^+	0.00	↑	↓	↑
CO	+0.15			
SO_3^{2-}	+0.22			
$P(C_6H_5)_3$	+0.23			
NO_2^-	+0.26			
$Sb(C_6H_5)_3$	+0.26			
NH_3	+0.26			
$As(C_6H_5)_3$	+0.29			
H_2O	+0.31	$\delta \sim \rho(0)\frac{\Delta R}{R}$		$^{57}Fe: \frac{\Delta R}{R} < 0$

zero point, one finds the ordering given in Table 2.2 which expresses the varying effects of d_π–p_π *backdonation* for the different sixth ligand X.

The isomer shift values become more positive on going from NO^+ to H_2O. The reason is that in the same ordering the strength of d_π–p_π *back donation* decreases causing an increasing d-electron density residing near the iron center and thus effecting stronger shielding of s-electrons by d-electrons, which finally creates lower s-electron density at the nucleus in the case of H_2O as compared to NO^+. The fact that the nuclear factor $\Delta R/R$ is negative for ^{57}Fe explains the increasingly positive isomer shift values in the given sequence from NO^+ to H_2O.

2.3.1.4 Effect of Ligand Electronegativity

In Fig. 2.12 isomer shift values of ferrous halides taken from the literature [7] are plotted as a function of Pauling electronegativity values. The electronegativity

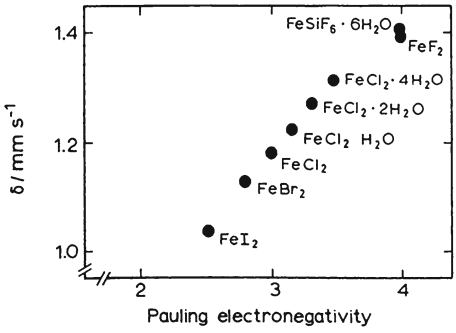

Fig. 2.12 The graph shows the influence of electronegativity on the isomer shift of ferrous halides. The electronegativity increases from iodine to fluorine. In the same ordering the 4s electron population decreases and as a direct consequence the s-electron density at the iron nucleus decreases, and due to the fact that $(R_a^2 - R_g^2) < 0$ for ^{57}Fe the isomer shift increases from iodide to fluoride

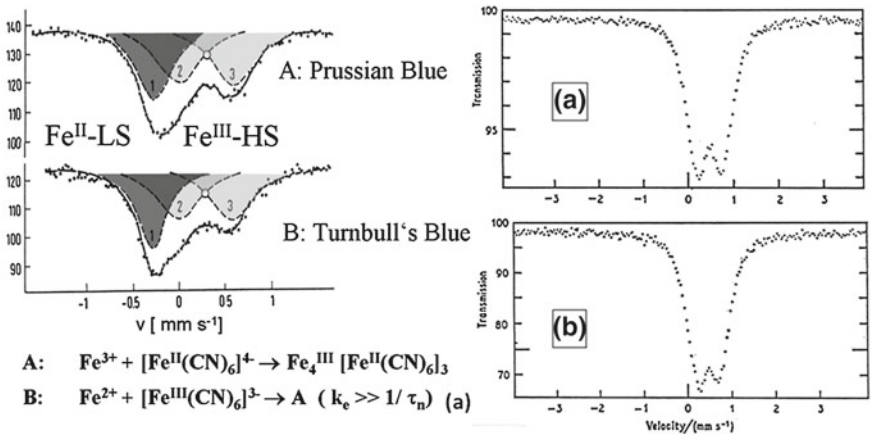

Fig. 2.13 **a** Mössbauer spectra of Prussian blue and Turnbull's Blue [21]. **b** Mössbauer spectra (77 K) of "Prussian Blue" prepared from (*A*) $^{57}Fe_2^{III}(SO_4)_3$ (enriched) + $K_4[Fe^{II}(CN)_6]$ (unenriched) and (*B*) $^{57}Fe^{II}Cl_2$ (enriched) + $K_3[Fe^{III}(CN)_6]$ (unenriched) [22]. The spectra *A* and *B* are identical and are indicative of the Fe^{III} cation outside the hexacyano complex. This confirms the occurrence of fast electron transfer in preparation *B*

increases from iodine to fluorine. In the same ordering the 4s electron population decreases and as a direct consequence the s-electron density at the iron nucleus decreases, and due to the fact that $\left(R_a^2 - R_g^2\right) < 0$ for ^{57}Fe the isomer shift increases from iodide to fluoride.

2.3.1.5 Prussian Blue vs. Turnbull's Blue

It has been stated in old textbooks of inorganic chemistry and hence it was recognized for many years that Prussian Blue and Turnbull's blue are different substances depending on their synthetic pathways [20]. However, a Mössbauer experiment originally performed by Fluck et al. [21] has demonstrated that the two end products prepared in different ways are chemically identical. In preparation A they prepared Prussian Blue, $Fe_4^{III}\left[Fe^{II}(CN)_6\right]_3$, by mixing equivalent amounts of ionic Fe^{III} and $\left[Fe^{II}(CN)_6\right]^{4-}$. Their Mössbauer spectrum shown in Fig. 2.13a reveals a singlet (dark grey) attributed to LS Fe^{II} ions and a quadrupole doublet (light grey) attributed to HS Fe^{III} ions. In preparation B, they mixed ionic Fe^{II} with $\left[Fe^{III}(CN)_6\right]^{3-}$ and also obtained $Fe_4^{III}\left[Fe^{II}(CN)_6\right]_3$ as shown in the Mössbauer spectrum (Fig. 2.13a). Indeed, a fast electron transfer occurs from Fe^{II} to Fe^{III} during mixing the two components, the rate constant for electron transfer being

$k_e \gg 1/\tau_n$, where τ_n is the lifetime of the 14.4 keV state of ^{57}Fe. This experiment was elegantly confirmed a few years later by Maer et al. (Fig. 2.13b) [22].

2.3.2 Switchable Molecules: Spin Crossover

2.3.2.1 Thermally Induced Spin State Switching in Fe^{II} Compounds

Thermally induced spin state transition from a HS state with maximum unpaired electrons to a LS state with minimum unpaired electrons can be encountered in certain transition metal compounds with d^4 up to d^7 electron configurations. Scheme 2.1 sketches the phenomenon in the case of Fe^{II} compounds with six valence electrons in the 3d shell. In Fe^{II} compounds with relatively weak ligands coordinated to the iron ions, e.g. water molecules, the 3d electrons are accommodated spin-free according to Hund's rule of maximum spin of $S = 2$. Such compounds, called *HS complexes*, are paramagnetic and are generally weakly colored. In Fe^{II} compounds with relatively strong ligands like CN^- ions, the six electrons are arranged spin-paired with total spin $S = 0$. Such compounds are called *LS complexes*; they are generally diamagnetic and often colored. If the right kinds of ligands are chosen, e.g. derivatives of tetrazole or triazole, one may observe spin state transition solely by varying the temperature, applying pressure or under irradiation with light [23–25].

Thermally induced spin crossover (SCO) in Fe^{II} compounds is reflected by changes in the electron configuration. In the notation of ligand field theoretical

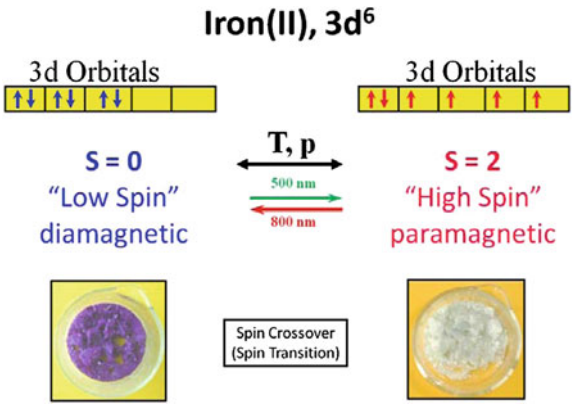

Scheme 2.1 Classification and physical properties of octahedral Fe^{II} coordination compounds. Most of them (an estimate of >95 %) show either HS or LS behavior depending on the ligand field strength set up at the metal center by the coordinated ligand molecules. Less than 5 % (about 200 as a rough estimate), mainly those with FeN_6 core, exhibit thermally induced spin crossover. Spin crossover is also possible by application of pressure and irradiation with light

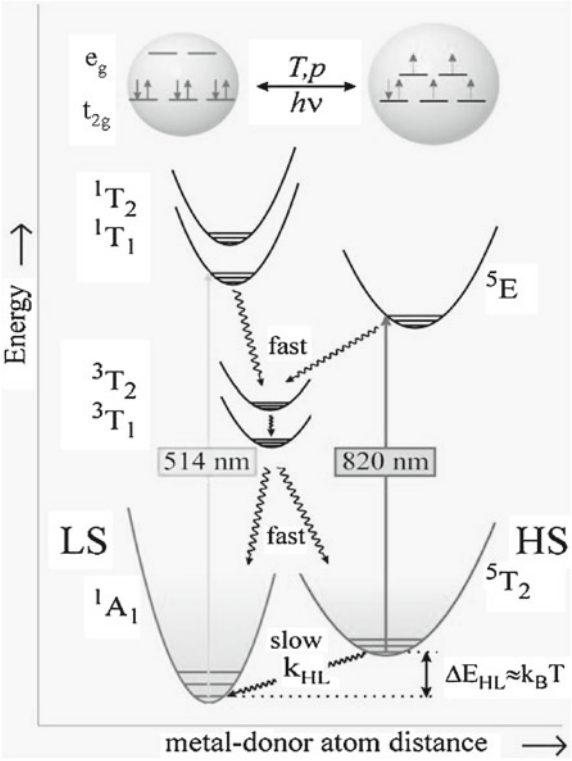

Fig. 2.14 Jablonski diagram depicting potential wells of the LS and HS sates for an Fe^{II} complex, illustrating the LIESST and reverse-LIESST mechanism. These phenomena refer to the possibility to reversibly address spin states of Fe^{II} complexes by light irradiation

concepts, the electron configuration changes from $(t_{2g})^4(e_g)^2$ in the HS state to $(t_{2g})^6$ in the LS state. This phase transition between paramagnetic and (nearly) diamagnetic is easily detected by magnetic susceptibility measurements. As the color changes simultaneously, too, the transition from one spin state to the other is also easily detected by optical means. The spin transition (ST) can also be afforded by applying external pressure, magnetic field or by irradiating the material with light, where green light converts the LS to the HS state and red light the HS to the LS state. This has become known as Light-Induced Excited Spin State Trapping (LIESST) and reverse-LIESST [26].

The condition that has to be met in order to observe thermal SCO is sketched in Fig. 2.14 using the term symbols known from ligand field theory. Thermal SCO may be observed if the ligand field strength of an Fe^{II} compound is such that the difference between the lowest "vibronic" energy levels of the HS state $^5T_2$ and the LS state $^1A_1$ state is comparable with thermal energy k_BT (k_B = Boltzmann constant). The ST behavior can be influenced by chemical alteration of the material, e.g. ligand replacement, change of non-coordinating anion and solvent molecule, substitution of spin state changing metal by another metal (e.g. iron by zinc). For a comprehensive coverage of chemical and physical influences on the ST behavior see Refs. [23–25].

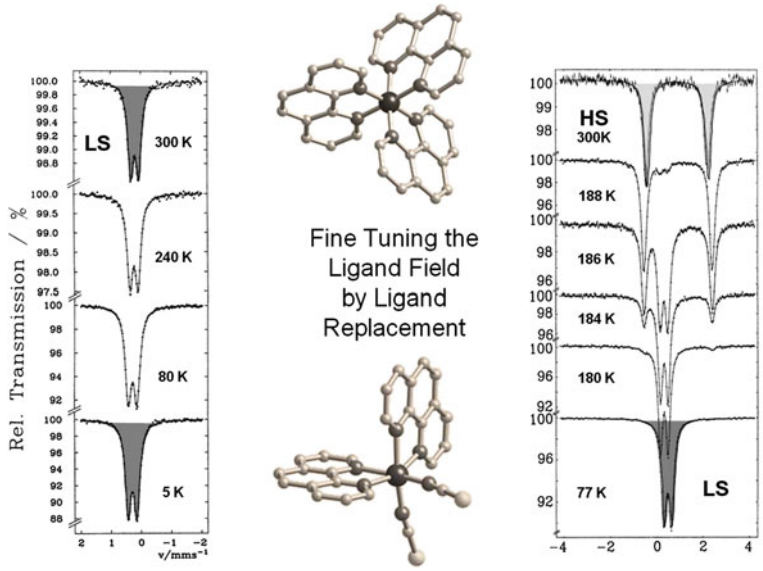

Fig. 2.15 $[Fe^{II}(phen)_3]X_2$ (phen = 1,10-phenanthroline) is a typical LS compound with characteristic Mössbauer spectra shown on the *left*. If one of the relatively strong phen ligands is replaced by two monofunctional NCS^- groups, the average ligand field strength becomes weaker such that now the condition for thermally induced SCO, viz. $\Delta E_{HL} \approx k_B T$ is met and the compound $[Fe^{II}(phen)_2(NCS)_2]$ adopts HS character at room temperature. The temperature dependent Mössbauer spectra shown on the *right* confirm that $[Fe^{II}(phen)_2(NCS)_2]$ undergoes ST between S = 2 and S = 0 near 180 K

The influence of the ligand molecules on the spin state of the central Fe^{II} ions is demonstrated with the two examples and their temperature dependent Mössbauer spectra shown in Fig. 2.15. $\left[Fe^{II}(phen)_3\right]X_2$ (phen = 1,10-phenanthroline) is a typical LS compound at all temperatures under study as confirmed by the characteristic Mössbauer spectra on the left with isomer shift of ca. 0.2 and quadrupole splitting ca. 0.5 mm s^{-1} independent of temperature. If one of the relatively strong phen ligands, which occupies two coordination positions of the octahedron, is replaced by two monofunctional isothiocyanato groups, the average ligand field strength becomes weaker than the mean spin pairing energy and the compound $\left[Fe^{II}(phen)_2(NCS)_2\right]$ adopts HS character at room temperature. The Mössbauer spectrum at 300 K shows the typical features of an Fe^{II} HS compound with isomer shift of ca. 1 mm s^{-1} and a large quadrupole splitting of ca. 3 mm s^{-1}. However, the compound $\left[Fe^{II}(phen)_2(NCS)_2\right]$ fulfils the condition for thermal SCO to occur, viz. $\Delta E_{HL} \approx k_B T$. As the temperature is lowered, the compound changes spin state from HS to LS near 180 K as is well documented by the Mössbauer spectra as a function of temperature on the right hand side of Fig. 2.15, which was first reported by Dezsi et al. in 1967 [27]. Since then more than 200 SCO compounds of Fe^{II} and Fe^{III} have been studied by Mössbauer spectroscopy (see e.g. [25]).

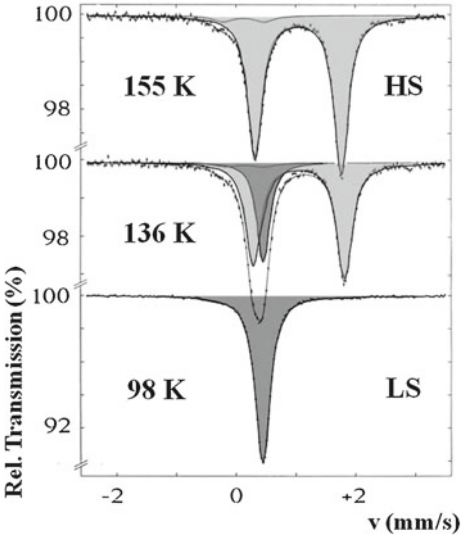

Fig. 2.16 The variable temperature ^{57}Fe Mössbauer spectra of $[Fe(ptz)_6](BF_4)_2$, reveals a thermally induced SCO with a transition temperature on warming $T^{\uparrow}_{1/2}$ of ca. 135 K. Above this temperature the spectra show a quadrupole doublet characteristic for the HS state of Fe^{II}. Near the transition temperature the quadrupole doublet disappears on further cooling at the favor of a singlet which is typical of the LS state [28]

$[Fe(ptz)_6](BF_4)_2$ (ptz = 1-propyl-tetrazole), is another model Fe^{II} coordination compound exhibiting thermal SCO with a transition temperature on warming $T^{\uparrow}_{1/2}$ of ca. 135 K. The ^{57}Fe Mössbauer spectra of Fig. 2.16, recorded on warming from 98 K, clearly confirm the transition at this temperature between the LS phase (singlet shown in dark grey) and the HS phase (quadrupole doublet shown in grey).

2.3.2.2 Light Induced Spin State Switching

With $[Fe(ptz)_6](BF_4)_2$ it was observed for the first time that the ST can also be induced by irradiating the crystals with light; green light converts the LS state to the HS state, which can have very long lifetimes, e.g. on the order of days at temperatures below ca. 20 K [26]. Figure 2.17 shows a single crystal of $[Fe(ptz)_6](BF_4)_2$ (size ca. 3×3 cm^2), which is colorless at room temperature. The absorption spectrum shows only a weak absorption band at ca. 12,000 cm^{-1}. At 80 K the crystal has changed totally to the LS state by thermal SCO and is now red and absorbs relatively strongly at 18,000 and 26,000 cm^{-1}. Irradiating the crystal at ca. 10 K converts the LS state to the metastable HS state. The optical spectrum of the white spot (ca. 1 mm in diameter) is practically identical to the one recorded at 300 K.

Mössbauer spectroscopy is ideally suited to follow the light-induced spin state conversion in $[Fe(ptz)_6]BF_4)_2$ as exemplified in Fig. 2.18. A polycrystalline sample of $[Fe(ptz)_6](BF_4)_2$ was cooled to 15 K. Before irradiation, the sample is in the LS state and shows the typical Mössbauer spectrum of Fe^{II}-LS (upper left). After irradiating with green light (Xe lamp with filters or 514 nm band of an Ar ion laser) at 15 K the sample is quantitatively converted to the metastable HS state (middle left). The asymmetry in the intensity of the two components of the

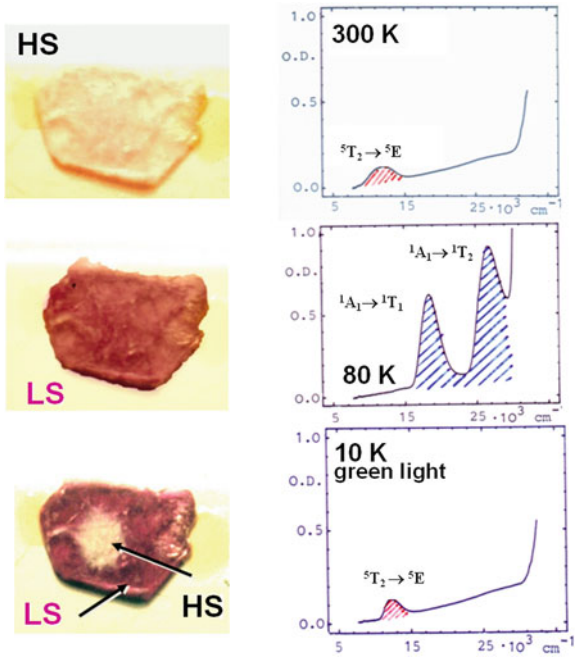

Fig. 2.17 A single crystal of $[Fe(ptz)_6](BF_4)_2$ (size ca. 3×3 cm^2) is colorless at room temperature. The absorption spectrum shows only a weak absorption band at ca. 12,000 cm^{-1}. At 80 K the crystal has changed totally to the LS state by thermal SCO and is now *red* and absorbs relatively strongly at 18,000 and 26,000 cm^{-1}. Irradiating the crystal at ca. 10 K converts the LS state to the metastable HS state. The optical spectrum of the white spot (ca. 1 mm in diameter) is practically identical to the one recorded at 300 K

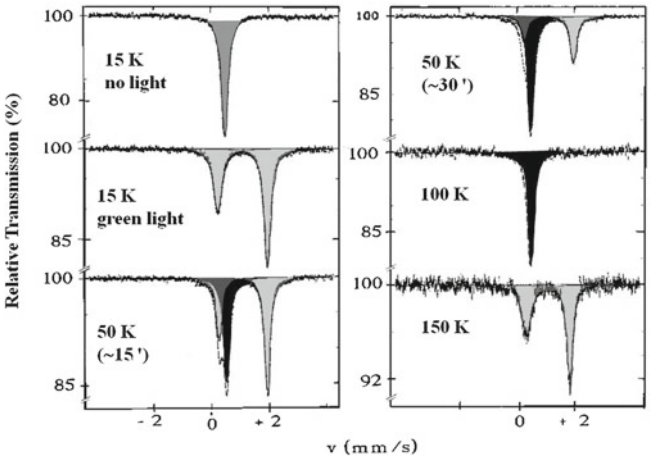

Fig. 2.18 Light induced spin state switching in $[Fe(ptz)_6](BF_4)_2$ followed by ^{57}Fe Mössbauer spectroscopy [26]

quadrupole doublet is due to the plate-like shape of the crystals (texture effect). Thermal relaxation on a 15 min-timescale sets in at 50 K (lower left and upper right: the sample was heated for 15 min at 50 K and then cooled to the measuring temperature of 15 K in two runs). Thermal relaxation to the stable LS state is

complete at 100 K. On further heating to 150 K the sample undergoes again thermal ST at 135 K to the (now stable) HS state.

This photophysical phenomenon has become known as LIESST. The processes involved in the LIESST effect are well understood on the basis of ligand field theory [23, 24]. Figure 2.14 explains the mechanisms of LIESST and reverse-LIESST. The energy level scheme shows in the uppermost part the distribution of the six valence electrons of Fe^{II} over the five d-orbitals split in an octahedral ligand field into the subgroups t_{2g} and $e._g$ resulting in the two spin states LS (left) and HS (right). The corresponding energy potentials are drawn in the lower part of the scheme. The complex molecules in the HS state are bigger than those in the LS state due to the fact that the antibonding e_g orbitals are partially occupied in the HS state, whereas in the LS state they are empty. Thus the HS potentials are placed in positions of larger metal-donor atom distances as compared to the LS potentials.

Green light (514 nm) excites the LS state ($^1A_1$) to the $^1T_1$ and $^1T_2$ states (spin-allowed, but parity-forbidden), which decay fast via the spin triplet states $^3T_{1,2}$ to the $^5T_2$ state. This double intersystem crossing decay path is favored by spin–orbit coupling over the direct decay path back to $^1A_1$. Decay of the $^5T_2$ state to the $^1A_1$ state is forbidden, the metastable HS state is trapped until radiationless thermal relaxation sets in by nonadiabatic multiphoton processes [23, 24]. Light-induced back conversion of the metastable LIESST state is possible by irradiating the sample with red light, thereby undergoing again double intersystem crossing processes similar to the LS to HS conversion with green light (reverse-LIESST) [29].

Replacing propyl by methyl in the tetrazole molecule yields $[Fe(mtz)_6](BF_4)_2$ with mtz = 1-methyl-1H-tetrazole which undergoes thermal ST around 74 K. The crystal structure at room temperature shows two lattice sites called A and B that only differ slightly by their Fe–N bond lengths (Fig. 2.19a) [30]. Mössbauer spectroscopy between room temperature and 160 K shows only one HS site. However, on further cooling, two sites with equal population become clearly distinguishable. Upon cooling to 60 K, the HS quadrupole doublet (green) attributed to B is not affected. However, a new signal (blue) appears at 85 K which is characteristics of the LS state indicating a SCO of the A site. At 60 K, the transition of the A site ions is complete while the B site ions fully remain in the HS state with ca. 50 % population evaluated from the resonance area fractions assuming equal Lamb-Mössbauer factors for both HS and LS states of Fe^{II} (Fig. 2.19b).

The $[Fe(mtz)_6](BF_4)_2$ compound with thermal ST at A site ions but HS behavior at B site ions is an interesting case for LIESST effect studies (Fig. 2.20). When the sample is irradiated with green light at 20 K, where all A site ions have turned to the LS state but all B site ions are still in the HS state, a complete LS(A) → HS(A) photo-conversion is observed. At around 65 K, thermal relaxation back to the LS state is observed for the A site ions. When the sample is irradiated with red light at 20 K, the signal corresponding to B site ions disappears almost totally, and a new resonance signal appears which is characteristic for Fe^{II} ions in the LS state. This is the first observation of a light induced excitation of a stable HS state into a long lived metastable LS state. Again, upon warming to ca. 65 K, complete thermal relaxation is observed back to the stable HS(B) state [31].

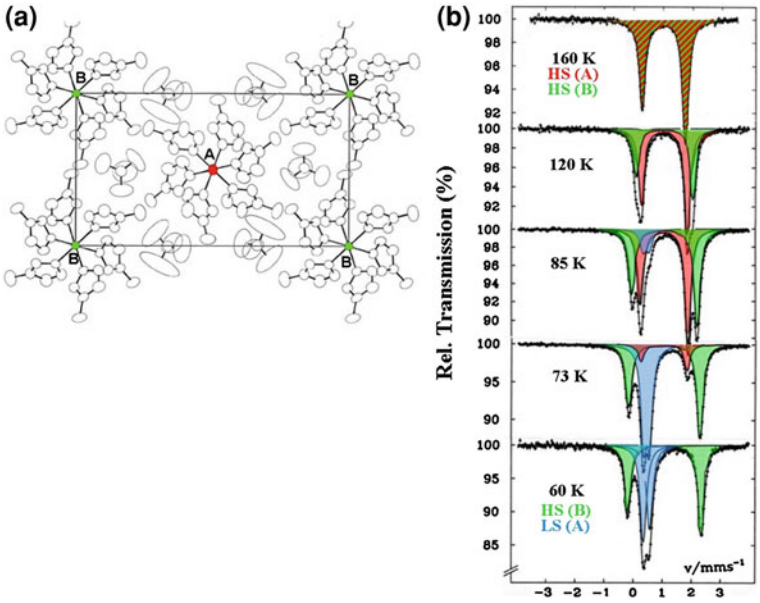

Fig. 2.19 **a** View of the crystal structure of $[Fe(mtz)_6](BF_4)_2$ showing two lattice sites, *A* and *B* at 300 K occupied by Fe^{II} ions in the HS state with metal to ligand bond distances Fe(A) − N = 2.181(5), 2.181(5), 2.181(7) Å and Fe(B)-N = 2.161(5), 2.197(5), 2.207(4) Å [30]. **b** Temperature dependent Mössbauer spectra of $[Fe(mtz)_6](BF_4)_2$ over the temperature range 160–60 K [31]. From room temperature down to ca. 160 K, only one quadrupole doublet arising from iron(II) ions in HS(A) and HS(B) state is observed, i.e. *A* and *B* site ions are not distinguishable in the Mössbauer spectrum. On further cooling, the *A* site ions undergo HS to LS transition whereas the *B* site ions remain in the HS state at all temperatures under study

2.3.2.3 Mechanism of Spin State Switching in Fe^{II} Dinuclear Compounds

The dinuclear Fe^{II} compound $[Fe(bpym)(NCS)_2]_2bpym$ (bpym = bipyrimidine) belongs to a family of materials that can combine both antiferromagnetic (AF) coupling and SCO phenomena. Its crystal structure, shown in Fig. 2.21a, consists of two Fe^{II} centers, each of them coordinated to a bidentate bpym and two monodentate isothiocyanato anions, and bridged by a bipyrimidine ligand to form a dinuclear unit [32]. This compound does not show thermal ST, but the magnetic susceptibility measurements reveal weak AF coupling ($J \approx -4.1\ cm^{-1}$). Replacing the NCS group by NCSe with slightly stronger ligand field strength causes temperature induced ST near 120 K as seen in Fig. 2.21b, which shows the temperature dependent magnetic properties of $[Fe(bpym)(NCSe)_2]_2bpym$ as a plot of $\chi_M T$ vs. *T*, where χ_M is the magnetic susceptibility corrected for diamagnetic contributions. It reveals the presence of weakly coupled HS Fe^{II} ions in the region between room temperature and ca. 120 K. Around this temperature, a dramatic decrease of $\chi_M T$ due to thermally induced ST is observed to reach a plateau with a

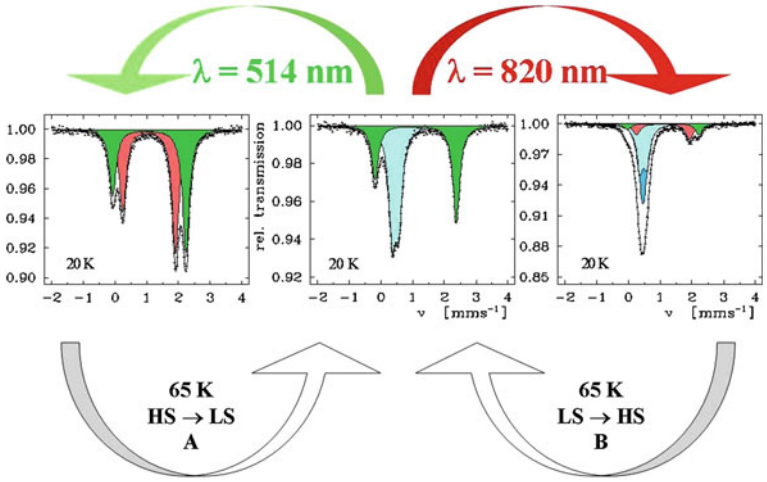

Fig. 2.20 LIESST effect at *A* sites of $[Fe(mtz)_6](BF_4)_2$ (LS to metastable HS conversion with green light, 514 nm) and at *B* sites (HS to metastable LS conversion with red light, 820 nm). Thermal relaxation from HS to LS at *A* sites and from LS to HS at *B* sites sets in at ca. 65 K in both cases [31]

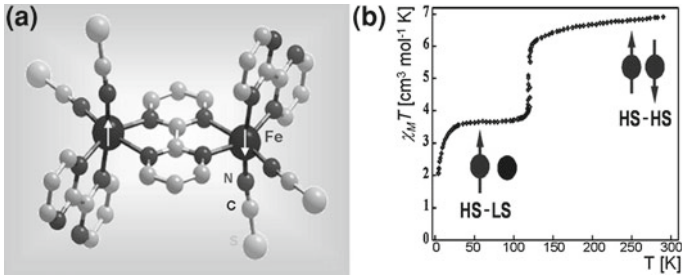

Fig. 2.21 **a** View of the crystal structure of $[Fe(bpym)(NCS)_2]_2bpym$ [32]. **b** Plot of $\chi_M T$ vs. T for $[Fe(bpym)(NCSe)_2]_2bpym$, where χ_M is the magnetic susceptibility corrected for diamagnetic contributions [33]

$\chi_M T$ value of ca. 3.5 cm^3 mol^{-1} K which indicates that about 50 % of the Fe^{II} ions have undergone ST to the LS state (Fig. 2.21b) [33]. The question, however, arises concerning the nature of the plateau region: Does the plateau originate from only [HS–LS] pairs or from a 1:1 mixture of [HS–HS] and [LS–LS] pairs?

Neither can this question be answered by magnetic susceptibility measurements nor by conventional Mössbauer spectroscopy. The latter would yield identical spectra for the HS state of Fe^{II} atoms in [HS–LS] and [HS–HS] spin pairs as seen in Fig. 2.22a. However, the Mössbauer spectrum recorded in applied magnetic field can give a conclusive answer based on the different effective hyperfine magnetic fields arising from different expectation values of the spin state of the

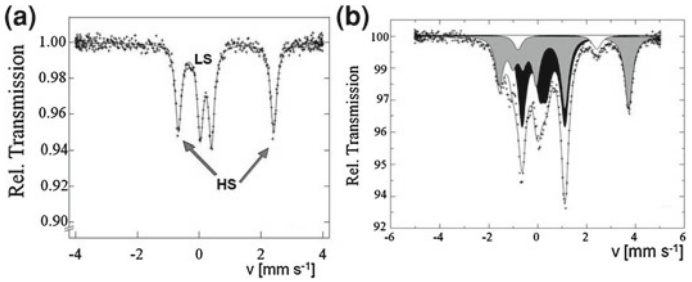

Fig. 2.22 Mössbauer spectra of $[Fe(bpym)(NCSe)_2]_2bpym$ at: **a** 4.2 K without applied magnetic field and **b** 4.2 K in applied magnetic field of 5 T. LS in [HS–LS] and [LS–LS] pairs (*black*), HS in [HS–LS] pairs (*grey*), HS in [HS–HS] pairs (*white*) [34, 35]

Fe^{II} ions [34, 35]. The effective hyperfine field H_{eff} at the iron nuclei of a paramagnetic non-conducting sample in an external field H_{ext} may be estimated as $H_{eff} \approx H_{ext} - [220 - 600(g - 2)]\langle S \rangle$ where $\langle S \rangle$ is the expectation value of the atomic spin moment and g the Landé splitting factor [36, 37]. The difference between the expectation values of S for the Fe^{II} atom in the LS and in the HS states in [HS–LS] and [HS–HS] pairs enables one to distinguish unambiguously between the dinuclear units consisting of two possible spin states in an external magnetic field. To do so, the strength of the external magnetic field should be sufficiently high and the temperature sufficiently low in order to avoid magnetic relaxation taking place within the characteristic time window of a Mössbauer experiment. The zero-field spectrum of the $[Fe(bpym)(NCSe)_2]_2bpym$ recorded at 4.2 K reflects, in agreement with the magnetic measurements, the nearly "one-half" ST according to the area fractions of the HS (48.0 %) and LS (52.0 %) components with parameters $\delta^{HS} = 0.86(1)\ \text{mms}^{-1}, \Delta E_Q^{HS} = 3.11(2)\ \text{mms}^{-1}$, and $\delta^{LS} = 0.22(1)\ \text{mms}^{-1}, \Delta E_Q^{LS} = 0.36(1)\ \text{mms}^{-1}$, respectively (Fig. 2.22a). The measurement in a magnetic field of 50 kOe (5 T) at 4.2 K yields a spectrum that consists of three components as can be seen in Fig. 2.22b. One of them (shown in black) with relative intensity (area fraction) 52.0 % and with isomer shift and quadrupole splitting indicative of Fe^{II} in LS state shows an expected effective hyperfine field that is practically the same as the applied field, $H_{eff} \approx H_{ext}$ (because S = 0). This subspectrum arises from LS-Fe^{II} ions in [HS–LS] and [LS–LS] pairs. The second component (shown in white) with area fraction of ca. 4.0 % is a doublet with isomer shift and quadrupole splitting values characteristic of Fe^{II} in HS state. The resonance lines are magnetically broadened through magnetic dipole interaction with a local effective hyperfine field of $H_{eff} = 14$ kOe, which is rather small and originates from a small $\langle S \rangle$ value as a result of antiferromagnetic coupling in [HS–HS] pairs. The third component (shown in grey) with relative intensity of ca. 44.0 % and isomer shift and quadrupole splitting values indicative of Fe^{II} in HS state can be unambiguously assigned to [HS–LS] pairs; because the measured effective magnetic field at the iron nuclei of 81 kOe clearly stems from a spin quintet ground state of Fe^{II} ($S = 2$). As a result, the complete distinction between

dinuclear units becomes possible and the nature of the plateau in Fig. 2.22b has been clarified: it is predominantly due to the presence of [HS–LS] pairs [34, 35].

The reason for the sharp decrease of $\chi_M T$ vs. T below ca. 30 K (Fig. 2.21b) has also become clear with the help of Mössbauer spectroscopy. It is due to zero-field splitting (ZFS) of the remaining HS–Fe^{II} ions and definitely not a continuation of ST upon further cooling; the Mössbauer spectrum recorded at temperatures below the plateau is nearly the same as that recorded in the region of the plateau (Fig. 2.22a).

Very similar studies were carried out with the dinuclear Fe^{II} complex $\left[Fe(phdia)(NCS)_2\right]_2$phdia (phdia = 4,7-phenanthroline-5,6-diamine), which exhibits an almost complete two-step thermally induced ST with a plateau around 100 K in the $\chi_M T$ vs. T magnetization curve [38]. After rapidly cooling the sample from the plateau down to 4.2 K the Mössbauer spectrum was recorded at that temperature in applied magnetic field of 5 T. The analysis of the magnetically perturbed spectrum indicated that the plateau consisted mainly of [HS–LS] pairs.

In another Mössbauer effect study the mechanism of the half-way ST in the dinuclear complex of formula $\left[Fe^{II}_2(pmatrz)_2\right](BF_4)_4 \cdot DMF$ with pmatrz = 4-amino-3,5-bis{[(2-pyridyl-methyl)amino]methyl}-4H-1,2,4-triazole could be elucidated by recording the spectra solely as a function of temperature in zero field. The results are in full agreement with the analysis of the structure determination [39]. The structure of this dinuclear compound is shown in Fig. 2.23 [39]. The Fe^{II} ions are in the HS state (shown in black) at room temperature as expected for [HS–HS] pairs. On cooling, only half of the Fe^{II} ions switch to the LS state as confirmed by the magnetic susceptibility measurements (Fig. 2.23). This is possible in two ways: (1) Both Fe^{II} complex ions have undergone ST but in only 50 % of the original [HS–HS] pairs; (2) Only one Fe^{II} center in all [HS–HS] pairs has switched. Mössbauer spectroscopy has confirmed that the second switching manner holds, viz. a ST between [HS–HS] to [LS–HS] pairs. Such a ST from [HS–HS] to [LS–HS] pairs on cooling is in agreement with the temperature dependence of the magnetic properties (Fig. 2.23). The HS to LS transition of half of the Fe^{II} ions occurs around 225 K to reach a plateau of very large length. The drop in $\chi_M T$ at very low temperature is definitely not due to a further HS to LS transition, because the Mössbauer spectrum recorded at 4.2 K shows a 50 % HS population. The sharp decrease of $\chi_M T$ at low temperatures is due to ZFS of HS Fe^{II} ions [40]. The Mössbauer spectra recorded as a function of temperature and shown in Fig. 2.24 not only confirm a 50 % spin state conversion, but also give insight into structural distortion that accompanies the spin transition (Fig. 2.23). The quadrupole doublet measured at 298 K refers to the original [HS–HS] pairs. At 240 K new signals appear corresponding to LS Fe^{II} ions (blue) in [HS–LS] pairs and HS Fe^{II} ions (dark red) in [HS–LS] pairs, both with the same area fraction. Upon further cooling to 180 K, a complete transition of HS ions in [HS–HS] pairs to a 50 % mixture of LS and HS ions in [HS–LS] pairs is identified, for the first time in zero-field Mössbauer spectroscopy [41].

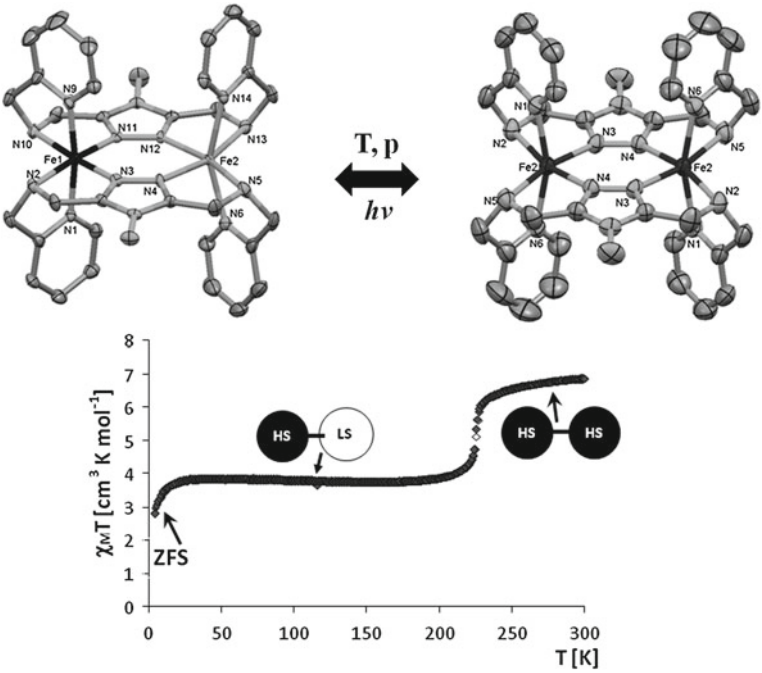

Fig. 2.23 View of the crystal structure of $\left[Fe^{II}_2(pmatrz)_2\right](BF_4)_4 \cdot DMF$ at 298 K in HS state (*right*) and at 123 K in LS state (*left*), and the magnetic susceptibility as a function of temperature for $\left[Fe^{II}_2(pmatrz)_2\right](BF_4)_4 \cdot DMF$ [39]

As seen from the 180 K spectrum the original quadrupole doublet (red) from [HS–HS] pairs has totally disappeared at the favor of the poorly resolved LS quadrupole doublet (blue) from [HS–LS] pairs and the new HS doublet (dark red) from [HS–LS] pairs. Its quadrupole splitting is significantly smaller than that in the original [HS–HS] pairs, and clearly points to the occurrence of a molecular distortion caused by the spin transition. In other words, the ST occurring in one Fe^{II} center is rapidly (in times characteristic of molecular vibrations) transmitted through the bridging ligand to the neighboring Fe^{II} center where it causes some molecular distortion such that the ligand field strength is weakened to such an extent that no more thermal SCO takes place with this Fe^{II} ion on further cooling. This is indicated in the structure (Fig. 2.23) by the black color for the Fe^{II} center remaining permanently in HS state. Clearly, Mössbauer spectroscopy has revealed such extreme subtleties in this study which is hardly possible with any other physical technique.

2.3.2.4 Thermal Spin Transition in a Trinuclear Fe^{II} Compound

The trinuclear Fe^{II} compound of formula $\left[Fe_3(iptrz)_6(H_2O)_6\right](CF_3SO_3)_6$ (iptrz = 4-isopropyl-1,2,4-triazole) was synthesized and its structure and magnetic

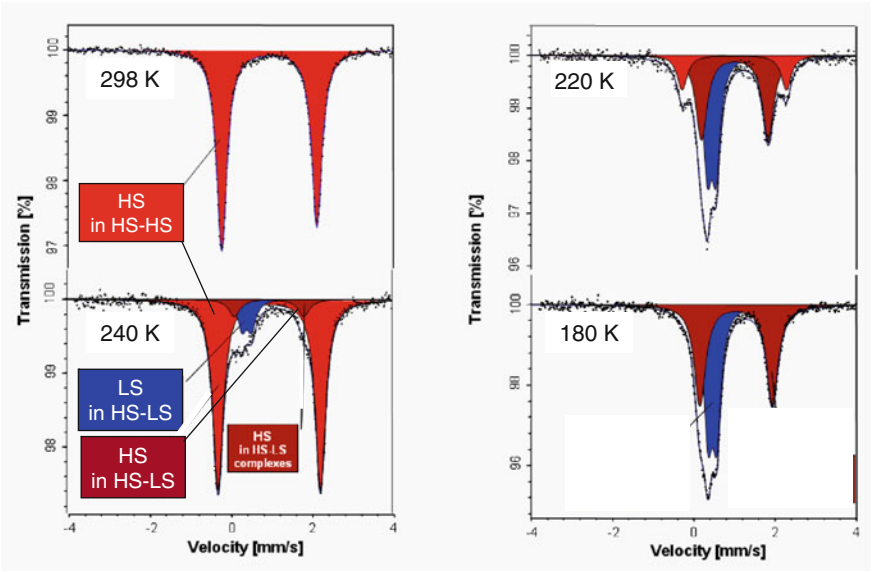

Fig. 2.24 Proof of [HS–LS] pair formation by variable temperature ^{57}Fe Mössbauer spectroscopy over the temperature range 298–180 K [41]

behavior characterized [42]. A perspective view of the structure is depicted in Fig. 2.25a. The central Fe^{II} is coordinated to three 1,2,4-triazole units and thus has FeN_6 core suitable to undergo thermal spin transition. The outer two Fe^{II} sites are each coordinated to three 1,2,4-triazole units and are capped by three water molecules, thus each having an FeN_3O_3 core, the ligand field strength of which is too weak for Fe^{II} to undergo thermal spin transition.

All three Fe^{II} centers are HS at 300 K as confirmed by Mössbauer spectroscopy (Fig. 2.25b). The quadrupole doublet shown in red, marked HSc, with the large splitting refers to the central Fe^{II}. The large splitting arises mainly from the valence electron contribution to the EFG; the lattice contribution is small due to the relatively high symmetry (close to O_h) of the FeN_6 core. The quadrupole doublet shown in yellow, marked HSo, refers to the two outer two Fe^{II} sites. The considerably smaller quadrupole splitting in this case arises from a relatively large lattice contribution to the EFG due to the low symmetry of the FeN_3O_3 core. This is opposite in sign to the valence electron contribution and thus reduces the total EFG giving a smaller total quadrupole splitting. The intensity ratio of the doublets of HSo to HSc is 1:2 as expected.

As the temperature is lowered, thermal ST from HS to LS takes place only at the central Fe^{II}. While the intensity of the yellow doublet of HSo remains unchanged, that of the red doublet of the central Fe^{II} diminishes at the favor of a new signal, shown in blue, which arises from LS state central Fe^{II} ions, marked by LSc. At the same time, a new quadrupole doublet (green) arising from the outer Fe^{II}–HS sites in HS–LS–HS trinuclear species, denoted as HS_o^{SC}, with twice the

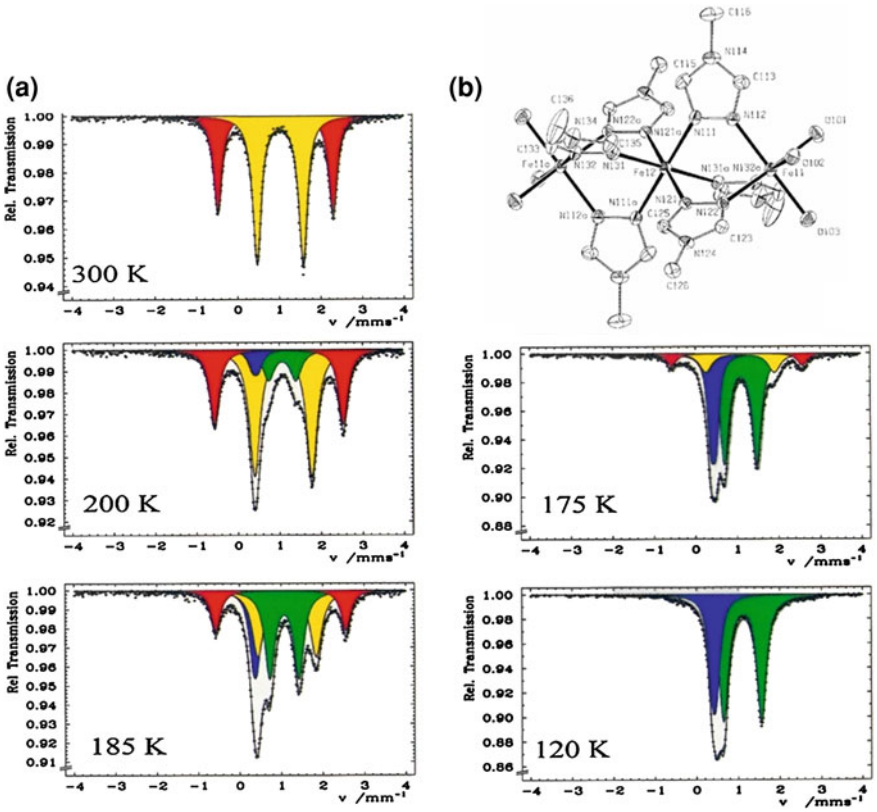

Fig. 2.25 a Projection showing the crystal structure of $[Fe_3(iptrz)_6(H_2O)_6](CF_3SO_3)_6$ [42]. **b** Temperature dependent ^{57}Fe Mössbauer spectra of $[Fe_3(iptrz)_6(H_2O)_6](CF_3SO_3)_6$ [42]. The *yellow*, *red* and *green* doublets correspond to HS_0, HS_c and HS_o^{SC}, respectively. The *blue* signal corresponds to LS_c

intensity of the blue LSc resonance signal. This 2:1 intensity ratio for HS_o^{SC}: LSc (green to blue) remains on further lowering the temperature. The same 2:1 intensity ratio remains for HSo: HSc (yellow to red) at any temperature until they entirely disappear after the ST is complete. The Mössbauer spectrum recorded at 120 K shows only the resonance signals for HS–LS–HS species. Clearly, the outer Fe^{II}–HS sites "feel" the process of thermal ST at the center, which is being communicated through the three rigid 1,2,4-triazole bridges and cause a noticeable structural distortion at the outer Fe^{II}–HS sites without influencing the spin state.

This is another "textbook example" for the high sensitivity of Mössbauer spectroscopy similar to the Mössbauer study of the $\left[Fe_2^{II}(pmatrz)_2\right](BF_4)_4 \bullet DMF$ discussed above. The tiny small distortion felt by the outer Fe^{II}–HS sites, which is caused by the ST from HS to LS in the center, is hardly detectable by diffraction techniques. Similarly, HS↔LS relaxation effects that are not seen by magnetic susceptibility measurements were detected at room temperature for the trinuclear

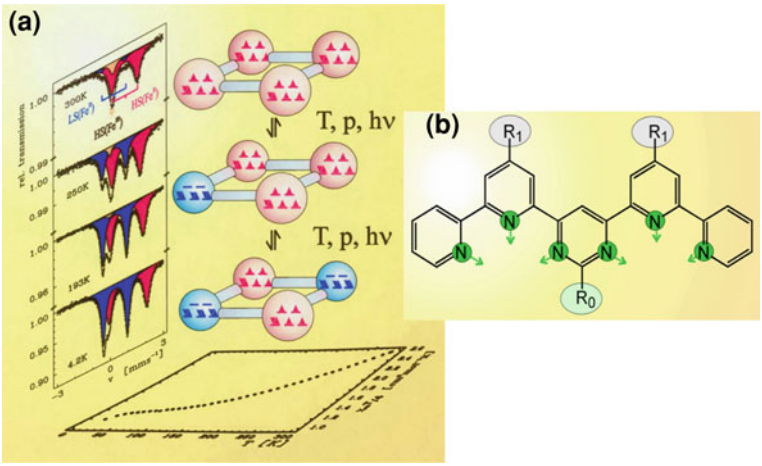

Fig. 2.26 **a** Temperature dependence of the magnetic susceptibility (*bottom*) and the Mössbauer spectra (*left*) reflect a very gradual and incomplete thermal spin conversion in the tetranuclear grid-like system $[Fe_4L_4]X_8$, with the anion $X = ClO_4^-$ and the L being depicted in Fig. 2.26b. The ST proceeds successively over the whole temperature range under study [45]. Spin transition in this system can also be achieved by application of pressure or irradiation with (*green*) light. **b** Four nitrogen donating ligands (derivative of terpyridine) as shown in the figure hold together four Fe^{II} ions to form a tetranuclear assembly, termed [2 × 2] grid, as schematized in the figure. With ligand molecules bearing CH_3 or Ph substituents in R_0 position the ligand field strengths at Fe^{II} ions becomes comparable to the mean spin pairing energy and thermally induced ST sets in successively at the iron centers [44]

SCO complex $[Fe_3(hyetrz)_6(H_2O)_6](CF_3SO_3)_6$ (hyetrz = 4-(2′-hydroxyethyl)-1,2,4-triazole) [43].

2.3.2.5 Spin Transition in "Grid-like" Tetranuclear Fe^{II} Complexes

The magnetism of a series of tetranuclear complexes of the $[Fe_4L_4]X_8$ [2 × 2]-grid-type was investigated, revealing the occurrence of ST behavior within this class of compounds. Four L-type ligands embrace four Fe^{II} ions as schematized in Fig. 2.26b. The magnetic behavior depends directly on the nature of the substituent R_0 in the 2-position of the central pyrimidine group of the ligand L. All Fe^{II} ions in compounds with R_0 substituents favoring strong ligand fields (R_0 = H; OH) remain completely in the diamagnetic LS state. Only complexes bearing R_0 substituents attenuating the ligand field strength by steric (and to a lesser extent electronic) effects (R_0 = Me; Ph) exhibit ST behavior triggered by variation of temperature. In general, gradual and incomplete transitions without hysteresis were observed for these magnetically active complexes. The spin conversion takes place successively at the iron centers which causes the very gradual decrease of the magnetic susceptibility stretched over the whole temperature range under study [44]. Figure 2.26a shows on the left some representative ^{57}Fe Mössbauer spectra

recorded between 300 and 4.2 K. The red quadrupole doublet refers to the HS–Fe^{II} ions, the one shown in blue to the LS–Fe^{II} ions. The approximately equal resonance areas of both doublets at 4.2 K indicates that the ST is incomplete and apparently has occurred only at two of the four Fe^{II} ions of a [2 × 2] grid unit. The question arises whether the two Fe^{II} ions exhibiting SCO are direct neighbors or placed diagonal in opposite positions of the grid. In relation to what one has learned from the studies of ST in dinuclear and trinuclear compounds (see Sects. 2.3.2.3 and 2.3.2.4), viz. that ST can cause a molecular distortion of a neighboring complex with accompanying weakening of the ligand field, it is not unreasonable to conclude that a similar process occurs in the present grid system. Thus it is likely that the two complex molecules which have converted to the LS state at low temperature are placed in diagonal positions as sketched in Fig. 2.26 [45].

2.3.2.6 Spin Transition in a 'Pentanuclear' Fe^{II} Coordination Compound

An unique pentanuclear Fe^{II} compound with the formula $[Fe_2L_5(NCS)_4]_2[FeL_2(NCS)_2(H_2O)_2]\cdot H_2O$, where L = 4-(p-tolyl)-1,2,4-triazole, has been synthesized and structurally characterized [46]. The structure was found to consist of two types of iron-containing structural units, a mononuclear unit and a dinuclear one (Fig. 2.27). The mononuclear unit has a crystallographic inversion center, and is coordinated by two NCS anions, two triazole nitrogen atoms, and two water molecules, each hydrogen-bonded to one of the two dinuclear units. The dinuclear units

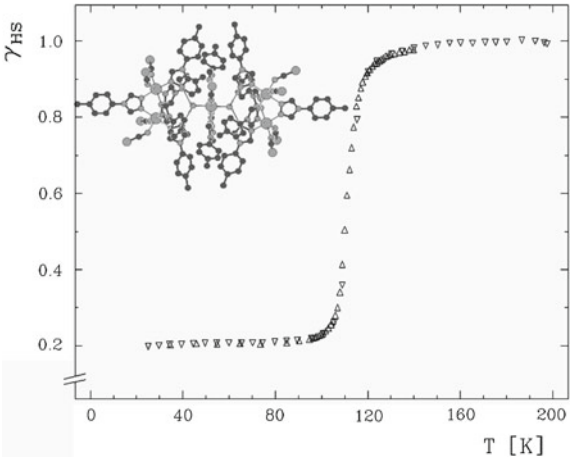

Fig. 2.27 Molar fraction of HS molecules of the pentanuclear Fe^{II} compound of formula $[Fe_2L_5(NCS)_4]_2[FeL_2(NCS)_2(H_2O)_2]\cdot H_2O$, derived from magnetic susceptibility measurements. A sharp ST between HS and LS state of Fe^{II} occurs near 111 K without hysteresis [46]. (Insert) Structure of the pentanuclear Fe^{II} compound $[Fe_2L_5(NCS)_4]_2[FeL_2(NCS)_2(H_2O)_2]\cdot H_2O$. Thermal ST takes place at the four outer Fe^{II} ions with FeN_6 core, but not at the central Fe^{II} ion with FeN_4O_2 core, where the ligand field strength is too weak such that the Fe^{II} ion remains in the HS state

consist of two Fe^{II} ions bridged by three triazole ligands in a 1,2-fashion. The coordination spheres of both iron ions are completed by two NCS anions and one monodentate 1,2,4-triazole ligand. The monodentate triazole ligands are connected through the non coordinating N atom to the mononuclear iron unit by hydrogen bonds from its coordinated water molecule. Magnetic susceptibility measurements indicate a ST only for the iron ions in the dinuclear units, centered at around $T_{1/2} = 111$ K. The transition takes place within a relatively narrow T range. The mononuclear iron ion with relatively weak ligand field strength of the FeN_4O_2 core remains in the HS state even at very low temperature, yielding a ratio of 4:1 of LS to HS iron ions. Temperature-dependent Mössbauer spectroscopy and magnetic susceptibility measurements confirm these results as seen from Figs. 2.27 and 2.28 [46].

2.3.2.7 Spin Transition in Metallomesogens

Metallomesogens belong to a class of metal-containing compounds which exhibit liquid–crystal (LC) properties. The possibility of combining LC properties with SCO behavior and accompanying change of color and magnetism in advanced functional materials has been a major objective of research in this field in recent years. In addition, the possibility of tuning the physical (mesomorphic, optical,

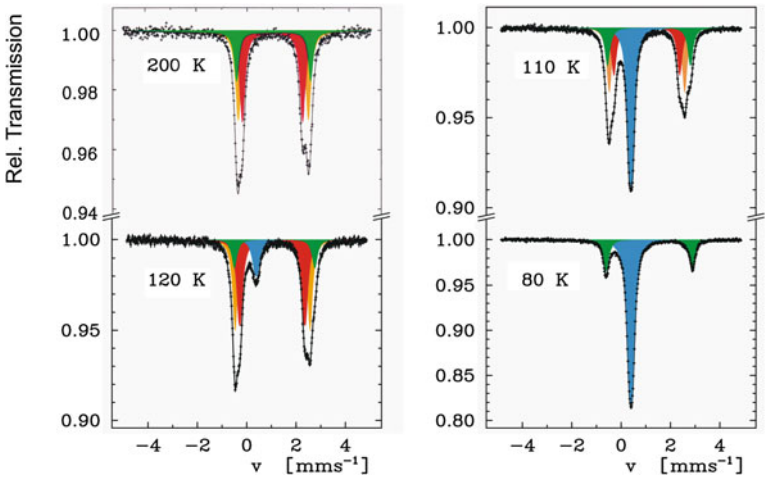

Fig. 2.28 Variable temperature ^{57}Fe Mössbauer spectra of $[Fe_2L_5(NCS)_4]_2[FeL_2(NCS)_2(H_2O)_2]\cdot H_2O$ [44]. Above the ST temperature of ca. 110 K the spectra show three doublets (*red*, *green*, *orange*) characteristic of Fe^{II} in HS state. The *green* doublet refers to the central Fe^{II} site, which remains in the HS state over the whole temperature range under study. The *red* and *orange* doublets with nearly equal intensity arise from the HS- Fe^{II} ions in the outer dinuclear units; the slight differences in quadrupole splitting point at slightly different molecular distortions. These two doublets decrease in intensity on lowering the temperature at the favor of a new signal (singlet shown in *blue*) with increasing intensity arising from the four LS-Fe^{II} ions in the dinuclear units after thermal spin transition

magnetic) properties of metallomesogens is significantly extended, since the organic ligand of these systems can be varied. Liquid crystalline materials in which a SCO center is incorporated into the mesogenic organic skeleton establish a separate class of compounds for which an interplay of structural transitions and liquid crystallinity is expected. This may lead to advantages in practical applications, for example, processing SCO materials in the form of thin films, enhancement of ST signals, switching and sensing in different temperature regimes, or achievement of photo- and thermochromism in metal-containing liquid crystals. The change of color in coexistence with liquid crystallinity is certainly a phenomenon of particular interest in the field of materials sciences.

Galyametdinov et al. [47] reported on temperature-dependent Mössbauer and magnetic susceptibility measurements of an Fe^{III} compound which exhibits liquid crystalline properties above and thermal ST below room temperature. This was the first example of SCO in metallomesogens. Later, different families of Fe^{II} and Co^{II} systems were also investigated [48–57]. The question whether the solid–liquid crystal phase transition provokes the spin-state change in SCO metallomesogens has been addressed in several series of Fe^{II} systems employing a variety of physical measurements [54, and references therein]. In all these studies ^{57}Fe Mössbauer spectroscopy has been extremely helpful, e.g. in controlling the completeness of ST in both the high and low temperature regions, where $\chi_M T$ data are often not reliable due to calibration difficulties. Also, one can unambiguously decide whether a significant decrease of the $\chi_M T$ vs. T plot towards lower temperatures is due to SCO or zero-field splitting. An example is the study of the one-dimensional (1D) 1,2,4-triazole-based compound $[Fe(C_{10}\text{–tba})_3](4\text{-}MeC_6H_4SO_3)_2 \cdot nH_2O$, with C_{10}–tba = 3,5-bis(decyloxy)-N-(4H-1,2,4-triazol-4-yl)benzamide, n = 1 or 0 [55, 56]. This system exhibits a spin state change on warming as a result of solvent release with a concomitant change of color between white (HS state) and purple (LS state) [58]. The magnetic properties of the pristine compound (n = 1) and the dehydrated sample (n = 0) are depicted in the form of $\chi_M T$ vs. T plots in Fig. 2.29.

At 300 K the value of $\chi_M T = 0.20$ cm^3 K mol^{-1} indicates that the compound is in the LS (purple) state. The Mössbauer spectrum recorded at 4.2 K is in agreement with the magnetic data, i.e. the HS population is 4.8 % and the LS population 95.2 % (Fig. 2.30a). Upon heating $\chi_M T$ increases abruptly within a few degrees, reaching the value of 3.74 cm^3 K mol^{-1} at 342 K. This clearly shows that a spin state change from LS to HS has occurred. The thermo-gravimetric analysis (TGA) of this system showed that dehydration takes place in the same temperature region where the spin state change occurs. The magnetic susceptibility of the dehydrated compound (n = 0) was recorded in a temperature loop, i.e. from 375 K down to 10 K and then up again to 375 K. The dehydrated complex reveals incomplete SCO, accompanied by hysteresis and color change (from purple in the LS state to white in the HS state), in the temperature region of 250–300 K. Around 50 % of Fe^{II} sites have changed the spin state as can be inferred from the value of $\chi_M T$ at 200 K. The Mössbauer spectrum recorded at 200 K (Fig. 2.30b) yields 49.3 % of Fe^{II} in the LS state and 50.7 % in the HS state. The further decrease of the

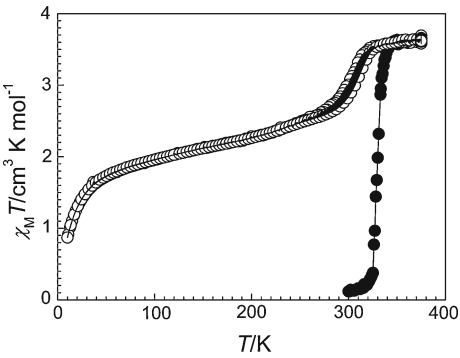

Fig. 2.29 Magnetic properties in the form of $\chi_M T$ vs. T of the one-dimensional 1,2,4-triazole-based mesogen of formula $[Fe(C_{10}\text{–tba})_3](4\text{-}MeC_6H_4SO_3)_2 \cdot nH_2O$, with n = 1 (*filled circles*) and n = 0 (*open circles*) [55, 56]. The pristine compound is in the LS state at 300 K, but loses crystal water on heating accompanied by sharp ST to the HS state. The dehydrated sample (n = 0) shows a entirely different SCO behavior

$\chi_M T$ value below 100 K, particularly below 50 K, is due to the ZFS of those iron atoms which remain in the HS state even at very low temperature, as derived from the Mössbauer spectrum at 4.2 K (HS population is 48.1 %, LS population is 51.9 %) (Fig. 2.30c).

Another member of the tba-based mesogen complexes is the room temperature operational 1D coordination polymer $[Fe(C_{12}\text{-tba})_3](CF_3SO_3)_2$ (C_{12}-tba = 3,5-bis(dodecyloxy)-*N*-(4*H*-1,2,4-triazol-4-yl)benzamide) which has been studied by Mössbauer spectroscopy [53]. The disk-like cations are self-assembled in columns, where the Fe^{II} ions are stacked on top of each other in the middle of the column as sketched in Fig. 2.31. The distance between the iron ions, determined by powder X-ray diffraction and Extended X-ray Absorption Fine Structure (EXAFS) measurements, varies with temperature and influences the spin state of the Fe^{II} ions as controlled by Mössbauer spectroscopy (Fig. 2.31). The variation of the chain length of the alkoxy substituent on the triazole ligand in $[Fe(C_n\text{-tba})_3](BF_4)_2 \cdot H_2O$ with C_n-tba = 5-bis(alkoxy)-*N*-(4*H*-1,2,4-triazol-4-yl)benzamide) can dramatically affect the spin state population as illustrated in Fig. 2.32 where the dark grey and light grey signals refer to the LS and HS states, respectively [53].

2.3.2.8 Nuclear Decay-Induced Excited Spin State Trapping (NIESST): Mössbauer Emission Spectroscopy

In conventional Mössbauer spectroscopy one uses a single-line source, e.g. ^{57}Co embedded in a rhodium matrix in the case of ^{57}Fe spectroscopy, and the iron containing material under study as absorber. This technique is termed *Mössbauer Absorption Spectroscopy* (MAS) in order to distinguish it from the so-called source experiment, also known as *Mössbauer Emission Spectroscopy* (MES). In a MES

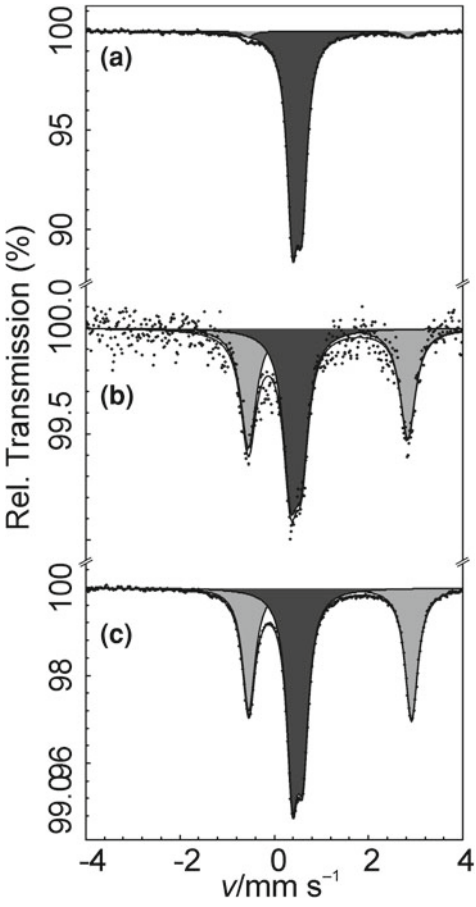

Fig. 2.30 ^{57}Fe Mössbauer spectra of the mesogen $[Fe(C_{10}–tba)_3](4\text{-}MeC_6H_4SO_3)_2 \cdot nH_2O$, with n = 1 at 4.2 K (**a**) of n = 0 at 200 K (**b**) and of n = 0 at 4.2 K (**c**) [53, 54]

experiment one uses a single-line absorber (free of electric quadrupole and magnetic dipole interaction), e.g. $K_4[Fe(CN)_6]$, and a ^{57}Co doped sample under study as source. In this case, the recorded Mössbauer spectrum refers to the hyperfine interactions in the source material, i.e. it yields information on the chemical and physical properties of the excited ^{57}Fe atoms before they decay to the ground state. The MES technique has been widely used to investigate chemical and physical *after-effects* of nuclear decay in various materials, particularly in coordination compounds [59]. The electron capture decay of radioactive ^{57}Co, whereby an electron from the K-shell is captured by the ^{57}Co nucleus leading to ^{57}Fe, ^{57}Co(EC)^{57}Fe, may lead to a variety of after-effects like bond rupture, ligand radiolysis, change of charge states and excited ligand field states to name the most important consequences of nuclear decay in solid coordination compounds. These after-effects may have lifetimes on the order of 10–500 ns. It is possible to cover this time regime and study the relaxation kinetics of such short-lived after effect species with *time-integral* and *time-differential* Mössbauer emission spectroscopy [60, 61].

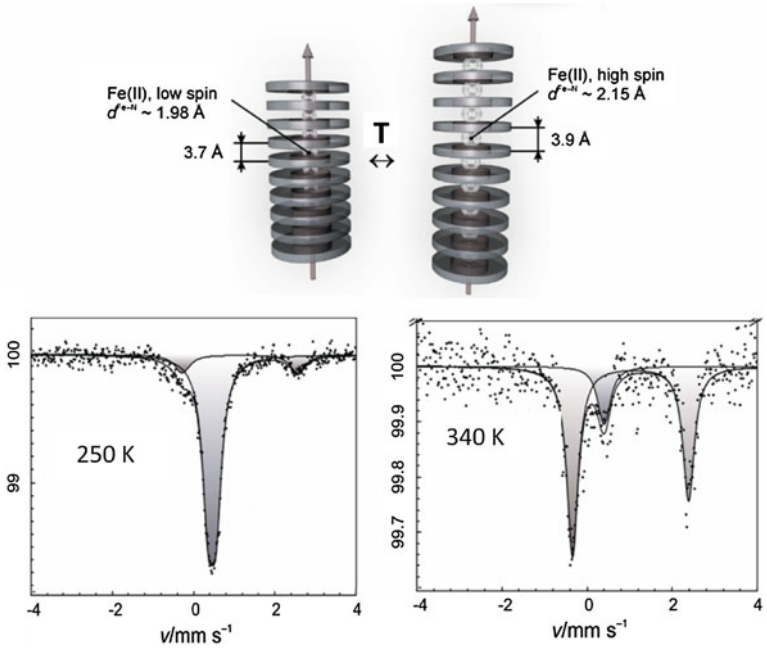

Fig. 2.31 The room temperature operational 1D polymeric mesogen $[Fe(C_{12}\text{-tba})_3](CF_3SO_3)_2$ arranges in disk-like columns with the iron ions stacked on *top* of each other in the *middle* of the columns. The spin state of the Fe^{II} ions depends on the distance d between the disks. At room temperature, d is relatively small and the LS state (singlet) is favored. On warming the distance d increases which favors the HS state (doublet) [53]

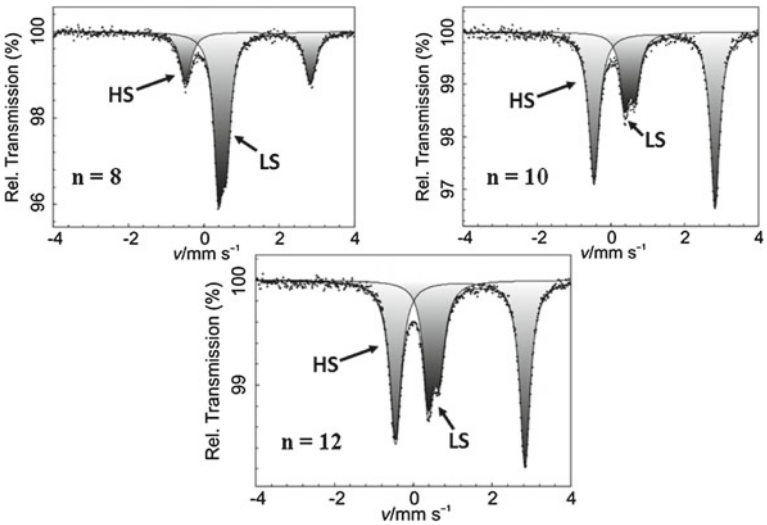

Fig. 2.32 Effect of chain length on the spin state population of $[Fe(Cn\text{-tba})_3](BF_4)_2{\cdot}H_2O$ (n = 8, 10, 12) investigated by Mössbauer spectroscopy at 80 K [53]

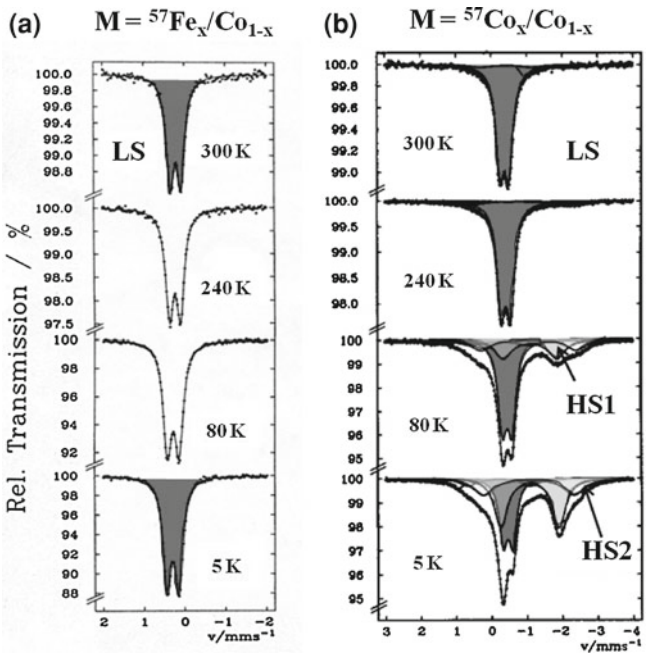

Fig. 2.33 **a** *Left* ^{57}Fe Mössbauer absorption spectra of $[^{57}Fe_x/Co_{1-x}(phen)_3](ClO_4)_2$ as a function of temperature vs. ^{57}Co/Rh (295 K) as source (x = 0.001) **b** *Right* Time-integral ^{57}Fe Mössbauer emission spectra of a $[^{57}Co_x/Co_{1-x}(phen)_3](ClO_4)_2$ source as a function of temperature vs. $K_4[Fe(CN)_6]$ (295 K) (x = 0.001). In (*a*) the source was moved relative to the absorber and in (*b*) the absorber was moved relative to the fixed source mounted in the crystal [63]

As an example, the coordination compound $[Co^{II}(phen)_3](ClO_4)_2$ doped with 0.1 % of ^{57}Fe was studied by Mössbauer absorption spectroscopy using a ^{57}Co/Rh source (Fig. 2.33; spectra on the left). The three phen ligands create a relatively strong ligand field at the Fe^{II} center, the compound shows LS behavior at all temperatures under study. The same system, however doped with ^{57}Co as Mössbauer source, was studied by Mössbauer emission spectroscopy using $K_4[Fe(CN)_6]$ as absorber. The MES spectra (Fig. 2.33, spectra on the right) also show the typical Fe^{II}–LS signal at 300 K down to ca. 200 K. On further cooling, however, the intensity of this signal decreases and at the same time two Fe^{II}–HS doublets, HS1 and HS2, appear with increasing intensity [62]. These unusual spin states are excited ligand field states with temperature-dependent lifetimes on the order of ca. 100 ns.

Similar experiments were carried out with systems whose corresponding Fe^{II} compounds possess intermediate ligand field strengths and show thermal spin crossover. $[Fe(phen)_2(NCS)_2]$ undergoes thermal ST as already discussed above (Sect. 2.3.2.1). The temperature dependent MAS spectra are shown on the left of Fig. 2.34. The analogous Co^{II} compound doped with ^{57}Co and used as Mössbauer source (or the corresponding iron compound doped with ^{57}Co as source which

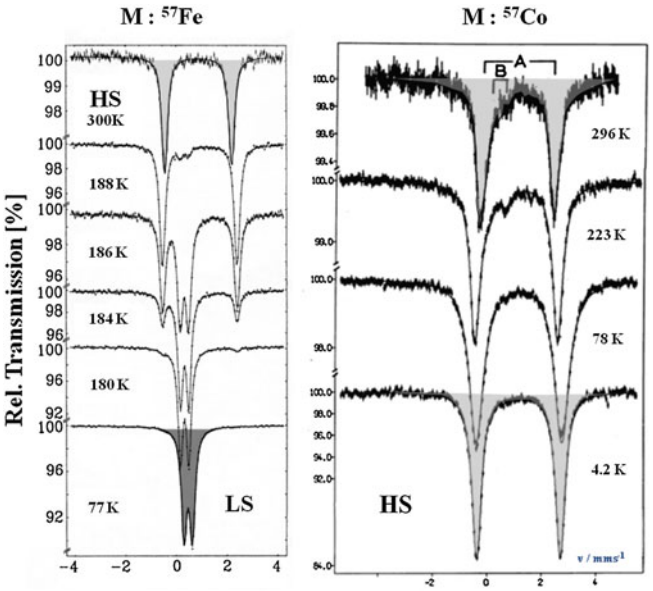

Fig. 2.34 [Fe(phen)$_2$(NCS)$_2$] undergoes thermal ST (MAS spectra on the *left*). The analogous Co^{II} compound doped with ^{57}Co and used as Mössbauer source (or the corresponding iron compound doped with ^{57}Co as source which gives the same results) yield the temperature dependent Mössbauer emission spectra (MES) shown on the *right*. The main result is that in the temperature region, where the MAS spectra reflect the transition to the LS state, the MES spectra still show the typical HS signals arising from short-lived excited ligand field states [64]

gives the same results) yield the temperature dependent MES spectra shown on the right [64]. The main result is that in the temperature region, where the MAS spectra reflect the transition to the LS state, the MES spectra still show the typical HS signals arising from excited ligand field states.

The mechanism of the formation of the excited ligand field states as a consequence of the EC nuclear decay of radioactive ^{57}Co is well understood. It is much related to that of the LIESST phenomenon (Fig. 2.14) and has therefore been termed *Nuclear Decay-Induced Excited Spin State Trapping* (NIESST) [59]. The main difference between the two phenomena lies in the primary step of excitation, which is the application of a light source in the case of LIESST, whereas in NIESST the nuclear decay serves quasi as an intrinsic molecular excitation source. The lifetime or probability of observing the metastable HS ($^5T_2$) state within the Mössbauer time scale (given by the lifetime of the 14.4 keV nuclear state of ^{57}Fe) at a given temperature is governed by the ligand field strength felt by the nucleogenic ^{57}Fe ion: The weaker the ligand field strength, the longer the lifetime of the metastable HS ($^5T_2$) state. It is worth emphasizing that this technique, Mössbauer emission spectroscopy, is most effective for the study of chemical and physical after-effects of nuclear decay processes, referred to as "Hot Atom Chemistry", in solids [63].

The NIESST effect was also studied in Co^{II} SCO compounds, viz. $[^{57}Co/Co(terpy)_2]X_2\,nH_2O$ ($X = ClO_4^-$, $n = 1/2$, $X = Cl^-$, $n = 5$), where terpy is the tridentate ligand terpyridine [65]. The perchlorate salt shows thermal SCO with $T_{1/2}$ around 200 K and a HS fraction of nearly 100 % at room temperature, whereas the chloride salt possesses a somewhat stronger ligand field giving rise to thermal ST at much higher temperatures (the HS fraction starts to rise around 200 K, reaches ca. 20 % at 320 K and obviously would increase further) [65]. Conventional Mössbauer absorption measurements were performed on the corresponding systems doped with 5 % Fe^{II}, which was found to be in the LS ($S = 0$) state at all temperatures under study [65]. The emission spectra of the ^{57}Co-labelled cobalt complexes were measured using a home-made resonance detector, which operates as conversion-electron detector with count rates 10–20 times higher than those of a conventional detector. At room temperature, the nucleogenic ^{57}Fe ions were found to have relaxed to the stable $^1A_1$ LS ground and gave the same MAS Mössbauer spectrum like the corresponding Fe^{II} compound. On lowering the temperature a doublet from a metastable Fe^{II}–HS state appears in the MES spectra with increasing intensities. The perchlorate derivative with the weaker ligand field strength shows, at comparable temperatures, a considerably higher amount of Fe^{II}–HS fraction than the chloride derivative with the stronger ligand field. For instance, the emission spectra recorded at 100 K displayed in Fig. 2.35 demonstrate this effect very clearly. Thus, it turns out that the lifetime of the nuclear decay-induced metastable HS state of Fe^{II} is short in strong ligand field surroundings and long in weak ligand fields. In other words in relation to Fig. 2.14, the stronger the ligand field, the larger is the difference between the lowest vibronic energy levels of HS and LS states, and the shorter is the lifetime at a given temperature. This is known as "reduced energy gap law" which holds for all these NIESST studies [59].

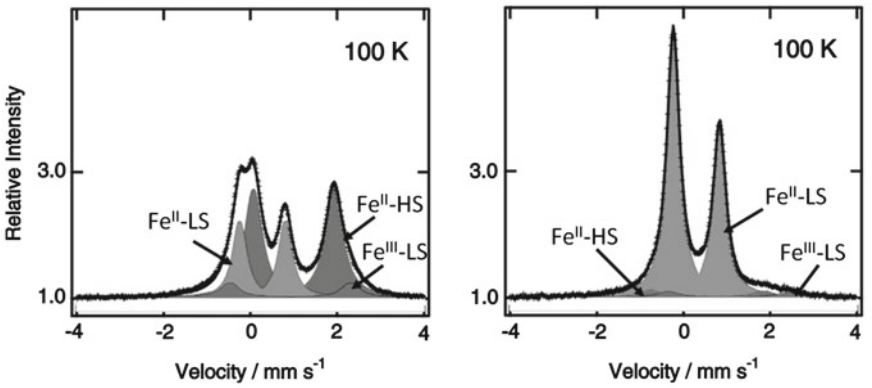

Fig. 2.35 Mössbauer emission spectra of $[^{57}Co/Co(terpy)_2]X_2nH_2O$ ($X = ClO_4^-$, $n = ½$; $X = Cl^-$, $n = 5$) as source material vs. $K_4[Fe(CN)_6]$ as absorber (which was kept at 298 K) recorded at 100 K with a conversion-electron detector. *Left* $X = ClO_4^-$, $n = ½$. *Right* $X = Cl^-$, $n = 5$ (from [65])

2.3.3 Mixed-Valence Compounds, Intramolecular Electron Transfer

Mixed-valence compounds are known to possess two or more transition metal ions with different oxidation states. Intramolecular electron transfer may take place between (generally two) heterovalent metal centers over suitable bridging atoms or ligand molecules. There may be three cases observed in the Mössbauer spectrum. (1) If the electron fluctuation rate τ_f is less than the reciprocal of the Mössbauer time window (given by the lifetime τ_n of the nuclear excited state of the Mössbauer probe), $\tau_f < \tau_n$, the spectrum will show two resolved resonance signals arising from the static ("localized") oxidation states. (2) If $\tau_f > \tau_n$, the spectrum will show a single time-averaged resonance signal which is different from the two signals of case (1) and points at an oxidation state in between those of the two static components. One speaks of a "delocalized" mixed-valence compound. (2) If $\tau_f \approx \tau_n$, the Mössbauer spectrum will be the sum of overlapping heavily broadened resonance lines of cases (1) and (2); the spectrum will be very complicated and difficult to analyze. As the fluctuation rate τ_f is temperature dependent, one often observes a transition between the localized and delocalized cases during variation of temperature.

In the following, we shall briefly discuss three examples of studies of mixed-valency systems with Mössbauer spectroscopy.

2.3.3.1 Mixed-Valence Biferrocenes

In Fig. 2.36 is schematized the molecular structure of biferrocenes which possess two iron atoms with different valence electron structures. Depending on the nature of the substituent R, the iron centers have either static but different electronic structures referred to as "localized" ferrocene and ferricinium, respectively. Or a rapid electron transfer between the two iron centers takes place and as a result of the fast fluctuation one observes a time-averaged species with an electronic structure between the two localized species. With the help of ^{57}Fe Mössbauer spectroscopy one has studied the biferrocenes containing ethyl groups as R substituents as a function of temperature. At 115 K, the spectrum shows two well resolved quadrupole doublets, the light-blue one being characteristic of ferrocene-like iron, the red one of ferrocinium-like iron. With increasing temperature a fast electron fluctuation sets in and the doublets of the two localized species turn into one quadrupole doublet (shown in green at 287 K) of a time-averaged species, the parameter values of which are different from those of the two localized species. From the sharpness of the quadrupole doublet of the time-averaged species one can conclude that the electron fluctuation rate must be faster than 10^7 s^{-1} corresponding to the time-window of ^{57}Fe Mössbauer spectroscopy. This example shows a thermally induced transition between localized and delocalized electronic structures in a mixed-valence organometallic compound.

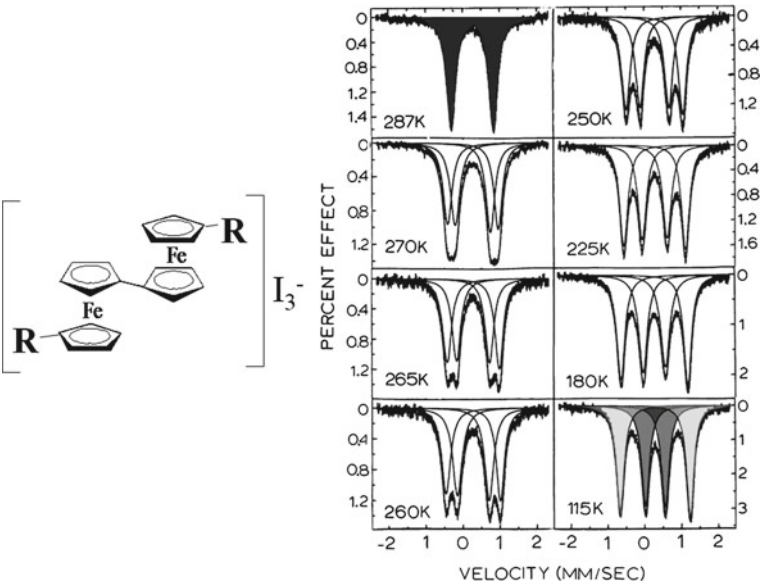

Fig. 2.36 Mixed valence biferrocene with R = Et shows temperature dependent electron fluctuation between the two iron centers. At low temperatures the fluctuation rate is comparatively slow (less than the reciprocal of the Mössbauer time window of ca. 100 ns) and the Mössbauer spectra show two subspectra indicative of "localized" ferrocene (*grey*) and ferrocinium (*dark grey*), respectively. At higher temperatures the fluctuation rate becomes so fast that the Mössbauer spectrum reflects a time-averaged "delocalized" species (*black*) which is neither ferrocene nor ferrocenium [66, 67]

2.3.3.2 Effect of Crystal Solvents Molecules on the Valence Detrapping of Mixed-Valence $[Fe_3O(O_2CCH_3)_3)_6(3\text{-Et-py})_3]\cdot S$

The molecular structure of the mixed-valence compound $[Fe_3O(O_2CCH_3)_3)_6(3\text{-Et-py})_3]\cdot S$ is visualized in Fig. 2.37. The molecule accommodates two HS–Fe^{III} ions and one HS–Fe^{II} ion which is confirmed by Mössbauer spectroscopy (Fig. 2.37) [68]. In all spectra the more intense quadrupole doublet (red) corresponds to the two HS Fe^{III}–HS ions and the less intense doublet (green) is for the one HS Fe^{II} ion. The ratio of the area fractions of Fe^{III} to Fe^{II} is close to 2 at low temperatures. Towards higher temperatures it tends to become larger than 2, which is due to the larger Lamb-Mössbauer factor of Fe^{III} compared to that of Fe^{II}. It is found [68] that the mixed valency properties of this compound depend on the nature of the crystal solvents molecules. Compounds A (with S = 0.5 benzene) and B (with S = CH_3CN) appear to be valence-trapped over the whole temperature range up to room temperature. The quadrupole doublets arising from HS–Fe^{III} (red) and HS–Fe^{II} (green) are well resolved and sharp. Thus the lifetimes of these trapped (localized) species are longer than the lifetime of the 14.4 keV nuclear excited state. Compound C (with S = CH_3CCl_3) are valence-trapped at low temperatures.

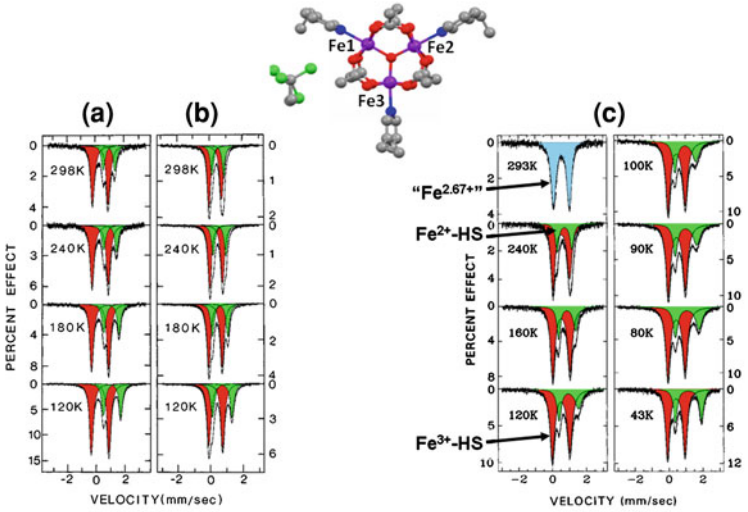

Fig. 2.37 Molecular structure and temperature dependent ^{57}Fe Mössbauer spectra of the mixed valence complex compound $[Fe_3O(O_2CCH_3)_3)_6(3\text{-Et-py})_3]\cdot S$ with S = 0.5 benzene (**a**), CH_3CN (**b**) and CH_3CCl_3 (**c**). Solvates A and B are "valence-trapped" (localized) with two HS–Fe^{III} ions (*red* doublet) and one HS–Fe^{II} ion (*green* doublet) in the molecular unit; the quadrupole doublets are well resolved without significant line-broadening. **c** Shows a transition from electron localization to delocalization (valence-trapped to detrapped) with increasing temperature. The sharp doublets of the trapped species begin to broaden on heating and finally disappear at the favor of a time-averaged new signal (*blue*) from a species with averaged oxidation state, "$Fe^{2.67+}$", due to fast electron fluctuation within the Fe_3O *triangle* [68]

The resonance lines of the two quadrupole doublets begin to broaden around 50 K. Further increase of temperature leads to valence-detrapping (delocalization) near room temperature, where the red and green doublets have disappeared at the favor of a new doublet (blue) which is a time-averaged resonance signal of a species with an "average" oxidation state of "$Fe^{2.67+}$" due to rapid electron circulation within the Fe_3O triangle of the complex.

2.3.3.3 Valence Fluctuation in a Trinuclear Cationic Complex

Another interesting example of valence fluctuation and temperature dependent transition between localized and delocalized electronic structures in a trinuclear transition metal compound was reported by Glaser et al. [69]. In this case the electron fluctuation takes place between two iron centers of different oxidation states and separated by a diamagnetic Co^{III} ion. The ^{57}Fe Mössbauer spectra clearly show that at sufficiently low temperatures, i.e. 5 K, the two iron centers are reflected as localized oxidation states with a well resolved doublet for LS–Fe^{III} (red) and a poorly resolved doublet for LS–Fe^{II} (light-blue). At higher temperatures the

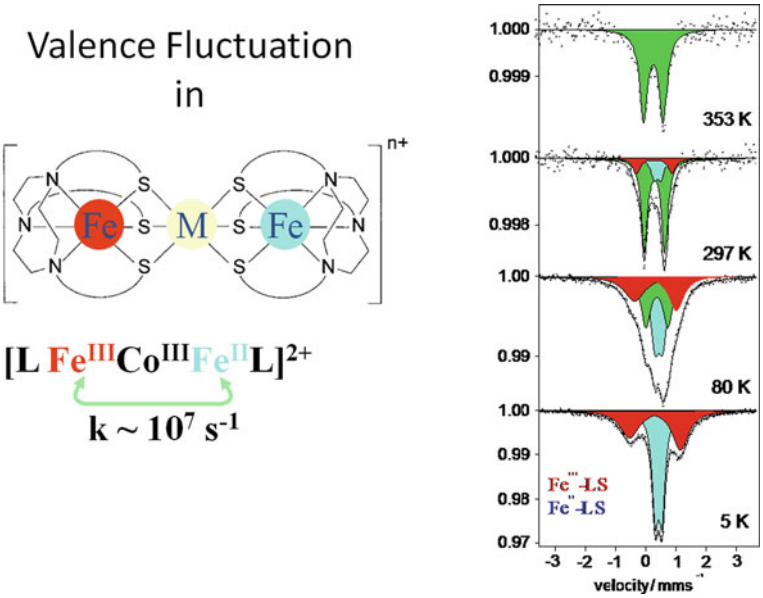

Fig. 2.38 Schematized molecular structure of a trinuclear cationic complex which accommodates LS-Fe^{III} (*red*) and LS-Fe^{II} (*blue*) ions separated by bridging LS-Co^{III} ion. At low temperatures two well resolved spectra are observed assigned to the localized LS-Fe^{III} and the LS-Fe^{II} species. With increasing temperature the intensities of these two doublets decrease at the favor of a new doublet (*green*) from a time-averaged species with intermediate oxidation state of the two iron sites. This species is the only one remaining at room temperature [69]

intensities of these two resonance signals decrease at the favor of a new resonance signal, another quadrupole doublet (blue), arising from a time-averaged species where both iron centers are in an intermediate oxidation state as a result of fast electron fluctuation through the bridging diamagnetic central Co^{III} ion (Fig. 2.38).

2.3.3.4 Valence Fluctuation in EuNiP

Mixed-valency and thermally induced transition between localized and delocalized valence states was observed with ^{151}Eu Mössbauer spectroscopy of the intermetallic compound EuNiP [70] (Fig. 2.39).

High temperature ^{151}Eu Mössbauer measurements between room temperature and ca. 500 K provide proof for mixed-valent behavior in the pnictide EuNiP. Two well resolved signals are observed at room temperature, one being typical for Eu^{2+} (dark grey) and the other one for Eu^{III} (light grey). With increasing temperature the electron fluctuation between Eu^{II} and Eu^{III} becomes faster than the time-window of ^{151}Eu Mössbauer spectroscopy and above ca. 450 K the resonance signals of localized Eu^{II} (dark grey) and Eu^{III} (light grey) gradually disappear at the favor of a new signal with time-averaged oxidation state of $Eu^{2.5+}$ (non shaded) [70].

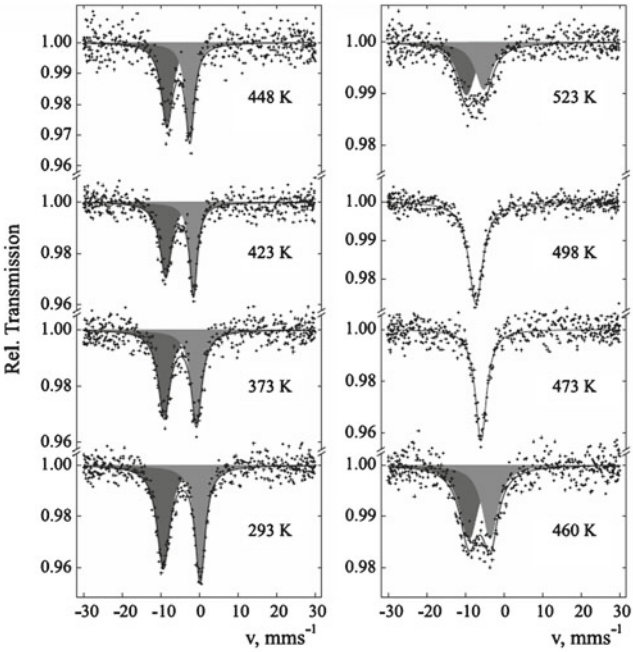

Fig. 2.39 Variable temperature ^{151}Eu Mössbauer spectra of the intermetallic compound EuNiP. Shaded subspectra correspond to Eu^{2+} (*dark grey*) and Eu^{3+} (*light grey*) [70]

EuNiP undergoes a Verwey-type charge delocalization transition when heated above 470 K prior to the structural gamma-beta phase transition at approximately 510 K. This finding confirms the results of photoemission spectroscopy of the isostructural compound EuPdP and of TB-LMTO-ASA (Tight-Binding Linear Muffin-Tin Orbital Atomic-Sphere Approximation) band structure calculations. It has been proposed that a van Hove singularity associated with a high density of 4f states close to the Fermi energy plays a particular role in mixed valency pnictide EuNiP [70].

2.3.4 Molecular Magnetism

Mössbauer spectroscopy, primarily employing ^{57}Fe as a nuclear probe, has developed to an enormously helpful complementary tool supporting standard SQUID and ac/dc magnetic measurements in studies of magnetic behavior of solid materials. Magnetic dipole interaction (see Sect. 2.2.3) will lead to a magnetically split Mössbauer spectrum, a sextet in the case of ^{57}Fe Mössbauer spectroscopy, provided a local effective magnetic field pointing sufficiently long (longer than the lifetime of the 14.4 keV nuclear excited state) in a fixed direction. Magnetic behavior of solid material is usually categorized into two classes: (1) *Long-range*

cooperative magnetism due to magnetic interactions (stronger than thermal energy) between metal ions with unpaired electrons, like in metals, alloys and simple inorganic compounds (oxides, halides etc.). (2) *Molecular magnetism* with weak or vanishing long-range spin–spin interactions, also known as "molecule-based magnetism" [71]. The latter kind of magnetism has attracted much interest in recent years [72]. Because of limited space we shall discuss only two examples.

2.3.4.1 Photo-Switchable Prussian Blue Analog $K_{0.1}Co_4[Fe(CN)_6]_{2.7}\cdot 18\ H_2O$

The Prussian-blue analog $K_{0.1}Co_4[Fe(CN)_6]_{2.7}\cdot 18\ H_2O$ with paramagnetic building blocks [Co^{II} (S = 3/2) –NC – Fe^{III}(S = 1/2)] was found to undergo photo-induced transition by irradiation with blue light, whereby electron transfer takes place to generate the diamagnetic buildings blocks [Co^{III}(S = 0) –NC – Fe^{II}(S = 0)]. This transition is reversible by irradiation with red light (Fig. 2.40). It was also found that the transition from Co^{II} (S = 3/2) –NC – Fe^{III}(S = 1/2)] to [Co^{III}(S = 0) –NC – Fe^{II}(S = 0)] is favored by increasing potassium concentration or by replacing

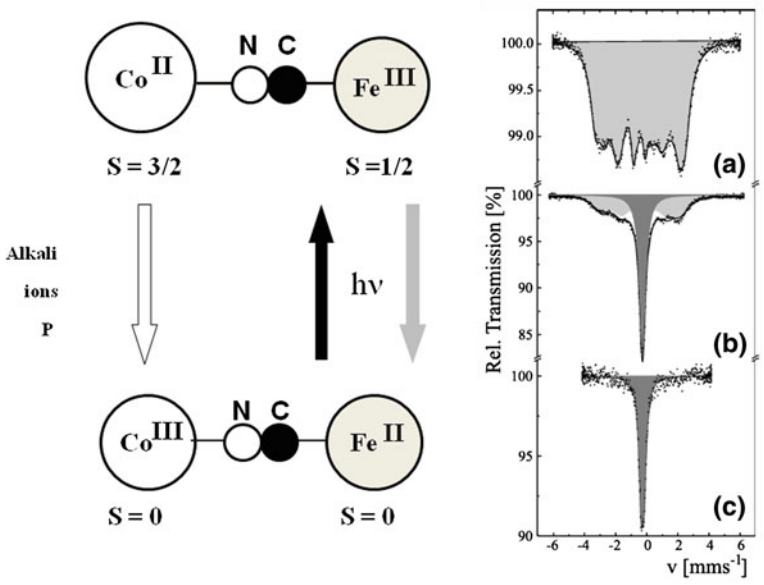

Fig. 2.40 The Prussian-blue analog $K_{0.1}Co_4[Fe(CN)_6]_{2.7}\cdot 18\ H_2O$ contains photosensitive paramagnetic [Co^{II} (S = 3/2) –NC – Fe^{III}(S = 1/2)] building blocks which can be converted by irradiation with blue light to diamagnetic [Co^{III}(S = 0)–NC – Fe^{II}(S = 0)] building blocks; back conversion is possible with *red* light. Increase of potassium content or replacement of potassium by bigger caesium ions or application of pressure favors the transition of the [Co^{III}(S = 0) –NC – Fe^{II}(S = 0)] entities to [Co^{III}(S = 0)–NC – Fe^{II}(S = 0)] as confirmed by Mössbauer spectroscopy at 4.2 K under different pressures **a** 1 bar, **b** 3 kbar, and **c** 4 kbar. Shaded subspectra correspond to Fe^{II}(S = 0) in *dark grey* and Fe^{III}(S = 1/2) in ~*light grey* [73]

potassium by bigger caesium ions. It was speculated that chemical pressure in the crystal lattice plays a decisive role in this process. To prove the validity of this idea, ^{57}Fe Mössbauer spectra of $K_{0.1}Co_4[Fe(CN)_6]_{2.7}\cdot 18\ H_2O$ were recorded at 4.2 K under applied pressure (Fig. 2.40). At ambient pressure the sample contains the paramagnetic [Co^{II} (S = 3/2) –NC – Fe^{III} (S = 1/2)] building blocks, and the electronic spins of Co^{II} and Fe^{III} sites are oriented sufficiently long in one direction such that the Mössbauer spectrum reflects a well resolved magnetically split sextet with effective field of 165 kOe at the ^{57}Fe nucleus. Increase of pressure to 3 kbar yields a spectrum that shows a dominating singlet (dark grey) characteristic of LS–Fe^{II} with S = 0 at the expense of the collapsing magnetic sextet from remaining LS–Fe^{III} ions. The spectrum recorded under 4 kbar shows only the singlet arising from LS–Fe^{II} ions [73].

2.3.4.2 Orbital Magnetism in a Rigorously Linear Two-Coordinate High-Spin Fe^{II} Compound

Reiff et al. have studied the linear two-coordinate HS Fe^{II} compound Bis (tris(trimethylsilyl)methyl) Fe^{II} with Mössbauer spectroscopy and observed an enormously large effective magnetic field at the Fe^{II} site of 152 T [74]. This is the largest field ever observed in an iron containing material. The molecular structure of the compound is shown in Fig. 2.41 [75].

The ^{57}Fe Mössbauer spectrum recorded at 4.2 K in zero applied magnetic field is also shown in Fig. 2.41. The authors have plausibly interpreted the origin of this extremely large field as being due to an unusually large orbital contribution, B_L, from electron movement around the molecular axis. In Sect. 2.2.3 above it has been outlined that the effective internal magnetic field B_{int} at the Mössbauer nucleus observed in a Mössbauer experiment results from several contributions, the Fermi-contact field B_c, the contribution from orbital motion of valence electrons, B_L, a contribution B_D, called spin-dipolar field, and eventually an externally applied magnetic field B_{ext}. The term B_c roughly contributes 12.5 T per electron spin, i.e. in total 50 T in the present case of HS–Fe^{II} with four unpaired valence electrons. B_D is generally comparatively small and can be neglected here. Since B_{ext} was zero in this experiment, one has found for the orbital contribution B_L a value of roughly 200 T (B_c and B_L have opposite signs). This surprisingly large orbital contribution arises from the fact that there are no in-plane ligands (only the axial ligands) to impede the orbital circulation of the electrons within the doubly degenerate E_g (d_{xy}, $d_x2_{-y}2$) ground state, which, in addition, does not suffer appreciably from a Jahn–Teller distortion.

2.3.5 Industrial Applications of Mössbauer Spectroscopy

The eminent capability of non-destructive phase analysis with Mössbauer spectroscopy has been used in the multidisciplinary field of materials science, particularly

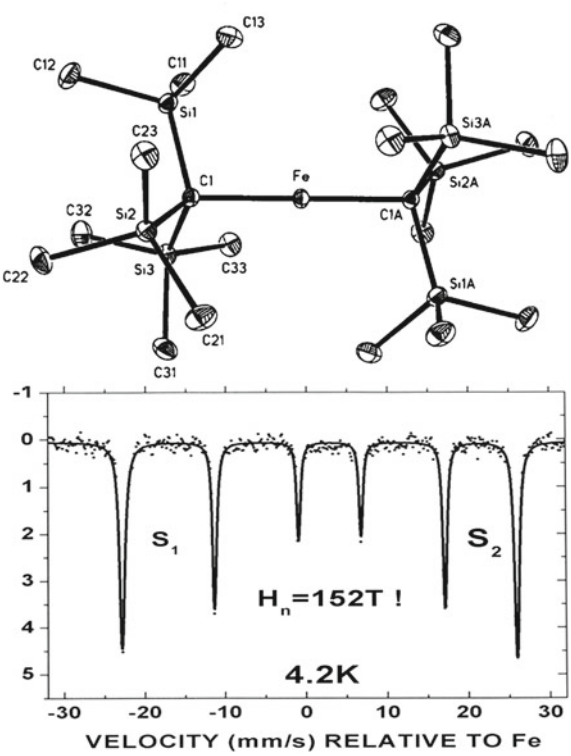

Fig. 2.41 Molecular structure of Bis(tris(trimethylsilyl) methyl)Fe^{II}, a rigorously linear two-coordinate compound of Fe^{II} in HS state with ideal staggered D_{3d} symmetry [75]. ^{57}Fe Mössbauer spectrum of Bis(tris(trimethylsilyl) methyl)Fe^{II}, recorded at 4.2 K in zero applied magnetic field [74]. The internal magnetic field derived from the distance between the two outermost resonance lines, S_1–S_2, is 152 T, the largest field ever observed in an iron compound

for the analysis of iron containing materials of technical relevance such as steel, alloys, pigments, oxides, corrosion products, to name a few. But other "Mössbauer-active" nuclides have also been used. Within the limited scope of this article we must confine the discussion in the following to only one representative example, viz. corrosion studies.

Roughly six different iron oxides and oxyhydroxides of iron are known as corrosion products, which may be formed by corrosion reactions in steel, metallic iron, and iron containing alloys under different conditions. These corrosion products can be distinguished by ^{57}Fe Mössbauer spectroscopy (Fig. 2.42). Magnetite, Fe_3O_4, is an inverse spinel compound of formula $Fe^{III}\left[Fe^{II}Fe^{III}\right]O_4$, where half of the Fe^{III} ions (those outside the square brackets) are in tetrahedral sites and the other half (inside the square brackets) in octahedral sites. All Fe^{II} ions are in octahedral sites. According to these three kinds of iron ions one should expect three different resonance signals in the Mössbauer spectrum. This, however, is not the case. Instead one observes at room temperature two overlapping sextets, one arising from Fe^{III} ions in tetrahedral sites, and the other one is a time-averaged sextet arising from Fe^{II} and Fe^{III} ions in octahedral sites with fast electron fluctuations between them (faster than the inverse of the lifetime of the 14.4 keV nuclear level). The oxides α- and γ-Fe_2O_3 show a magnetically split sextet with a

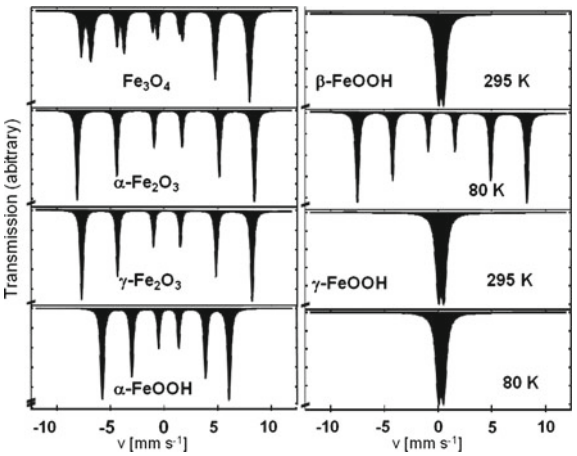

Fig. 2.42 ^{57}Fe Mössbauer spectra of various corrosion products which may be formed under different conditions. The spectra are discussed in the text

slightly different size of the internal magnetic field. The oxyhydroxides α-, *β*- and *γ*-FeOOH can be distinguished by temperature dependent Mössbauer spectroscopy. While α-FeOOH (Goethite) shows a magnetically split sextet at room temperature, *β*- and *γ*-FeOOH have the same poorly resolved quadrupole doublet and therefore cannot be distinguished at room temperature. At liquid nitrogen temperature (ca. 80 K), however, *β*-FeOOH is magnetically ordered and shows the typical magnetically split sextet, whereas *γ*-FeOOH still shows the same poorly resolved quadrupole doublet as at 295 K. This phase orders magnetically only below ca. 30 K yielding then a similar sextet as the other modifications. Thus, Mössbauer spectroscopy enables one to distinguish between these corrosion products, even in the form of highly dispersed particles (>ca. 10 nm), where powder X-ray diffraction measurements are no longer applicable.

Figure 2.43 shows an example of routine Mössbauer analysis of finely dispersed particles formed in the cooling system of a power plant. The particles were collected from the coolant with a special filter and analyzed with standard

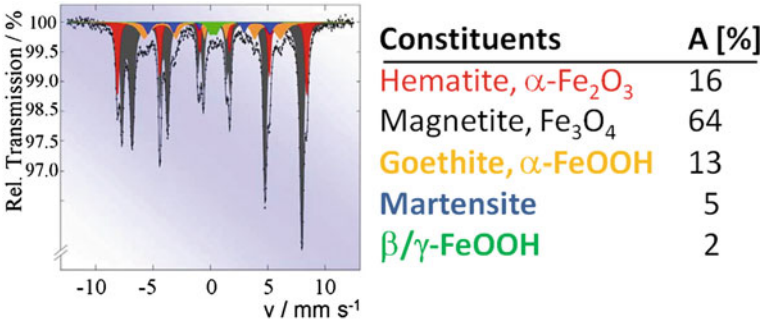

Fig. 2.43 Routine Mössbauer analysis of finely dispersed corrosion particles formed in the cooling system of a power plant [76]

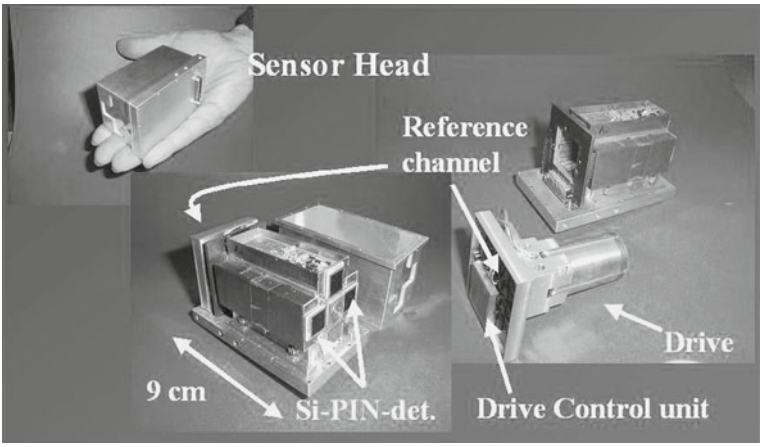

Fig. 2.44 The sensor head of the miniaturized Mössbauer spectrometer MIMOS contains the drive (vibrating) unit, the Mössbauer source, the detectors and amplification electronics. MIMOS is set up in backscattering geometry [77, 78]

transmission Mössbauer spectroscopy. The spectrum is a superposition of the spectra of five different iron-containing species with percentages given in the table on the right in Fig. 2.43. Such measurements are carried out routinely in the context of regular maintenance works in nuclear and conventional power plants.

2.3.6 Miniaturized Portable Mössbauer Spectroscopy

The miniaturization of Mössbauer instrumentation started under the guidance of E. Kankeleit at Technical University of Darmstadt and continued to completion ready for in-field-experiments by G. Klingelhöfer et al. at University of Mainz. The result is a portable miniaturized Mössbauer spectrometer (abbreviated as MIMOS) [77] as displayed in Fig. 2.44. This instrument is set up in backscattering geometry, which renders sample preparation such as the production of powders or thin slices for many applications unnecessary and thus also enables one to perform non-destructive measurements. The instrument can be taken to the field and simply placed, for example, on a rock surface of interest to be analyzed as realized by the MIMOS II instruments on the NASA Mars Exploration Rovers, which act as robotic field geologists. Another example is the analysis of rare and precious samples such as archaeological artefacts. The instrument is still developed further: Currently, for the advanced MIMOS IIa [78], the Si-PIN diode detectors are replaced by Si Drift Detectors, which have a much higher energy resolution. This result in (a) significantly improved signal-to-noise ratios and therefore shorter measurement times, and (b) allows for the simultaneous acquisition of X-Ray Fluorescence spectra for elemental analysis, whereby the ^{57}Co Mössbauer source also acts as the X-ray excitation source.

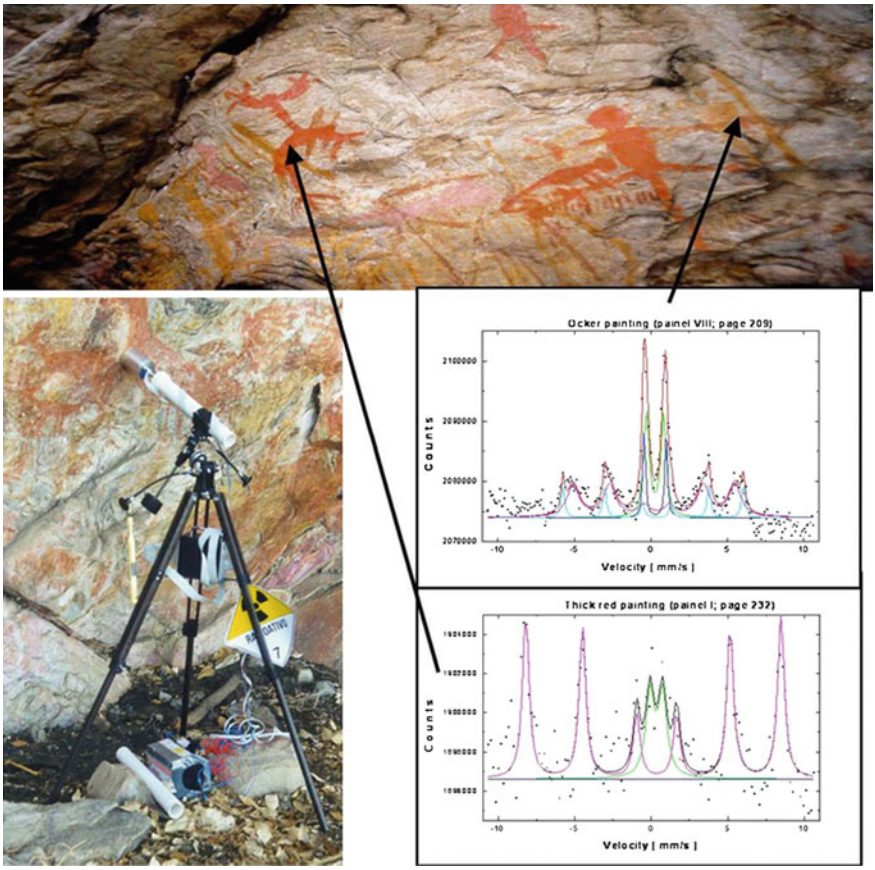

Fig. 2.45 Non-destructive analysis with MIMOS of ancient rock painting in Brazil (near Belo Horizonte). Two Mössbauer backscattering spectra were recorded, one of a darker paint, the other for a light-colored paint. Different iron oxide pigments are responsible for the different colors [80]

2.3.6.1 Archaeometric Applications

Studies of ancient ceramics became the first instance of the use of Mössbauer spectroscopy in what one commonly calls archaeometry—the application of scientific methods in studies of archaeological sites and artefacts. Changes which pottery clays undergo during firing are reflected in the Mössbauer spectra of the fired ceramics and hence can be used, even after millennia of burial, to gain information on the original firing conditions and thus on the techniques. Other areas of archaeological interest are, for example, corrosion or steel properties in iron artefacts, slags from prehistoric copper, tin and iron production, and pigments and paintings (e.g. [79], and references therein).

The portability and ability to perform non-destructive analyses with MIMOS have been exploited in the investigation of ancient rock paintings in Brazil (near Belo Horizonte, Minas Gerais, Fig. 2.45). MIMOS was mounted on a tripod and

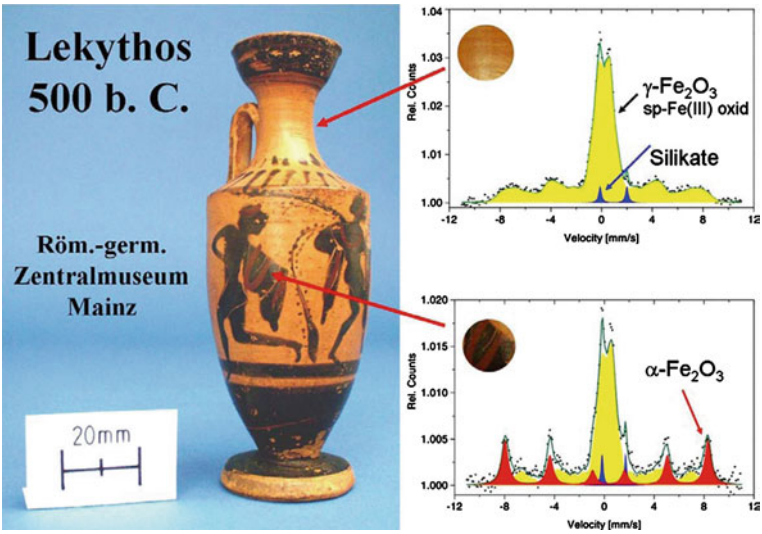

Fig. 2.46 Mössbauer backscattering spectra of a Greek lekythos vase. The different spectra taken from light and dark color positions result from different iron oxide pigments as discussed in the text [81]

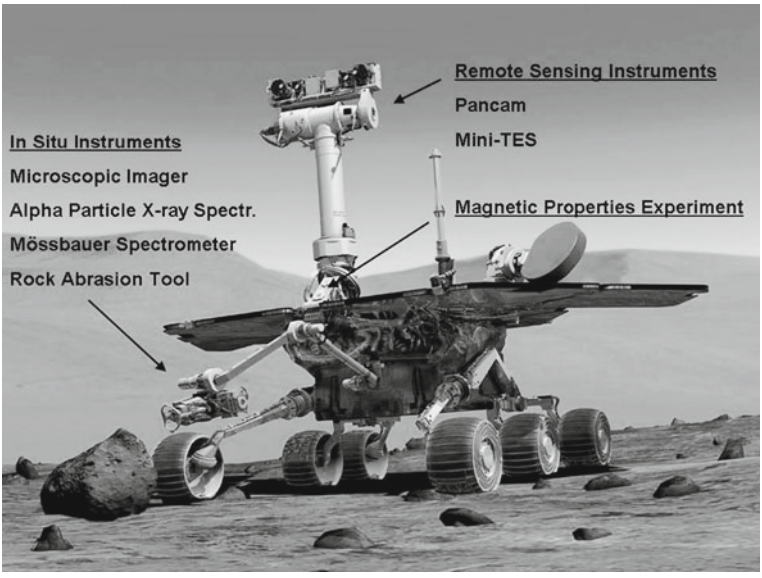

Fig. 2.47 The scientific payload of the Mars Exploration Rovers consists of the remote sensing Panoramic Camera (Pancam) and the Miniature Thermal Emission Spectrometer (*Mini-TES*); the in situ or contact instruments Microscopic Imager (*MI*), Alpha Particle X-ray Spectrometer (*APXS*), Mössbauer spectrometer (*MB*), and the Rock Abrasion Tool (*RAT*); the Magnetic Properties Experiment (NASA/JPL/Cornell) [77]

brought in contact with the painting on the wall for measurement. The two Mössbauer spectra in Fig. 2.45, one of a darker paint and the other for a light-colored paint, distinguish between different iron oxide pigments [80].

A similar application is shown in Fig. 2.46. A Greek lekythos vase was investigated non-destructively with the help of MIMOS II [81]. The unpainted surface shows a broad spectrum that can be associated with poorly crystallized iron oxides produced during the firing clay process. The painted surface shows, in addition to the characteristic spectrum of the non-painted area, a well-defined sextet corresponding to a well-crystallized hematite. The Mössbauer spectrum taken over the red painted details shows no significant difference from the non-painted surface. Therefore, the red details are presumably iron-free. However, the room-temperature analysis shows that the vase itself has a poorly crystallized iron oxide (hematite, α-Fe_2O_3, or maghemite, γ-Fe_2O_3) and some small Fe^{III} particles (intense lines in the middle of the measured spectral range). The poorly crystallized iron oxide would have been formed from heated clay minerals (e.g. Fe-rich smectites).

2.3.6.2 In Situ Mössbauer Spectroscopy on Mars

The NASA twin Mars Exploration Rovers (MER), Spirit and Opportunity, carry a MIMOS II instrument each [77] (Fig. 2.47). They were launched in June 2003 and landed successfully in January 2004 in Gusev Crater and at Meridiani Planum, respectively. Their nominal mission was only planned to be three months long, but both rovers exceeded expectations considerably and have been actively exploring the martian surface in their eight Earth year at the time of writing this paragraph (March 2011). Both Mössbauer instruments continue to work as well, although their decaying ^{57}Co sources (half-life 270 days) have resulted in significantly longer integration times necessary to obtain statistically good quality spectra than at the beginning of the mission.

The primary MER objective is to explore two sites on the Martian surface where water may once have been present, and to assess past environmental conditions at those sites and their suitability for life [82]. The Red Planet owes its color to Fe-oxides, and surface materials are enriched in Fe relative to Earth. The distribution of Fe between Fe-bearing minerals and its oxidation states constrains the primary rock type (e.g. olivine-bearing vs. non-olivine-bearing basalt), the redox conditions under which primary minerals crystallized (e.g. presence or absence of magnetite), the extent of alteration and weathering (e.g. value of Fe^{III}/Fe_{Total}), the type of alteration and weathering products (e.g. oxides vs. sulphates vs. phyllosilicates), and the processes and environmental conditions for alteration and weathering (e.g. neutral vs. acid-chloride vs. acid-sulphate aqueous process under ambient or hydrothermal conditions) [83], making ^{57}Fe Mössbauer spectroscopy an extremely useful tool for Mars exploration.

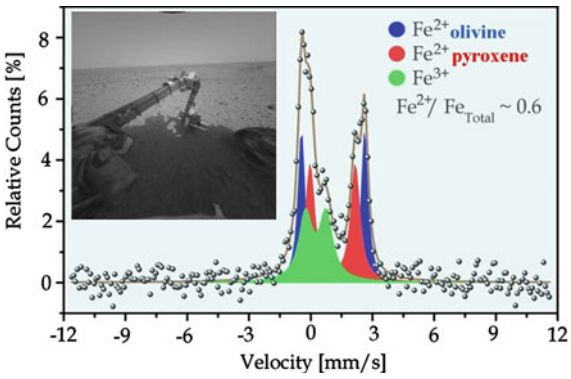

Fig. 2.48 First Mössbauer spectrum recorded on the Martian surface at Gusev crater (17th January 2004, measuring time 3 h 25 min). The inset shows a view of the Rover and of the MIMOS spectrometer operating on Mars [84, 85]

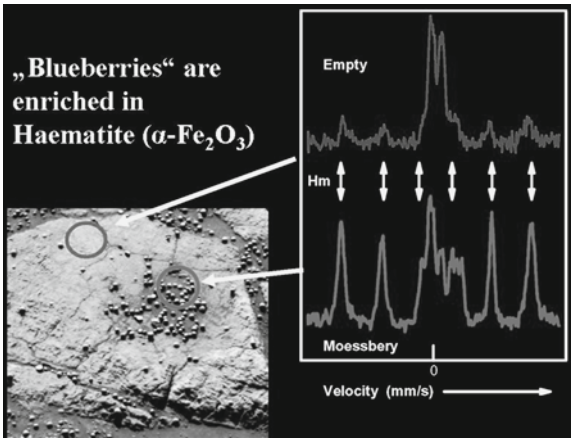

Fig. 2.49 "Blueberry"-like spherules found in *Meridiani Planum* on Mars surface were analyzed by Mössbauer spectroscopy and found to be enriched in haematite, α-Fe_2O_3 [86, 87]

The first Mössbauer spectrum recorded on the surface of Mars was obtained in the Columbia Hills of Gusev Crater [83] close to the Rover landing site (Fig. 2.48). It clearly revealed Fe^{II} containing species (olivine and pyroxene) as well as some Fe^{III} species, not yet identified at that stage. The discovery of olivine, commonly found in lava on earth, was quite informative since this mineral is known to weather to clays and iron oxides in the presence of water [84, 85].

Nests with bluish mineral spherules similar to blueberries [86, 87] (Fig. 2.49) were discovered in a region near the landing site of the Rover *Opportunity* in Meridiani Planum [88, 89]. Mössbauer spectra were recorded in places with and without such 'Blueberry' spherules. The 'blueberries' minerals were found to be enriched in haematite (α-Fe_2O_3).

One of the major discoveries of the MER mission was the identification of the mineral jarosite by Mössbauer spectroscopy in S-rich, layered outcrop rocks at Meridiani Planum [90] (Fig. 2.50). Jarosite is a ferric sulphate hydroxide whose generalized formula can be written $(K,Na,H_3O)(Fe_{3-x}Al_x)(SO_4)_2(OH)_6$, where $x < 1$. The end members $KFe_3(SO_4)_2(OH)_6$, $NaFe_3(SO_4)_2(OH)_6$, and $(H_3O)Fe_3(SO_4)_2(OH)_6$ are jarosite, natrojarosite, and hydronium jarosite, respectively. For

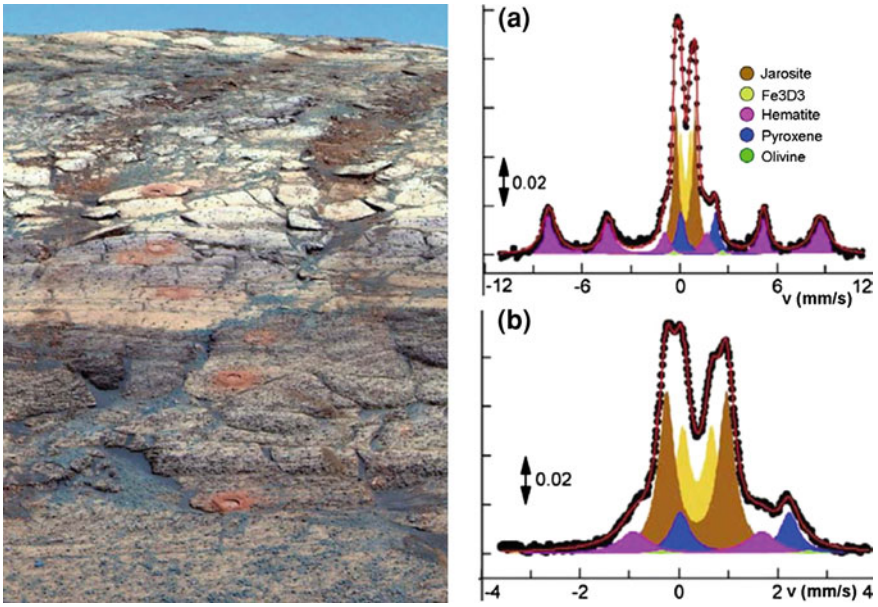

Fig. 2.50 On the left is a false color Pancam image of the 'Karatepe' section, a piece of the layered S-rich outcrop at Meridiani Planum exposed in the wall of Endurance crater. The image was obtained with Mars Exploration Rover Opportunity's Panoramic Camera (Pancam; http://marswatch.astro.cornell.edu/pancam_instrument/images/Sol173B_P2401_L257_false.jpg). One can see the tracks of the rover wheels curving down and where fresh outcrop has been exposed by the Rock Abrasion Tool (*RAT*) for analyses with the APXS and Mössbauer spectrometers. On the right are typical Mössbauer spectra of the outcrop material **a** a spectrum obtained at a velocity range of ±12 mm/s and **b** at a reduced velocity range of ±4 mm/s to increase the resolution of the central features in the spectrum where the Jarosite peaks occur. Fe_3D_3 stands for the as yet unassigned ferric mineral phase, possibly super paramagnetic hematite or $Fe(SO_4)(OH)$ [90]

jarosites, the quadrupole splitting ΔE_Q increases in the order K > Na > H_3O and with Al^{III} substitution for Fe^{III}. The ΔE_Q value for Martian jarosite is most consistent with $(K,Na)(Fe,Al)_3(SO_4)_2(OH)_6$ that is Na^+- or K^+-rich jarosite with possible Al substitution.

Jarosite is a mineralogical marker for aqueous processes because it contains the equivalent of ~10 wt. % H_2O in its structure as the OH anion. The average S-rich outcrop rock at Meridiani Planum has the equivalent of ~2 % H_2O associated with jarosite alone. An important aspect of the jarosite detection is that acidic conditions (pH < 4 at room temperature) are required for its formation. The alteration of basaltic precursor material under oxidizing, acid-sulphate conditions to form jarosite and other phases in the S-rich outcrop rocks at Meridiani Planum could have occurred under conditions provided, for example, by interactions with acid-sulphate, possibly hydrothermal waters and/or condensation of SO_2-rich volcanic emanations [91].

The past environmental conditions characterized by low pH inferred from the detection of jarosite at Meridiani Planum have implications for the suitability for life at Meridiani Planum. While microbial populations on Earth have adapted to low pH levels, they would have challenged prebiotic chemical reactions thought to have played a role in the origin of life on Earth [92].

2.4 Conclusion and Outlook

The examples of chemical applications of Mössbauer spectroscopy discussed in this Tutorial Lecture have mostly been selected from the authors' own research work and can, of course, only provide the reader with ideas about the kind of problems that can be solved with this nuclear resonance technique. Since the discovery of *recoilless nuclear resonance absorption* ("Mössbauer effect") by the german physicist Rudolf Mössbauer more than fifty years ago, Mössbauer spectroscopy has developed to a powerful tool in solid state research, making use of more than twenty "Mössbauer-active" nuclides from the list of more than fourty isotopes for which the Mössbauer effect has been observed [17]. Mössbauer spectroscopy has mostly been employed in conjunction with other physical techniques in order to gain more conclusive information in certain studies, but also in cases where certain problems could not be solved by other techniques.

Two important technical developments have recently opened new pathways in Mössbauer spectroscopy and will undoubtedly play a significant role in future: (1) The realization of a miniaturized portable Mössbauer spectrometer (MIMOS) for material characterization outside the laboratory as briefly described above, and (2) the use of synchrotron radiation for observing nuclear resonance fluorescence. The latter was initiated by E. Gerdau et al. in 1985 who proposed an unconventional Mössbauer technique using synchrotron radiation to observe nuclear resonance in two ways: Nuclear forward scattering (NFS) to study hyperfine interactions, as obtained with conventional Mössbauer spectroscopy, and nuclear inelastic scattering (NIS) to investigate local phonon spectra (partial density of states, PDOS) at the Mössbauer probe nucleus [93]. NFS and NIS, are certainly on their way to a great future [94].

Acknowledgments We thank the Deutsche Forschungsgemeinschaft, the Fonds der Chemischen Industrie and the Fonds National de la Recherche Scientifique (FNRS) for financial support.

Dedicated to Professor Wolfgang Kaim on the occasion of his 60th birthday.

Message to the Next Generation

Looking back over nearly five decades of working with Mössbauer spectroscopy in combination with other physical methods for characterizing inorganic compounds, mainly those exhibiting electronic structure phenomena, I can now state with great

satisfaction that it was an excellent decision to learn Mössbauer spectroscopy and apply it as a "forefront tool" in our research projects. I had first learned about it as a young postdoctoral fellow at Brookhaven National Laboratory in USA in the early sixties, shortly after the discovery of the "recoilless nuclear resonance absorption" by the young german physicist Rudolf L. Mössbauer, who made this magnificent discovery while he was working on his doctoral thesis at the Max Planck Institute in Heidelberg. Rudolf Mössbauer was only 32 years old when he received the Nobel in Physics in 1961. It was very fortunate for me to be accepted in a team of excellent physicists at Brookhaven National Laboratory, who had concentrated on applying the Mössbauer effect to characterize inorganic compounds and alloys by measuring the hyperfine interactions. It soon became clear that Mössbauer's unique discovery would develop rapidly to a powerful spectroscopic tool in materials science. Now, nearly five decades later, close to 100,000 published reports dealing with Mössbauer spectroscopy, many textbooks, and more than fifty international conferences, symposia and workshops held so far bear testimony to the firm establishment of this nuclear spectroscopic technique in various branches of solid state research, spreading over physics, chemistry, biology, earth- and geoscience, archaeology and industrial applications. Professor Mössbauer was an excellent speaker, and everybody was fascinated when he spoke about the experiments for his doctoral thesis that led him to the discovery of recoilless nuclear resonance absorption. Also, in many unforgettable personal conversations with him I had the pleasure to learn about details concerning his work. Such occasions never ended without discussions about piano music.

During the many years of my teaching spectroscopy in chemistry and physics, Mössbauer spectroscopy has always been my favourite for several reasons: The students become familiar with fundamental aspects on solid state and experimental physics, cry physics, quantum mechanics and theoretical chemistry to name a few. I consider it therefore highly recommendable, even necessary, that Mössbauer spectroscopy and relevant neighbouring fields are always part of the education in physics and chemistry.

Mössbauer spectroscopy has undoubtedly established as an elegant and versatile tool in materials science, mostly in conjunction with other physical techniques in order to reach deeper and more conclusive information in certain studies, but also in cases where certain problems could not be solved with other techniques. Quo vadis, Mössbauer effect research? Two outstanding developments have opened new pathways in Mössbauer spectroscopy and will definitely play a remarkable role in future: Without quality ranking, (1) the instrumental progress regarding the miniaturization of a Mössbauer spectrometer (MIMOS), and (2) the use of synchrotron radiation for observing nuclear resonance fluorescence. MIMOS has most spectacularly demonstrated its usefulness for extraterrestrial studies, viz. the NASA missions to the planet Mars. There are, of course, also hundreds of possibilities to use it on earth in mobile analytical studies outside the laboratory. A real breakthrough in Mössbauer spectroscopy research was initiated by E. Gerdau et al. in 1985 who proposed an unconventional Mössbauer technique based on the possibility to use synchrotron radiation to observe nuclear resonance.

Nuclear forward scattering (NFS) allows to study hyperfine interactions, as obtained with conventional Mössbauer spectroscopy; nuclear inelastic scattering (NIS) allows to investigate local phonon spectra (partial density of states, PDOS) at the Mössbauer probe nucleus. Compared, for instance, to Raman spectroscopy, NIS can achieve a higher resolution without perturbation of surrounding vibrations. Both synchrotron radiation techniques, NFS and NIS, are certainly on their way to a great future.

References

1. R.L. Mössbauer, Fluorescent nuclear resonance of γ-radiation in Iriridium-191. Z. Physik **151**, 124–143 (1958)
2. R.L. Mössbauer, Kernresonanzabsorption von gammastrahlung in Ir^{191}. Naturwissenschaften **45**, 538–539 (1958)
3. R.L. Mössbauer, Recoiless nuclear resonance absorption of γ-radiation. Science **137**, 731–738 (1962)
4. R.L. Mössbauer, The discovery of the Mössbauer effect. Hyperfine Interact. **126**, 1–12 (2000)
5. O.C. Kistner, A.W. Sunyar, Evidence for quadrupole interaction of Fe^{57m}, and influence of chemical binding on nuclear γ-ray energy. Phys. Rev. Lett. **4**, 412–415 (1960)
6. V.I. Goldanskii, R. Herber (eds.), *Chemical Applications of Mössbauer Spectroscopy* (Academic, New York, 1968)
7. N.N. Greenwood, T.C. Gibb, *Mössbauer Spectroscopy* (Chapman and Hall, London, 1971)
8. U. Gonser (ed.), *Mössbauer Spectroscopy, in Topics in Applied Physics*, vol. 5 (Springer, Berlin, 1975)
9. T.C. Gibb, *Principles of Mössbauer Spectroscopy* (Wiley, New York, 1976)
10. P. Gütlich, R. Link, A.X. Trautwein, *Mössbauer Spectroscopy and Transition Metal Chemistry. Inorganic Chemistry Concepts Series*, vol. 3, 1st edn. (Springer, Berlin, 1978)
11. G.J. Long, *Mössbauer Spectroscopy Applied to Inorganic Chemistry, Modern Inorganic Chemistry Series*, vol. 1 (Plenum, New York, 1984)
12. R.H. Herber, *Chemical Mössbauer Spectroscopy* (Plenum, New York, 1984)
13. G.J. Long, *Mössbauer Spectroscopy Applied to Inorganic Chemistry, Modern Inorganic Chemistry Series*, vol. 2 (Plenum, New York, 1989)
14. G.J. Long, F. Grandjean, *Mössbauer Spectroscopy Applied to Inorganic Chemistry, Modern Inorganic Chemistry Series*, vol. 3 (Plenum, New York, 1989)
15. G.J. Long, F. Grandjean, *Mössbauer Spectroscopy Applied to Magnetism and Materials Science*, vol. 1 (Plenum, New York, 1993)
16. G.J. Long, F. Grandjean, *Mössbauer Spectroscopy Applied to Magnetism and Materials Science*, vol. 2 (Plenum, New York, 1996)
17. P. Gütlich, E. Bill, A.X. Trautwein, (Mössbauer Spectroscopy and Transition Metal Chemistry, Springer, 2011)
18. N.E. Erickson, A.W. Fairhall, Mössbauer spectra of iron in $Na_2[Fe(CO)_4]$ and $Na[Fe_3(CO)_{11}H]$ and comments regarding the structure of $Fe_3(CO)_{12}$. Inorg. Chem. **4**, 1320–1322 (1965)
19. R. Greatrex, N.N. Greenwood, Mössbauer spectra, structure, and bonding in iron carbonyl derivatives. Discuss. Faraday Soc. **47**, 126–135 (1969)
20. E. Müller, Berlin blue and Turnbull's blue. Chemik. Zeit. **38**, 281–282 (1914)
21. E. Fluck, W. Kerler, W. Neuwirth, Der Mößbauer-Effekt und seine bedeutung für die chemie. Angew. Chem. **75**, 461–472 (1963)
22. K. Maer Jr, M.L. Beasley, R.L. Collins, W.O. Milligan, Structure of the titanium-iron cyanide complexes. J. Am. Chem. Soc. **90**, 3201–3208 (1968)

23. P. Gütlich, A. Hauser, H. Spiering, Thermal and optical switching of iron(II) complexes. Angew. Chem. Int. Ed. Engl. **33**, 2024–2054 (1994)
24. P. Gütlich, Y. Garcia, H.A. Goodwin, Spin crossover phenomena in Fe(II) complexes. Chem. Soc. Rev. **29**, 419–427 (2000)
25. P. Gütlich, H.A. Goodwin (eds.), Spin crossover in transition metal compounds. Top. Curr. Chem. 233–235 (2004)
26. S. Decurtins, P. Gütlich, C.P. Köhler, H. Spiering, A. Hauser, Light-induced excited spin state trapping in a transition-metal complex: the hexa-1-propyltetrazole-iron(II) tetrafluoroborate spin crossover system. Chem. Phys. Lett. **105**, 1–4 (1984)
27. I. Dezsi, B. Molnar, T. Tarnoczi, K. Tompa, On the magnetic behaviour of iron(II)-bis-(1,10 phenantroline)-thiocyanate between −190° and 30° C. J. Inorg. Nucl. Chem **29**, 2486–2490 (1967)
28. E.W. Müller, J. Ensling, H. Spiering, P. Gütlich, High-spin ↔ low-ST in hexacoordinate complexes of iron(II) with monodentate 1-alkyltetrazole ligands: a variable-temperature Mössbauer, magnetic susceptibility, and far-infrared study. Inorg. Chem. **22**, 2074–2078 (1983)
29. A. Hauser, Reversibility of light-induced excited spin state trapping in the $[Fe(ptz)_6](BF_4)_2$, and the $[Zn_{1-x}Fe_x(ptz)_6](BF_4)_2$ spin crossover systems. Chem. Phys. Lett. **124**, 543–548 (1986)
30. L. Wiehl, Structures of hexakis(1-propyltetrazole)iron(II) bis(tetrafluoroborate), $[Fe(CHN_4C_3H_7)_6](BF_4)_2$, hexakis(1-methyltetrazole)iron(II) bis(tetrafluoroborate), $[Fe(CHN_4CH_3)_6](BF_4)_2$, and the analogous perchlorates. Their relation to spin crossover behaviour and comparison of Debye-Waller factors from structure determination and Mössbauer spectroscopy. Acta Cryst. B **49**, 289–303 (1993)
31. P. Poganiuch, S. Decurtins, P. Gütlich, Thermal- and light-induced spin transition in $[Fe(mtz)_6](BF_4)_2$: first successful formation of a metastable low-spin state by irradiation with light at low temperatures. J. Am. Chem. Soc. **112**, 3270–3278 (1990)
32. G. De Munno, M. Julve, J.A. Real, F. Lloret, R. Scopelliti, Synthesis, crystal structure and magnetic properties of the chiral iron(II) chain $[Fe(bpym)(NCS)_2]_n$ (bpym = 2,2′-bipyrimidine). Inorg. Chim. Acta **250**, 81–85 (1996)
33. V. Ksenofontov, A.B. Gaspar, J.A. Real, P. Gütlich, Pressure-induced spin state conversion in antiferromagnetically coupled Fe(II) dinuclear complexes. J. Phys. Chem. B **105**, 12266–12271 (2001)
34. V. Ksenofontov, H. Spiering, S. Reiman, Y. Garcia, A.B. Gaspar, N. Moliner, J.A. Real, P. Gütlich, Direct monitoring of spin state in dinuclear iron(II) coordination compounds. Chem. Phys. Lett. **348**, 381–386 (2001)
35. V. Ksenofontov, H. Spiering, S. Reiman, Y. Garcia, A.B. Gaspar, J.A. Real, P. Gütlich, Determination of spin state in dinuclear iron(II) coordination compounds using applied field Mössbauer spectroscopy. Hyperfine Interact. **141/142**, 47–52 (2002)
36. R. Zimmermann, G. Ritter, H. Spiering, Mössbauer spectra of the tetrakis-(1,8-naphthyridine) iron(II) perchlorate in external magnetic fields. Evidence of slow relaxation ln paramagnetic iron(II). Chem. Phys. **4**, 133–141 (1974)
37. R. Zimmermann, G. Ritter, H. Spiering, D.L. Nagy, A further example of slow relaxation in high-spin iron(II) compounds: $Fe(papt)_2 \bullet C_6H_6$. J. Phys. **35-C6**, 439 (1974)
38. V. Ksenofontov, A.B. Gaspar, V. Niel, S. Reiman, J.A. Real, P. Gütlich, On the nature of the plateau in two-step dinuclear spin crossover complexes. Chem. Eur. J. **10**, 1291–1298 (2004)
39. Klingele, M. H., Moubaraki, B., Cashion, J. D., Murray, K. S., Brooker, S.: The first X-ray crystal structure determination of a dinuclear complex trapped in the [LS-HS] state $\left[Fe_2^{II}(PMAT)_2\right](BF_4)_4$:·DMF. Chem. Comm. 8, 987-989 (2005)
40. Y. Garcia, C.M. Grunert, S. Reiman, O. van Campenhoudt, Gütlich P (2006) The two-step spin conversion in a supramolecular triple helicate dinuclear iron(II) complex studied by Mössbauer spectroscopy. Eur. J. Inorg. Chem. **17**, 3333–3339 (2006)
41. C.M. Grunert, S. Reiman, H. Spiering, J.A. Kitchen, S. Brooker, P. Gütlich, Mixed spin-state [HS–LS] pairs in a dinuclear spin transition complex: confirmation by variable-temperature ^{57}Fe Mössbauer Spectroscopy. Angew. Chem. Inter. Ed. **47**, 2997–2999 (2008)

42. J.J.A. Kolnaar, G. vanDijk, H. Kooijman, A.L. Spek, V.G. Ksenofontov, P. Gütlich, J.G. Haasnoot, J. Reedijk, Synthesis, structure, magnetic behavior, and Mössbauer spectroscopy of two new iron(II) spin transition compounds with the ligand 4-Isopropyl-1,2,4-triazole. X-ray structure of $[Fe_3(4\text{-isopropyl-}1,2,4\text{-triazole})_6(H_2O)_6](\text{tosylate})_6{\cdot}2H_2O$. Inorg. Chem. **36**, 2433–2440 (1997)
43. Y. Garcia, P. Guionneau, G. Bravic, D. Chasseau, J.A.K. Howard, O. Kahn, V. Ksenofontov, S. Reiman, P. Gütlich, Synthesis, crystal structure, magnetic properties and ^{57}Fe Mossbauer spectroscopy of the new trinuclear $[Fe_3(4\text{-}(2'\text{-hydroxyethyl})\text{-}1,2,4\text{-triazole})_6(H_2O)_6](CF_3SO_3)_6$ spin crossover compound. Eur. J. Inorg. Chem. **7**, 1531–1538 (2000)
44. M. Ruben, E. Breuning, J.M. Lehn, V. Ksenofontov, F. Renz, P. Gütlich, G.B.M. Vaughan, Supramolecular Spintronic Devices: Spin transitions and magnetostructural correlations in $[Fe^{II}_4L_4]^{8+}$ [2 × 2]-grid-type complexes. Chem. Eur. J. **9**, 4422–4429 (2003)
45. E. Breuning, M. Ruben, J.-M. Lehn, F. Renz, Y. Garcia, V. Ksenofontov, P. Gütlich, E. Wegelius, K. Rissanen, Spin crossover in a supramolecular Fe^{II}_4 [2x2] grid triggered by temperature, pressure, and light. Angew. Chem. Inter. Ed. **39**, 2504–2507 (2000)
46. J.J.A. Kolnaar, M.I. de Heer, H. Kooijman, A.L. Spek, G. Schmitt, V. Ksenofontov, P. Gütlich, J.G. Haasnoot, J. Reedijk, Synthesis, structure and properties of a mixed mononuclear/dinuclear iron(II) spin crossover compound with the ligand 4-(p-tolyl)-1,2,4-triazole. Eur. J. Inorg. Chem. **5**, 881–886 (1999)
47. Y. Galyametdinov, V. Ksenofontov, A. Prosvirin, I. Ovchinnikov, G. Ivanova, P. Gütlich, W. Haase, First example of coexistence of thermal spin transition and liquid-crystal properties. Angew. Chem. Int. Ed. **40**, 4269–4271 (2001)
48. T. Fujigaya, D.L. Jiang, T. Aida, Switching of spin states triggered by a phase transition: spin-crossover properties of self-assembled iron(II) complexes with alkyl-tethered triazole ligands. J. Am. Chem. Soc. **125**, 14690–14691 (2003)
49. S. Hayami, K. Danjobara, K. Inoue, Y. Ogawa, N. Matsumoto, Y. Maeda, A photoinduced spin transition iron(II) complex with liquid-crystal properties. Adv. Mater. **16**, 869–872 (2004)
50. S. Hayami, R. Moriyama, A. Shuto, Y. Maeda, K. Ohta, K. Inoue, Spin transition at the mesophase transition temperature in a cobalt(II) compound with branched alkyl chains. Inorg. Chem. **46**, 7692–7694 (2007)
51. S. Hayami, N. Motokawa, A. Shuto, N. Masuhara, T. Someya, Y. Ogawa, K. Inoue, Y. Maeda, Photoinduced spin transition for iron(II) compounds with liquid-crystal properties. Inorg. Chem. **46**, 1789–1794 (2007)
52. M. Seredyuk, A.B. Gaspar, V. Ksenofontov, Y. Galyametdinov, J. Kusz, P. Gütlich, Iron(II) metallomesogens exhibiting coupled spin state and liquid crystal phase transitions near room temperature. Adv. Funct. Mater. **18**, 2089–2101 (2008)
53. M. Seredyuk, A.B. Gaspar, V. Ksenofontov, Y. Galyametdinov, M. Verdaguer, F. Villain, P. Gütlich, One-dimensional iron(II) compounds exhibiting spin crossover and liquid crystalline properties in the room temperature region. Inorg. Chem. **47**, 10232–10245 (2008)
54. M. Seredyuk, A.B. Gaspar, V. Ksenofontov, Y. Galyametdinov, J. Kusz, P. Gütlich, Does the solid–liquid crystal phase transition provoke the spin-state change in spin-crossover metallomesogens? J. Am. Chem. Soc. **130**, 1431–1439 (2008)
55. M. Seredyuk, A.B. Gaspar, V. Ksenofontov, S. Reiman, Y. Galyametdinov, W. Haase, E. Rentschler, P. Gütlich, Room temperature operational thermochromic liquid crystals. Chem. Mater. **18**, 2513–2519 (2006)
56. M. Seredyuk, A.B. Gaspar, V. Ksenofontov, S. Reiman, Y. Galyametdinov, W. Haase, E. Rentschler, P. Gütlich, Multifunctional materials exhibiting spin crossover and liquid-crystalline properties. Interplay between spin crossover and liquid-crystal properties in iron(II) coordination complexes. Hyperfine Interact. **166**, 385–390 (2006)
57. A.B. Gaspar, M. Seredyuk, P. Gütlich, Spin crossover in metallomesogens. Coord. Chem. Rev. **253**, 2399–2413 (2009)
58. Y. Garcia, P.J. Van Koningsbruggen, R. Lapouyade, L. Fournes, L. Rabardel, O. Kahn, V. Ksenofontov, G. Levchenko, P. Gütlich, Influences of temperature, pressure, and lattice solvents on the spin transition regime of the polymeric compound $[Fe(hyetrz)_3]A_2{\cdot}3H_2O$

(hyetrz = 4-(2′-hydroxyethyl)-1,2,4-triazole and A^- = 3-nitrophenylsulfonate). Chem. Mater. **10**, 2426–2433 (1998)
59. P. Gütlich, Nuclear decay induced excited spin state trapping (NIESST). Top. Curr. Chem. **234**, 231–260 (2004)
60. R. Grimm, P. Gütlich, E. Kankeleit, R. Link, Time and temperature dependence of aftereffects in $[^{57}Co(phen)_3](ClO_4)_2{\cdot}2H_2O$ from time-differential Mössbauer emission spectroscopy. J. Chem. Phys. **67**, 5491 (1977)
61. R. Albrecht, M. Alfen, P. Gütlich, Z. Kajcsos, R. Schulze, H. Spiering, F. Tuczek, A new spectrometer for time-differential Mössbauer emission spectroscopy (TDMES). Nucl. Instr. Methods **257**, 209–214 (1987)
62. J. Ensling, B.W. Fitzsimmons, P. Gütlich, K.M. Hasselbach, Anomalous spin states of iron(II) in $[Fe(phen)_3](ClO_4)_2{\cdot}2H_2O$. Angew. Chem. Int. Ed. **9**, 637 (1970)
63. H. Sano, P. Gütlich, Hot atom chemistry in relation to Mössbauer emission spectroscopy, in *Hot Atom Chemistry*, ed. by T. Matsuura (Kodansha Ltd., Tokyo, 1984), p. 26
64. J. Ensling, P. Gütlich, K.M. Hasselbach, B.W. Fitzsimmons, Anomalous spin states of iron(II) in ^{57}Fe Mössbauer emission spectra of $[^{57}Co(phen)_2(NCS)_2]$ and $[^{57}Co(bipy)_2(NCS)_2]$(cis). Chem. Phys. Lett. **42**, 232–236 (1976)
65. A. Oshio, H. Spiering, V. Ksenofontov, F. Renz, P. Gütlich, Electronic relaxation phenomena following $^{57}Co(EC)^{57}Fe$ nuclear decay in $[Mn^{II}(terpy)_2](ClO_4)_2{\cdot}1/2H_2O$ and in the spin crossover complexes $[Co^{II}(terpy)_2]X_2{\cdot}nH_2O$ (X = Cl and ClO_4): a Mössbauer emission spectroscopic study. Inorg. Chem. **40**, 1143–1150 (2001)
66. S. Iijima, R. Saida, I. Motoyama, H. Sano, The temperature dependence of the trapped and averaged-valence state in mono-oxidized dialkylbiferrocenes. Bull. Chem. Soc. Jpn. **54**, 1375–1379 (1981)
67. M.J. Cohn, M.D. Timken, D.N. Hendrickson, Mössbauer spectroscopy of mixed-valence biferrocenes in high magnetic fields. J. Am. Chem. Soc. **106**, 6683–6689 (1984)
68. C.C. Wu, H.G. Jang, A.L. Rheingold, P. Gütlich, D.N. Hendrickson, Solvate molecule effects and unusual ^{57}Fe Mössbauer line broadening in the valence detrapping of mixed-valence $[Fe_3O(O_2CCH_3)_6(3\text{-Et-py})_3]{\cdot}S$. Inorg. Chem. **35**, 4137–4147 (1996)
69. T. Glaser, T. Beissel, E. Bill, T. Weyhermüller, V. Schünemann, W. Meyer-Klaucke, A.X. Trautwein, K. Wieghardt, Electronic structure of linear thiophenolate-bridged heterotrinuclear complexes [LFeMFeL]n + (M = Cr, Co., Fe; n = 1–3): localized vs delocalized models. J. Am. Chem. Soc. **121**, 2193–2208 (1999)
70. V. Ksenofontov, H.C. Kandpal, J. Ensling, M. Waldeck, D. Johrendt, A. Mewis, P. Gütlich, C. Felser, Verwey type transition in EuNiP. Europhys. Lett. **74**, 672–678 (2006)
71. O. Kahn, *Molecular Magnetism* (VCH Publishers Inc, Weinheim, 1993)
72. J.S. Miller, M. Drillon (eds.), *Magnetism: Molecules to Materials*, vol. I–III (Wiley, Weinheim, 2001)
73. V. Ksenofontov, G. Levchenko, S. Reiman, P. Gutlich, A. Bleuzen, V. Escax, M. Verdaguer, Pressure-induced electron transfer in ferrimagnetic Prussian blue analogs. Phys. Rev. B **68**, 024415 (2003)
74. W.M. Reiff, A.M. LaPointe, E. Witten, Virtual free ion magnetism and the absence of Jahn–Teller distortion in a linear two-coordinate complex of high-spin iron(II). J. Am. Chem. Soc. **126**, 10206–10207 (2004)
75. A.M. LaPointe, $Fe[C(SiMe_3)_3]_2$: synthesis and reactivity of a monomeric homoleptic iron(II) alkyl complex Inorg. Chim. Acta **345**, 359–362 (2003)
76. J. Ensling, P. Gütlich, Laboratory Report, University of Mainz, 1985; Gütlich, P., Schröder, C.: Mössbauer spectroscopy. Bunsen-Magazin **1**, 4–22 (2010)
77. G. Klingelhöfer, R.V. Morris, B. Bernhardt, D. Rodionov, P.A. de Souza Jr, S.W. Squyres, J. Foh, E. Kankeleit, U. Bonnes, R. Gellert, C. Schröder, S. Linkin, E. Evlanov, B. Zubkov, O. Prilutski, The Athena MIMOS II Mössbauer spectrometer investigation. J. Geophys. Res. **108**, 8067 (2003)
78. G. Klingelhöfer, D. Rodionov, M. Blumers, L. Strüder, P. Lechner, B. Bernhardt, H. Henkel, I. Fleischer, C. Schröder, J. Girones Lopez, G. Studlek, J. Maul, J. Fernandez-Sanchez, C.

d'Uston, The advanced miniaturised Mössbauer spectrometer MIMOS IIa: increased sensitivity and new capability for elemental analysis. Lunar Planet. Sci. **39**, 2379 (2008)
79. E. Wagner, A. Kyek, Mössbauer spectroscopy in archaeology: introduction and experimental considerations. Hyperfine Interact. **154**, 5–33 (2004)
80. G. Klingelhöfer, G.M. da Costa, A. Prous, B. Bernhardt, Rock paintings from Minas Gerais, Brasil, investigated by in situ Mössbauer spectroscopy. Hyperfine. Interact. C **5**, 423–426 (2002)
81. P.A. de Souza Jr, B. Bernhardt, G. Klingelhöfer, P. Gütlich, Surface analysis in archaeology using the miniaturized Mössbauer spectrometer MIMOS II. Hyperfine Interact. **151**, 125–130 (2003)
82. S.W. Squyres, R.E. Arvidson, E.T. Baumgartner, J.F. Bell III, P.R. Christensen, S. Gorevan, K.E. Herkenhoff, G. Klingelhöfer, M.B. Madsen, R.V. Morris, R. Rieder, R.A. Romero, Athena Mars rover science investigation. J. Geophys. Res. **108**, 8062 (2003)
83. S.W. Squyres, R.E. Arvidson, J.F. Bell III, J. Brückner, N.A. Cabrol, W. Calvin, M.H. Carr, P.R. Christensen, B.C. Clark, L. Crumpler, D.J. Des Marais, C. d'Uston, T. Economou, J. Farmer, W. Farrand, W. Folkner, M. Golombek, S. Gorevan, J.A. Grant, R. Greeley, J. Grotzinger, L. Haskin, K.E. Herkenhoff, S. Hviid, J. Johnson, G. Klingelhöfer, A. Knoll, G. Landis, M. Lemmon, R. Li, M.B. Madsen, M.C. Malin, S.M. McLennan, H.Y. McSween, D.W. Ming, J. Moersch, R.V. Morris, T. Parker, J.W. Rice Jr, L. Richter, R. Rieder, M. Sims, M. Smith, P. Smith, L.A. Soderblom, R. Sullivan, H. Wänke, T. Wdowiak, M. Wolff, A. Yen, The spirit Rover's Athena science investigation at Guser crater, Mars. Science **305**, 794–799 (2004)
84. G. Klingelhöfer, E. De Grave, R.V. Morris, A. Alboom, V.G. Resende, P.A. Souza Jr, D. Rodionov, C. Schroeder, D.W. Ming, A. Yen, Mössbauer spectroscopy on Mars: goethite in the Columbia Hills at Gusev crater. Hyperfine Interact. **166**, 549 (2006)
85. R.V. Morris, G. Klingelhöfer, B. Bernhardt, C. Schröder, D.S. Rodionov, P.A. Jr de Souza, A. Yen, R. Gellert, E.N. Evlanov, J. Foh, E. Kankeleit, P. Gütlich, D.W. Ming, F. Renz, T. Wdowiak, S.W. Squyres, R.E. Arvidson, Mineralogy at Gusev crater from the Mössbauer spectrometer on the spirit rover. Science **305**, 833–836 (2004)
86. S.W. Squyres, R.E. Arvidson, J.F. Bell III, J. Brückner, N.A. Cabrol, W. Calvin, M.H. Carr, P.R. Christensen, B.C. Clark, L. Crumpler, D.J. Des Marais, C. d'Uston, T. Economou, J. Farmer, W. Farrand, W. Folkner, M. Golombek, S. Gorevan, J.A. Grant, R. Greeley, J. Grotzinger, L. Haskin, K.E. Herkenhoff, S. Hviid, J. Johnson, G. Klingelhöfer, A.H. Knoll, G. Landis, M. Lemmon, R. Li, M.B. Madsen, M.C. Malin, S.M. McLennan, H.Y. McSween, D.W. Ming, J. Moersch, R.V. Morris, T. Parker, J.W. Rice Jr, L. Richter, R. Rieder, M. Sims, P. Smith, L.A. Soderblom, R. Sullivan, H. Wänke, T. Wdowiak, M. Wolff, A. Yen, The opportunity rover's Athena science investigation at Meridiani planum, Mars. Science **306**, 1698–1703 (2004)
87. L.A. Soderblom, R.C. Anderson, R.E. Arvidson, J.F. Bell III, N.A. Cabrol, W. Calvin, P.R. Christensen, B.C. Clark, T. Economou, B.L. Ehlmann, W.H. Farrand, D. Fike, R. Gellert, T.D. Glotch, M.P. Golomber, R. Greeley, J. Grotzinger, K.E. Herkenhoff, D.J. Jerolmack, J.R. Johnson, B. Joliff, G. Klingelhöfer, A.H. Knoll, Z.A. Learner, R. Li, M.C. Malin, S.M. McLennan, H.Y. McSween, D.W. Ming, R.V. Morris, J.W. Rice Jr, L. Richter, R. Rieder, D. Rodionov, C. Schröder, F.P. Seelos IV, J.M. Soderblom, S.W. Squyres, R. Sullivan, W.A. Watters, C.M. Weitz, M.B. Wyatt, A. Yen, J. Zipfel, Soils of Eagle crater and Meridiani planum at the opportunity rover landing site. Science **306**, 1723–1726 (2004)
88. S.W. Squyres, J.P. Grotzinger, R.E. Arvidson, J.F. Bell III, W. Calvin, P.R. Christensen, B.C. Clark, J.A. Crisp, W.H. Farrand, K.E. Herkenhoff, J.R. Johnson, G. Klingelhöfer, A.H. Knoll, S.M. McLennan, H.Y. McSween Jr, R.V. Morris, J.W. Rice Jr, R. Rieder, L.A. Soderblom, In situ evidence for an ancient aqueous environment at Meridiani planum, Mars. Science **306**, 1709–1714 (2004)
89. S.W. Squyres, A.H. Knoll, R.E. Arvidson, B.C. Clark, J.P. Grotzinger, B.L. Jolliff, S.M. McLennan, N. Tosca, J.F. Bell III, W. Calvin, W.H. Farrand, T.D. Glotch, M.P. Golombek, K.E. Herkenhoff, J.R. Johnson, G. Klingelhöfer, H.Y. McSween, A.S. Yen, Two years at Meridiani planum: results from the opportunity rover. Science **313**, 1403–1407 (2006)

90. G. Klingelhöfer, R.V. Morris, B. Bernhardt, C. Schroeder, D.S. Rodionov, P.A. Jr de Souza, A. Yen, R. Gellert, E.N. Evlanov, B. Zubkov, J. Foh, U. Bonnes, E. Kankeleit, P. Gütlich, D.W. Ming, F. Renz, T. Wdowiak, S.W. Squyres, R.E. Arvidson, Jarosite and hematite at Meridiani Planum from Opportunity's Mossbauer spectrometer. Science **306**, 1740–1745 (2004)
91. R.V. Morris, G. Klingelhöfer, C. Schröder, D.S. Rodionov, A. Yen, D.W. Ming, P.A. De Souza Jr, T. Wdowiak, I. Fleischer, R. Gellert, B. Bernhardt, U. Bonnes, B.A. Cohen, E.N. Evlanov, J. Foh, P. Gütlich, E. Kankeleit, T. McCoy, D.W. Mittlefehldt, F. Renz, M.E. Schmidt, B. Zubkov, S.W. Squyres, R.E. Arvidson, Mössbauer mineralogy of rock, soil, and dust at Meridiani Planum. Mars: Opportunity's journey across sulfate-rich outcrop, basaltic sand and dust, and hematite lag deposits. J. Geophys. Res. **111**, 1215 (2006)
92. A.H. Knoll, M. Carr, B. Clark, D.J. Des Marais, J.D. Farmer, W.W. Fischer, J.P. Grotzinger, S.M. McLennan, M. Malin, C. Schröder, S. Squyres, N.J. Tosca, T. Wdowiak, An astrobiological perspective on Meridiani Planum. Earth Planet. Sci. Lett. **240**, 179–189 (2005)
93. E. Gerdau, R. Rüffer, H. Winkler, W. Tolksdorf, C.P. Klages, J.P. Hannon, Nuclear Bragg diffraction of synchrotron radiation in yttrium iron garnet. Phys. Rev. Lett. **54**, 835–838 (1985)
94. P. Gütlich, Y. Garcia, Mössbauer spectroscopy: elegance and versatility in chemical diagnostics. J. Phys. Conf. Ser. **217**, 012001 (2010)

Curriculum Vitae

Philipp Gütlich, Professor Dr.-Ing.
Born August 5th, 1934 in Rüsselsheim/Germany Married, 2 children

1941–1946 Elementary School in Rüsselsheim and Karben (Germany)

1946–1955 High school (Gymnasium) in Rüsselsheim

1955–1961 Technische Hochschule Darmstadt (Inorganic, Organic, Analytical, Technical and Physical Chemistry, Physics, Mathematics) Diplom-Ingenieur "Mit Auszeichnung" Master's thesis in Physical Inorganic Chemistry Academic Prize of Technical University of Darmstadt for best thesis

1961–1963 Ph.D. thesis "Surface Investigations Using the BET-Method and Heterogeneous Isotope Exchange on Barium Sulfate", Ph.D."Mit Auszeichnung"

1964 Postdoctoral research stay at "Centre d'Etudes Nucléaires à Saclay in France (Paris), 6 months

1964–1965	Postdoctoral research stay in Brookhaven National Laboratory (USA), work on Mössbauer spectroscopy of transition metal compounds
1966	Return to Technische Hochschule Darmstadt, research work towards "Habilitation" ("Applications of Mössbauer Spectroscopy in Inorganic Chemistry")
1976–1970	Participation in Theoretical Chemistry Schools C.A. Coulson (Oxford), P.O. Löwdin (Uppsala), H. Hartmann (Frankfurt)
1969	Habilitation in Inorganic Chemistry and Nuclear Chemistry
1972	Professor of Theoretical Inorganic Chemistry at Technische Hochschule Darmstadt
1974	2 offers for Full-Professorships a) Chair of Inorganic and Analytical Chemistry, University of Mainz b) Chair of Theoretical Inorganic Chemistry, University of Hamburg
1975	Professorship at Mainz University accepted
1989-1991	Dean of the Department of Chemistry and Pharmacy
1996-2001	Director of the Institute of Inorganic and Analytical Chemistry
April 2001	Professor Emeritus

Memberships

Gesellschaft Deutscher Chemiker
Bunsengesellschaft für Physikalische Chemie
Deutsche Gesellschaft für Metallkunde (until 2001)
Deutsche Physikalische Gesellschaft
American Chemical Society (for ca. 30 years, until 2001)
Chemical Society of London (for ca. 30 years, until 2001)

Guestprofessorships

University of Geneva and Bern in Switzerland (1985)
University of Lima/Peru (for UNESCO, 1985)
Tamkang University Taipei (1986)
University of Louvain-la-Neuve/Belgium (1991)
University of Fribourg/Switzerland (1994)
Ochanomizu University Tokyo (1994)
Université Pierre et Marie Curie, Paris (1997)
Vienna University of Technology (1998)
Toho University Tokyo (2007)

Awards and Honors

1961 Academic Prize of Technische Hochschule Darmstadt
1964 Fellowship of German Gouvernment for research stay in France
1965 Fellowship of Volkswagen-Foundation for research stay in USA
1989 Research Award of Japanese Society for the Promotion of Science
1993 Max Planck Research Award
2002 Honorary Member of the Internat. Board on the Applications of the Müssbauer Effect
2002 Foreign Member of the Russian Academy of Natural Science
2003 Honorary Doctor and Professor of the University of Budapest
2007 Member of Academia Europaea
2007 Honorary Doctor of Toho-University Tokyo

Teaching Experience

- Physical Methods in (Inorganic) Chemistry
- Theoretical Inorganic Chemistry

– Introduction to Quantum Mechanics
– Electrons in Atoms and Molecules
– Ligand Field Theory
– Molecular Orbital Theory
– Group Theory

- Coordination Chemistry
- Magnetochemistry

Research Fields

- Electronic structure (static and dynamic) of transition metal compounds

– Bond and valence state properties
– Molecular structure
– Spin crossover (thermally, optically and pressure-induced)
– Magnetic properties
– Photochemical and photophysical phenomena
– Phase transformations
– Kinetic and thermodynamic properties
– Chemical and physical aftereffects of nuclear transformation

- Surface physics and chemistry

– Thin metallic layers by Langmuir–Blodgett technique
– Corrosion
– Structure and reactivity on glass surfaces

- Industrial applications of Mössbauer spectroscopy

– Magnetic and optical recording material
– Battery material
– Glasses
– Corrosion

Research equipment

- ca. 8 Mössbauer spectrometers for transmission, scattering, CEMS, DEC-EMS, time-integral and time-differential measurements, also under pressure or in applied magnetic field and variable temperature ($\geq$ 2 K)
- 2 Magnetometers (Foner, SQUID) for 350 $\geq$ T $\geq$ 2 K
- ESCA-spectrometer
- AUGER-spectrometer
- UV/Vis spectrometer, also for single crystals in the range 300 $\geq$ T $\geq$ 5 K

Raman spectrometer, T-dependent in the range 1500 $\geq$ T $\geq$ 4 K

- FT-FIR spectrometer, T-dependent in the range 300 $\geq$ T $\geq$ 4 K
- Single crystal X-ray diffractometer, T-dependent 300 $\geq$ T $\geq$ 10 K, CCD

Publications

- ca. 475 original papers
- 1 book ("Mössbauer Spectroscopy and Transition Metal Chemistry")
- Chapters in ca. 15 books
- Editor (together with N. Sutin, USA) of "Comments on Inorganic Chemistry", which was launched in 1981)
- Editor of proceedings of 5 Seeheim Workshops on Mössbauer Spectroscopy
- Editor (with H.A. Goodwin) of the series of Spin Crossover Transition Metal Compounds, 3 volumes (Nr. 233, 234, 235) in Topics in Current Chemistry (Springer), 2004
- Book "Mössbauer Spectroscopy and Transition Metal Chemistry", Second Edition, Springer-Verlag, 2010

Seminars and Presentations

- More than 300 Invited Talks/Plenary Lectures
- Ca. 500 contributions to conferences (oral and posters)

Yann Garcia

Communication: French, English, Spanish, German (basic knowledge)

Research domains: Supramolecular functional (photo)magnetic materials, Crystal growth and design of MOFs and coordination polymers, Applications of Mössbauer and muon spin relaxation spectroscopies

Teaching area:

- Analytical chemistry and instrumental methods in solid state physics/chemistry
- 122 international publications, 9 book chapters, 2 patents, h index: 22
- Guest editor of three special issues (Eur. J. Inorg. Chem., Möss. Eff. Ref. Data J.)
- Author of 4 cover page articles
- 93 oral communications and 169 posters
- 104 oral communications and 191 posters
- Invited lectures at conferences (23) and universities (14)

Positions

2009	Professor at UCL
2004–2009	Associate professor at UCL
2001–2004	Tenure track assistant professor at UCL
1999–2001	EU-TMR Post-doctoral research fellow with Prof. Dr. P. Gütlich Institut für Anorganische und Analytische Chemie, Mainz (Germany).
1995–1999	Doctoral fellow of the University of Bordeaux I –Laboratory of Molecular Sciences, Bordeaux Institute of Condensed Matter Chemistry, CNRS (France) - supervisor: Prof. Dr. O. Kahn, academician.

Education

At the University of Bordeaux I (France):

1995–1999	Doctoral thesis in Materials Science and Solid State Chemistry (highest distinction), Bordeaux Institute of Condensed Matter Chemistry—CNRS
1994–1995	DEA of Materials Science
1993–1994	MSc in Physical Sciences
1992–1993	BSc in Physical Sciences
1990–1992	DEUG A in Chemistry and Physics
1987–1990	High school, Bachelor C (Mathematics, Physics, Chemistry), Bergerac

Services

Since 2007	President, Groupe Francophone de spectrométrie Mössbauer (GFSM)
Since 2009	Member, International Board on the Applications of the Mössbauer Effect (IBAME)
Since 2012	President of the thematic doctoral school of the French speaking community of Belgium 'Molecular, supramolecular and functional chemistry'

Referees for international grant applications, doctoral thesis outside UCL and one academic position

Editorial boards

Since 2005	Member, International advisory board of Eur. J. Inorg. Chem. (Wiley-VCH)
Since 2007	Member, International advisory board of Open Inorg. Chem. J. (Bentham Sc. Pub).
Since 2011	Editor-in-Chief of Curr. Inorg. Chem. (Bentham Sc. Pub).
Since 2011	Associate Editor of MERDJ Regular referee for high impact factor international chemistry journals (Angew. Chem. Int. Ed., J. Am. Chem. Soc., Chem. Comm., Chem. Eur. J., Dalton Trans., CrystEngComm, Eur. J. Inorg. Chem. ...)

Award

2009	Nominated as emerging leader of the future Mössbauer community by the Mössbauer Effect Data Center (Vienna, July 2009).

http://www.springer.com/978-3-642-32219-8

Mössbauer Spectroscopy
Tutorial Book
Yoshida, Y.; Langouche, G. (Eds.)
2013, X, 310 p., Hardcover
ISBN: 978-3-642-32219-8